MINISTÉRIO DA CIÊNCIA, TECNOLOGIA E INOVAÇÃO
INSTITUTO NACIONAL DE PESQUISAS ESPACIAIS

sid.inpe.br/mtc-m21d/2023/02.23.15.20-TDI

COMPARATIVE ANALYSIS OF THE TRIGRS AND SINMAP MODELS FOR ASSESSING LANDSLIDE-PRONE AREAS: SUBSIDIES FOR THE DEVELOPMENT OF AN EARLY WARNING SYSTEM

Tèhrrie Caroline König Ferraz Pacheco

Doctorate Thesis of the Graduate Course in Remote Sensing, guided by Drs. Hermann Johann Heinrich Kux, and Alessandra Cristina Corsi, approved in February 16, 2023.

URL of the original document:
<http://urlib.net/8JMKD3MGP3W34T/48JT36E>

INPE
São José dos Campos
2023

PUBLISHED BY:

Instituto Nacional de Pesquisas Espaciais - INPE
Coordenação de Ensino, Pesquisa e Extensão (COEPE)
Divisão de Biblioteca (DIBIB)
CEP 12.227-010
São José dos Campos - SP - Brasil
Tel.:(012) 3208-6923/7348
E-mail: pubtc@inpe.br

BOARD OF PUBLISHING AND PRESERVATION OF INPE INTELLECTUAL PRODUCTION - CEPPII (PORTARIA Nº 176/2018/SEI-INPE):

Chairperson:

Dra. Marley Cavalcante de Lima Moscati - Coordenação-Geral de Ciências da Terra (CGCT)

Members:

Dra. Ieda Del Arco Sanches - Conselho de Pós-Graduação (CPG)

Dr. Evandro Marconi Rocco - Coordenação-Geral de Engenharia, Tecnologia e Ciência Espaciais (CGCE)

Dr. Rafael Duarte Coelho dos Santos - Coordenação-Geral de Infraestrutura e Pesquisas Aplicadas (CGIP)

Simone Angélica Del Ducca Barbedo - Divisão de Biblioteca (DIBIB)

DIGITAL LIBRARY:

Dr. Gerald Jean Francis Banon

Clayton Martins Pereira - Divisão de Biblioteca (DIBIB)

DOCUMENT REVIEW:

Simone Angélica Del Ducca Barbedo - Divisão de Biblioteca (DIBIB)

André Luis Dias Fernandes - Divisão de Biblioteca (DIBIB)

ELECTRONIC EDITING:

Ivone Martins - Divisão de Biblioteca (DIBIB)

André Luis Dias Fernandes - Divisão de Biblioteca (DIBIB)

MINISTÉRIO DA CIÊNCIA, TECNOLOGIA E INOVAÇÃO
INSTITUTO NACIONAL DE PESQUISAS ESPACIAIS

sid.inpe.br/mtc-m21d/2023/02.23.15.20-TDI

COMPARATIVE ANALYSIS OF THE TRIGRS AND SINMAP MODELS FOR ASSESSING LANDSLIDE-PRONE AREAS: SUBSIDIES FOR THE DEVELOPMENT OF AN EARLY WARNING SYSTEM

Tèhrrie Caroline König Ferraz Pacheco

Doctorate Thesis of the Graduate Course in Remote Sensing, guided by Drs. Hermann Johann Heinrich Kux, and Alessandra Cristina Corsi, approved in February 16, 2023.

URL of the original document:
<http://urlib.net/8JMKD3MGP3W34T/48JT36E>

INPE
São José dos Campos
2023

Cataloging in Publication Data

Pacheco, Tèhrrie Caroline König Ferraz.

P115c Comparative analysis of the TRIGRS and SINMAP models for assessing landslide-prone areas: subsidies for the development of an early warning system / Tèhrrie Caroline König Ferraz Pacheco. – São José dos Campos : INPE, 2023.

xxiv + 132 p. ; (sid.inpe.br/mtc-m21d/2023/02.23.15.20-TDI)

Thesis (Doctorate in Remote Sensing) – Instituto Nacional de Pesquisas Espaciais, São José dos Campos, 2023.

Guiding : Drs. Hermann Johann Heinrich Kux, and Alessandra Cristina Corsi.

1. Landslides. 2. TRIGRS. 3. Early warning system. I.Title.

CDU 528.8:504.2

Esta obra foi licenciada sob uma Licença Creative Commons Atribuição-NãoComercial 3.0 Não Adaptada.

This work is licensed under a Creative Commons Attribution-NonCommercial 3.0 Unported License.

MINISTÉRIO DA CIÊNCIA, TECNOLOGIA E INOVAÇÃO

INSTITUTO NACIONAL DE PESQUISAS ESPACIAIS
Serviço de Pós-Graduação - SEPGR

DEFESA FINAL DE TESE DE TÈHRRIE CAROLINE KÖNIG FERRAZ PACHECO
REG. 136727/2019, BANCA Nº 011/2023

No dia 16 de fevereiro de 2023, de forma online, o(a) aluno(a) mencionado(a) acima defendeu seu trabalho final (apresentação oral seguida de arguição) perante uma Banca Examinadora, cujos membros estão listados abaixo. O(A) aluno(a) foi APROVADO(A) pela Banca Examinadora, por unanimidade, em cumprimento ao requisito exigido para obtenção do Título de Doutora em Sensoriamento Remoto, com a exigência de que o trabalho final a ser publicado deverá incorporar as correções sugeridas pela Banca Examinadora, com revisão pelo(s) orientador(es).

Novo Título: "Comparative Analysis of the TRIGRS and SINMAP Models for Assessing Landslide-prone Areas: Subsidies for the Development of an Early Warning System"

Membros da banca:

Dra. Cláudia Maria de Almeida – Presidente – INPE
Dr. Hermann Johann Heinrich Kux – Orientador – INPE
Dra. Alessandra Cristina Corsi – Orientadora – IPT
Dr. Thales Sehn Körting – Membro Interno – INPE
Dr. Estéfano Seneme Gobbi – Membro Externo – PUC-Campinas
Dr. Nelson Ferreira Fernandes – Membro Externo – UFRJ

Documento assinado eletronicamente por **Thales Sehn Korting**, **Pesquisador**, em 20/03/2023, às 10:49 (horário oficial de Brasília), com fundamento no § 3º do art. 4º do Decreto nº 10.543, de 13 de novembro de 2020.

Documento assinado eletronicamente por **Alessandra cristina corsi (E)**, **Usuário Externo**, em 20/03/2023, às 11:38 (horário oficial de Brasília), com fundamento no § 3º do art. 4º do Decreto nº 10.543, de 13 de novembro de 2020.

Documento assinado eletronicamente por **Cláudia Maria de Almeida**, **Pesquisador**, em 20/03/2023, às 11:44 (horário oficial de Brasília), com fundamento no § 3º do art. 4º do Decreto nº 10.543, de 13 de novembro de 2020.

Documento assinado eletronicamente por **Estéfano Seneme Gobbi (E)**, **Usuário Externo**, em 20/03/2023, às 13:08 (horário oficial de Brasília), com fundamento no § 3º do art. 4º do Decreto nº 10.543, de 13 de novembro de 2020.

Documento assinado eletronicamente por **nelson ferreira fernandes (E)**, **Usuário Externo**, em 29/03/2023, às 13:49 (horário oficial de Brasília), com fundamento no § 3º do art. 4º do Decreto nº 10.543, de 13 de novembro de 2020.

Documento assinado eletronicamente por **Hermann johann heinrich kux (E)**, **Usuário Externo**, em 30/03/2023, às 14:25 (horário oficial de Brasília), com fundamento no § 3º do art. 4º do Decreto nº 10.543, de 13 de novembro de 2020.

A autenticidade deste documento pode ser conferida no site https://sei.mcti.gov.br/verifica.html, informando o código verificador **10930620** e o código CRC **46687C14**.

Referência: Processo nº 01340.000812/2023-61 SEI nº 10930620

"*If you care about something, you fight for it*".

Hergé (1907-1983)

Aos meus queridos pais, meus grandes exemplos de vida, que sempre estiveram ao meu lado, em todos os momentos de minha vida. Ao meu marido, por seu apoio incondicional nessa jornada. E a minha amada Nonô, que me acompanhou durante as inúmeras madrugadas de pesquisa e realização desse trabalho.

AGRADECIMENTOS

Aos meus amados pais, por todo o amor, apoio, força e incentivo ao longo de toda a minha vida.

Ao meu companheiro e amado Alex, pelo apoio incondicional durante esta jornada, pela amizade, carinho e por sempre acreditar em mim.

Aos meus orientadores Dr. Hermann Kux e Dra. Alessandra Cristina Corsi, pela oportunidade, apoio, orientação, confiança e amizade.

Aos meus avós, por todo o carinho, apoio e abraços apertados.

Aos meus amigos que mesmo distante sempre me apoiaram, me ouviram reclamar e fizeram de tudo para me animar: Victor, Nagela e Édino.

À Coordenação de Aperfeiçoamento de Pessoal de Nível Superior (CAPES) do Ministério da Educação (MEC) pela concessão de bolsa de estudos.

ABSTRACT

A landslide is a natural phenomenon that becomes a disaster when occurring in urban areas. Usually triggered by heavy rainfall, the landslides can cause economic damage, social impact, and fatalities. In Brazil, the region called Serra do Mar is one of the most affected areas, where several landslides are recorded every year. Therefore, the identification, analysis, and monitoring of landslide-prone areas are essential to avoid disasters. This doctoral thesis identifies the landslide-prone areas in the Guarujá municipality, performs a temporal analysis of urban sprawl from 1990-2021, correlates it with landslide occurrences, and develops a landslide early warning system, to avoid disasters. The temporal analysis was performed using satellite images from the Landsat series and an orthophoto for image classification of the study area. To identify landslide-prone areas, two mathematical models were tested: TRIGRS (Transient Rainfall Infiltration and Grid-based Regional Slope-Stability Model), and SINMAP (Stability Index Mapping). The results were validated using a landslide inventory, prepared from satellite images and Guarujá Civil Defense data. The susceptibility map developed by IPT (Technological Research Institute) supports the validation. The performance of both models was compared using statistical indexes and the TRIGRS model performed the best. Therefore, an early warning system was developed in Python using TRIGRS to model the landslide-prone areas. The system automatically acquired weather forecasts from the Climatempo website, calculates the slope stability, and if necessary, sends an alert. The results of this study are a landslide susceptibility map for the Vila Baiana neighborhood in Guarujá municipality, the correlation between rainfall events, landslides, and urban sprawl, and an early warning system using TRIGRS.

Keywords: Landslides. TRIGRS. Early warning system.

ANÁLISE COMPARATIVA ENTRE OS MODELOS TRIGRS E SINMAP PARA A DETERMINAÇÃO DE ÁREAS DE DESLIZAMENTO: SUBSÍDIOS PARA O DESENVOLVIMENTO DE UM SISTEMA DE PREVISÃO E ALERTA

RESUMO

Deslizamentos de terra são um fenômeno natural, que se tornam desastres quando ocorrem em áreas urbanas. Geralmente desencadeados por chuvas intensas, os deslizamentos de terra podem causar prejuízos econômicos, sociais e fatalidades. No Brasil, a região chamada de Serra do Mar é uma das áreas mais atingidas, registrando diversos deslizamentos todos os anos. Desta forma, a identificação, análise e monitoramento das áreas suscetíveis à deslizamentos de terra são essenciais para evitar desastres. Esta tese de doutorado identifica as áreas suscetíveis à deslizamentos de terra no município do Guarujá, realiza uma análise temporal da expansão urbana de 1990-2021, relacionando-a com as ocorrências de deslizamentos, e desenvolve um sistema de previsão e alerta de deslizamentos, a fim de evitar desastres. Uma análise temporal foi realizada utilizando imagens de satélite da série Landsat, e uma ortofoto para classificar a área de estudo. A identificação das áreas suscetíveis à deslizamento de terra foram realizadas utilizando-se dois modelos matemáticos: TRIGRS (*Transient Rainfall Infiltration and Grid-based Regional Slope-Stability Model*) e SINMAP (*Stability Index Mapping*). Os resultados foram validados a partir de um inventário de cicatriz de deslizamentos, preparado a partir de imagens de satélite e dados da Defesa Civil do Guarujá. O mapa de suscetibilidade desenvolvido pelo IPT (Instituto de Pesquisas Tecnológicas) auxilia na validação dos resultados. Comparou-se a performance de ambos os modelos usando índices estatísticos, e o modelo TRIGRS obteve os melhores resultados. Diante disso, um Sistema de previsão e alerta foi desenvolvido em *Python*, utilizando-se do modelo TRIGRS para a identificação das áreas suscetíveis à deslizamento de terra. O sistema automaticamente adquire dados de previsão do tempo, a partir do site do Climatempo, calcula a estabilidade das encostas e, se necessário, envia um alerta. Como resultado desse estudo, gerou-se um mapa da suscetibilidade à deslizamentos de terra, no bairro da Vila Baiana localizada no município do Guarujá, a correlação entre eventos de chuva, deslizamentos e expansão urbana, e um sistema de previsão e alerta usando o modelo TRIGRS.

Palavras-chave: Deslizamento de terra. TRIGRS. Sistema de previsão e alerta.

LIST OF FIGURES

LIST OF TABLES

ABBREVIATION LIST

API	Application Programming Interface
CART	Classification and Regression Trees
CEMADEN	Centro Nacional de Monitoramento e Alerta de Desastres Naturais National Center for Monitoring and Early Warning
COMPDEC	Coordenadoria Municipal de Proteção e Defesa Civil Civil Municipal Defense Coordination
CSI	Critical Success Index
DAEE	Departamento de Águas e Energia Elétrica Water and Eletrical Energy Department
DEM	Digital Elevation Model
dSLAM	Physically based Slope Stability Model
EI	Error Index
ENOS	El-Niño South Oscillation
FAR	False Alarm Ratio
Fd	Frequency of Distribution
FN	False Negative
FP	False Positive
FPR	False Positive Ratio
FS	Factor of Safety
GIS	Geographic Information System
GCP	Ground Control Point
GNSS	Global Navigation Satellite System
IBGE	Instituto Brasileiro de Geografia e Estatística – Brazilian Institute of Geography and Statistics
IPT	Instituto de Pesquisas Tecnológicas - Technological Research Institute
KDD	Knowledge Discovery in Databases
LAI	Leaf Area Index
LiDAR	Light Detection and Ranging

LP	Landslide Potential
NDVI	Normalized Difference Vegetation Index
NOAA	National Oceanic and Atmospheric Administration
OBIA	Objected-based Image Analysis
ONI	Ocean Niño Index
POD	Probability of Detection
PPDC	Civil Defense Preventive Plan
ROC	Receiver Operating Curve
SI	Success Index
SINMAP	Stability Index Mapping
SOM	Self-Organized Maps
SC	Scar Concentration
SHALSTAB	Shallow Slope Stability Model
SST	Sea Surface Temperature
SSURGO	Soil Survey Geographic
TRIGRS	Transient Rainfall Infiltration and Grid-based Regional Slope Stability Model
TN	True Negative
TP	True Positive

CONTENTS

1. INTRODUCTION

The number of registered disasters has been increasing worldwide, especially since the 1950s (MARCELINO et al., 2006). Some authors, such as Nicholls (2001) and Pielke (2005; 2006), associate the increase in disasters with a higher vulnerability of society. However, for Houghton (2003), there is a correlation between disasters and global climate change.

In Brazil, landslides are a natural phenomenon, usually triggered by high precipitation rates. This phenomenon can be called “deslizamento” (landslide) or “escorregamento” (slip) in Portuguese. Both terms are used to describe a surface rupture with the displacement of soil and rocks. Despite that, this study will use the term landslide.

When landslides happen in urban areas, they become disasters due to economic damage, social impact, and fatalities. As an example, in January 2011, several landslides occurred in the mountainous region of Rio de Janeiro State, killing 947 people, leaving more than 300 missing, and thousands homeless. It was considered one of the worst disasters in the country (CEMADEN, 2016).

Most landslides registered in Brazil occurred during the rainy season, corresponding to the summer season (December through March). From 1991 to 2019, 1146 landslides were registered, and 69% of them happened in the southeast region of the country, as presented in Figure 1.1. Furthermore, Figure 1.2 shows the distribution of how landslides affected the population (CENAD, 2013; CEPED-UFSC, 2013; 2020).

Analyzing Figure 1.2, one observes that more than 1.5 million people were affected somehow by landslides. These people account for the homeless, injured (hurt, disease), or missing. Therefore, identifying, analyzing, and monitoring landslide-prone areas is critical. When preventive actions are not applied, there is an increase in the intensity, magnitude, and frequency of hazard impacts (KOBIYAMA et al., 2006). Moreover, the development of a warning system with different risk levels also helps avoid and minimize the disaster impact.

In 1987-1988, several landslides occurred in a region called "Serra do Mar", in São Paulo State. Consequently, the Civil Defense Preventive Plan – PPDC (in Portuguese: Plano Preventivo da Defesa Civil), was created to identify, evaluate, and monitor the susceptible

geological areas, mainly related to landslides. One of the essential actions of PPDC is the preventive removal of people living in risk areas during rainfall events (MACEDO et al., 2004; MENDES; FILHO, 2015).

Figure 1.1. Landslides documented in Brazil from 1991 to 2019.

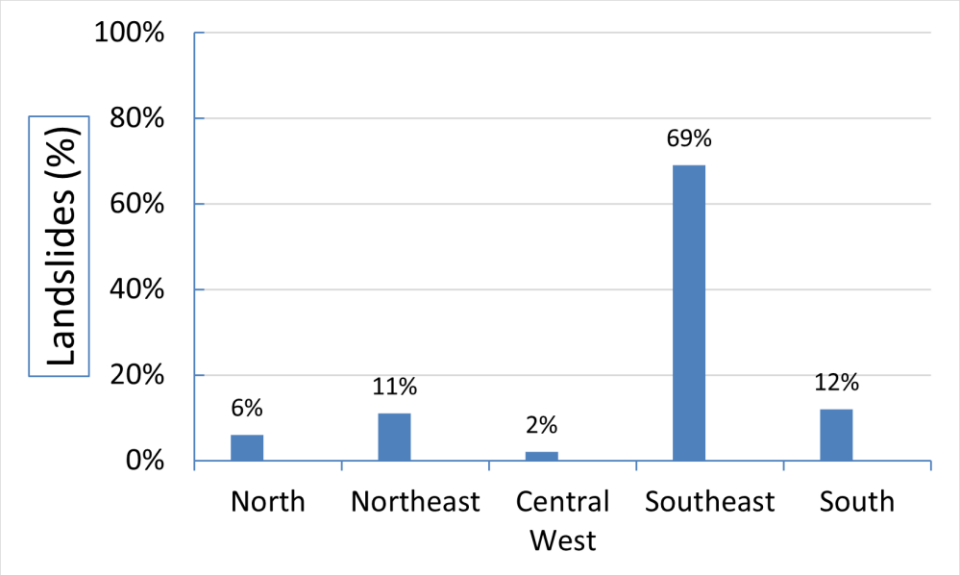

Source: Adapted from CEPED-USFC (2020).

Figure 1.2. The social impact caused by landslides in the southeastern region of Brazil, from 1991 to 2019.

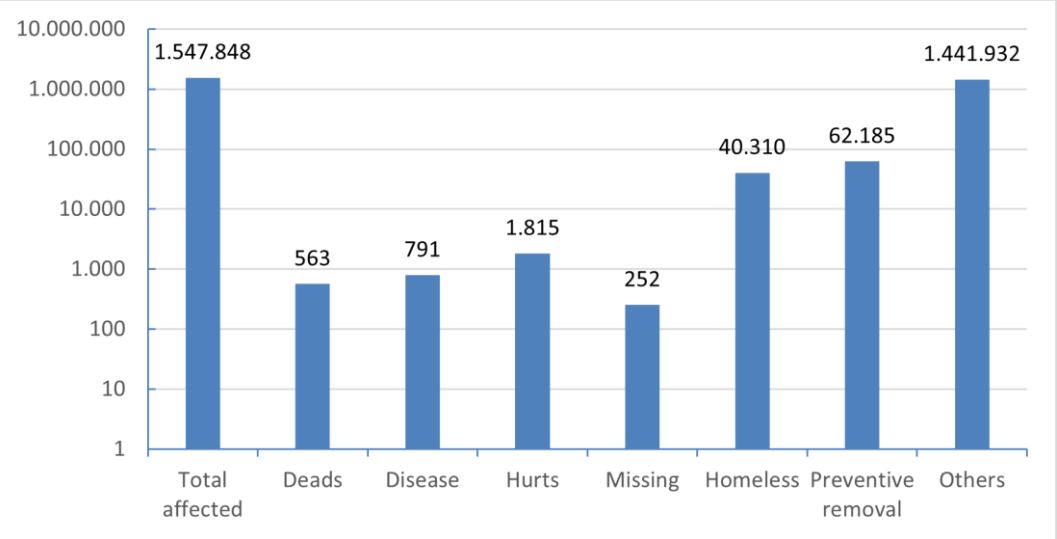

Source: Adapted from CEPED-USFC (2020).

With the current climate variability, there is a tendency to increase extreme weather conditions, either with long periods of drought or heavy and long-term rainfall (HOUGHTON, 2003). According to Brollo and Ferreira (2016), in São Paulo State from 2000 to 2015, 10,893 geodynamic phenomena were registered, affecting 971,849 people and killing 534. Among these phenomena, 1,430 had geological nature (landslides, debris flow, rock displacement), 6,064 hydrological characteristics (flooding, flash flooding), 2,444 were meteorological (rainfall, storms, hailstones), and 955 related to climate (drought, frost).

Heavy rainfall might trigger landslides; however, the area's susceptibility is strongly related to its geological and geomorphological characteristics. For that reason, it is crucial to study how climate and soil's geotechnical properties interact to understand the hydro-mechanical aspects responsible for triggering landslides.

The identification of landslide-prone areas can be performed using statistical methods (CARRARA et al., 1991; BAI et al., 2009; CERVI et al., 2010; LI et al., 2012) and physically-based models such as the Shallow Slope Stability Model (SHALSTAB) (MONTGOMERY; DIETRICH, 1994; DIETRICH, W. E.; MONTGOMERY, 1998; DIETRICH; et. al., 2011), Stability Index Mapping (SINMAP) (PACK et al. 1998), Transient Rainfall Infiltration and Grid-based Regional Slope Stability Model (TRIGRS) (BAUM et al., 2008), physically-based Slope Stability Model (dSLAM) (WU; SIDLE, 1995), SLOPE/W and SEEP/W (GEO-SLOPE, 2016).

The Shalstab - Shallow Landsliding Stability Model, developed by Dietrich and Montgomery (1998), is a deterministic mathematical model to identify landslide-prone areas. Its formula is based on the infinity slope stability model, defined by the Mohr-Coulomb Law, and on the steady-state hydrological model, developed by O'Loughlin (1986). Shalstab calculates the critical threshold of rainfall for the occurrence of a surface rupture and, consequently, a landslide (MONTGOMERY; DIETRICH, 1994; DIETRICH AND MONTGOMERY, 1998; VIEIRA; RAMOS, 2015; KÖNIG et al., 2019).

The Sinmap – Stability Index Mapping, developed by Pack et al. (1998), is a probabilistic model based on the steady-state hydrologic concepts and the infinite slope stability model, "that balances the destabilizing components of gravity and the restoring

components of friction and cohesion on a failure plane parallel to the ground surface" (PACK et al., 1998, p. 1).

Baum et al. (2008) developed the mathematical model TRIGRS (Transient Rainfall Infiltration and Grid-based Regional Slope Stability Model) to calculate the variations of the Factor of Safety (FS) due to changes in the transient pore-pressure and soil moisture during a rainfall infiltration.

The dSLAM software is a distributed, physically based model that combines the mathematical formulation of an infinite slope model with a groundwater kinematic model. It uses the continuous changes in vegetation to analyze landslides and the variation of the Factor of Safety (FS) on steep slope forests (WU; SIDLE, 1995; 1997).

The GeoSlope software, developed by the Geo-Slope company in Canada, is a mathematical model based on the principle of limit equilibrium to analyze the deformation and stability of geotechnical structures. It has two modules: Seep/W and Slope/W. The Seep/W module uses numerical analysis to calculate the water infiltration process in the soil, for both saturated and unsaturated soil conditions (GEO-SLOPE, 2012, 2016; GHOSH, 2012; MENDES et al., 2018a). The results from Seep/W are used in the Slope/W module to analyze the terrain´s stability and calculate the Factor of Safety (FS). (GEO-SLOPE, 2016; MENDES et al., 2018a).

This doctoral research project is committed to use the TRIGRS model to identify landslide-prone areas based on the successful results reported in the literature (CHIEN-YUAN et al., 2005; GODT et al., 2008; SORBINO et al., 2010; LIAO et al., 2011; PARK et al., 2013; ZIZIOLI et al., 2013). The expected outcome is a landslide-prone map for the Vila Baiana neighborhood in Guarujá municipality, and the evaluation of TRIGRS as a tool for early warning systems.

This project is based on the hypothesis that TRIGRS has a higher degree of accuracy in identifying landslide-prone areas. And it can be used as an early warning system, providing alerts based on the soil moisture and variation from the slope Factor of Safety. Moreover, a temporal analysis of urban sprawl helps to understand if anthropic changes in slope areas induced landslides.

2. OBJECTIVES

The main objective of this work is the development of an early warning system using the mathematical model TRIGRS to identify landslide-prone areas in the Guarujá municipality.

2.1. Specific objectives

- Perform a temporal analysis of urban sprawl, using satellite images and machine learning techniques, and correlate it with landslide occurrences.
- Analyze the correlation between rainfall events and landslides.
- Investigate the topographic and lithological aspects of the Guarujá municipality.
- Comparative evaluation of the TRIGRS and SINMAP models for assessing landslide-prone areas
- Development of an early warning system that combines weather forecast and TRIGRS predictive analysis to determine risk levels, and issue alerts based on the variation of the Factor of Safety.

3. THEORETICAL FRAMEWORK

3.1 Definitions

Natural phenomena, which occur worldwide, might become a disaster when it affects a group of people, disrupting their everyday life (KOBIYAMA et al., 2006; KÖNIG et al., 2018). Communities that live in areas affected by natural hazards are vulnerable to their consequences, and these people are at risk due to financial damage and losses of life. There is a correlation among disaster, hazard, risk, susceptibility, vulnerability, and resilience; thus, some definitions are necessary.

The hazard is related to the natural phenomena recurrence, affecting different areas individually or combined (one or more natural phenomena happening simultaneously, in the same place). It is common for a hazard to cause problems in the affected region. The risk happens due to a combination of hazard and vulnerability. It is related to social impacts, economic and structural damages. Risk levels (high or low risks) agree with vulnerability (e.g., severe hazards affecting a vulnerable group of people constitute high risk) (KOBIYAMA et al., 2006).

The vulnerability is related to people and communities. It is associated with the preexisting conditions of material and a social life affected by natural phenomena. The susceptibility is related to areas and regions affected by natural hazards (WISNER et al., 2003; MACEDO; BRESSANI, 2013; TOBIN; WHITEFORD, 2013; KÖNIG et al., 2018). For example, Etna is an active volcano with frequent eruptions. The cities near Etna are in susceptible areas, meaning they are susceptible to volcano hazards. People who live in those cities are vulnerable to the same hazards. In a Brazilian context, the neighborhood Vila Baiana in Guarujá-SP is susceptible to landslides, and the population is vulnerable to the consequences.

The disasters occur when a group of people or a community is affected by a natural hazard, and there is a disturbance in their development and everyday life (e.g., livestock, crops, homes, roads, bridges, schools, and hospitals are destroyed) (WISNER et al., 2003; MACEDO; BRESSANI, 2013).

Resilience is related to the population´s capability to be prepared, cope with, resist and recover from a significant disruption caused by a natural hazard within an acceptable time (AVEN, 2011; MACEDO; BRESSANI, 2013; BITAR et al., 2015).

3.2 Pedology and characteristics of mass movements

Pedology is the study of soil formation, its properties characterization, and the mapping of its geographic distribution (SOUZA, 1995). Moreover, a pedological study determines the best use for a specific area (i.e.: agriculture, preservation areas, urban expansion).

The soils consist of roughly parallel sections, called horizons (Figure 3.1), which differ from the parent material (hard bedrock) due to pedogenesis. Pedogenesis is the process of soil formation, which involves addition, losses, transformation, and translocation of matter. The types of soils differ accordingly to the parent material, topography, biota, climate, and length of time during pedogenesis (JENNY, 1945; SOUZA, 1995; PHILLIPS, 2017; EMBRAPA, 2018). They can be classified based on their morphological characteristics: color, texture, structure, porosity, and cohesion. It is also analyzed the concentration of iron, aluminum, silica, clay, and organic matter (BOCKHEIM et al., 2005). The soil layers have specific characteristics. Horizon O is characterized by decomposed and undecomposed organic matter. Horizon A (surface horizon) is characterized as the mineral horizon and has a high concentration of organic matter. Horizon B is the subsoil, formed due to intense pedogenetic processes, with sandy loam or finer texture and a high concentration of clay. The C horizon is the substratum (regolith). In this horizon, the rock is partially weathered with fragments of different sizes (SOUZA, 1995; EMBRAPA, 2018). There is also a colluvial cover, which is the accumulation of soil material and small fragments of rocks on the base of slopes, mainly by gravity.

Each soil has its own physical and chemical properties, which determine the soil´s susceptibility to landslides and erosive processes (MENEZES; PEJON, 2010).

Gravitational mass movements are surface transformations with a displacement of soil, rocks, and debris (FELL et al., 2008; KÖNIG et al., 2019). They can be classified into four types accordingly to the soil type, water moisture content, velocity, rupture, and deformation (VARNES, 1978; CRUDEN; VARNES, 1996; CENAD, 2013), as presented in Table 3.1.

Figure 3.1. Schematic soil horizons.

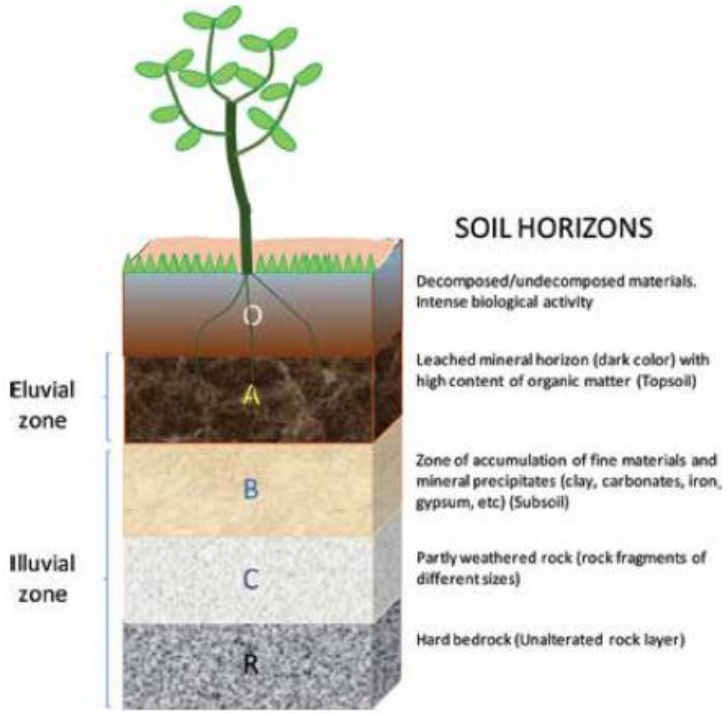

Source: Adapted from Larramendy and Soloneski (2019).

Table 3.1. Types of Mass Movements.

Types of Mass Movements	**Description**
Slide	A large volume of soil displacement moving down on the slope. (i.e., translational, and rotational landslides)
Falls	Rock and sediment displacement falling through the air.
Flows	A mix of soil, rocks, and sediments with high water moisture volume flowing rapidly down the slope. (i.e., Debris flow, mudflows/lahar)
Creeps	A very slow process (years) of mass movement that happened deeper in the ground.

In Brazil, the slide is the mass movement type that causes several disasters, thus it will be emphasized and described as a landslide. According to Cruden and Varnes (1996), landslides occur when there is a surface rupture, with soil and rock sliding down slopes. The landslides are classified as rotational and translational slides.

The translational slides occur in steep parallel surfaces when there is a rupture between the shallow soil layer and the impermeable substrate beneath it. They usually happen in residual and colluvial soil layers, with the soil rupture occurring at depths from 0.5m to 5.0m (VIEIRA, 2007; VIEIRA; RAMOS, 2015; MENDES et al., 2018a). Subsequently, the impermeable substrate can be a rock or soil layer with high values of clay. The rotational slides are characterized by a deep surface rupture that deforms this surface concavely. Its occurrence usually happens in landfills and dams (AHRENDT, 2005; ZÊZERE et al., 2005). Figure 3.2 presents the two types of landslides.

To understand and predict soil behavior, the knowledge of geotechnical and hydrological properties is essential. Some geotechnical properties related to the prediction of landslides are shear strength, soil cohesion, and internal friction angle; while the hydrological properties are hydraulic conductivity and diffusivity. The definitions of these parameters are presented in Table 3.2.

Figure 3.2. Representation of a rotational slide (A) and translational slide (B).

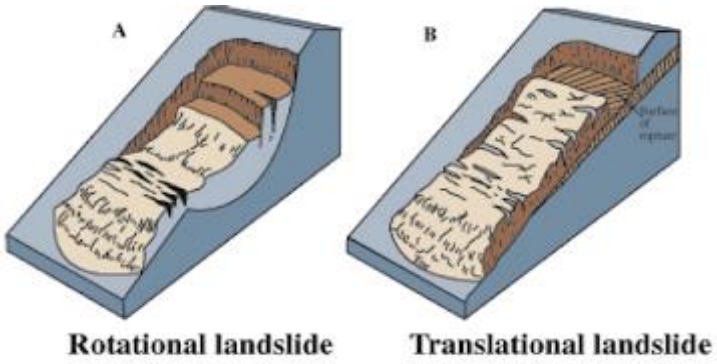

Source: Adapted from CEMADEN (2016).

Table 3.2. Definitions of soil properties.

	Soil Properties	Definitions
Geotechnical Properties	Soil Cohesion	It is the force that holds the soil particles.
	Internal Friction Angle	The angle between the shear strength and the normal effective stress in which a failure occurs.
	Shear Strength	It is related to the maximum shear stress a soil can sustain.
Hydrological Properties	Hydraulic Conductivity	Also called the Coefficient of Permeability - It is a measure of velocity with which the water can pass through soil layers.
	Hydraulic Diffusivity	It is the ratio of Hydraulic Conductivity to the effective porosity, i.e., the water capacity to infiltrate.

Source: Ahrendt (2005); Das and Kondraivendhan (2012); Roy et al. (2017).

3.3 Satellite images

Satellite images have been used in several different types of research: change detection of land use and land cover, occupation, disasters management, and detection of burning areas or forest degradation, among others (GUILD et al., 2004; HENRIQUE et al., 2008; NOVACK, 2009; PINHO et al., 2012; RODRIGUES, 2014; LIBONATI et al., 2015; PECHINCHA; ZAIDAN, 2015; KÖNIG et al., 2019).

Today, there are several satellite sensors, each of them with specific characteristics. They have different spectral, spatial, and radiometric resolutions. The revisit frequency and swath width also change. Some satellite sensors with high spatial resolution have a more refined spectral resolution, like IKONOS, WorldView-2, and 3, QuickBird, and Planet, among others. These images are widely used in urban areas studies because they provide the opportunity to differentiate individual trees, different vegetation species, landslides scars, and types of constructions (houses, buildings) or roads (PINHO; et. al., 2005; SANTOS; et. al., 2011; PU; LANDRY, 2012; MENEGHETTI; KUX, 2014; KÖNIG, 2018).

In 1972, the Landsat 1 was launched into space, and despite the low spatial resolution of the Landsat program (30 m), they are useful for temporal analysis. Furthermore, this doctoral project use Planet images to identify landslide scars and the Landsat collection

(Landsat 5, 7, and 8) for the temporal analysis of the study area. Table 3.3 presents a summary of each satellite´s spatial resolution that will be used in this project.

Table 3.3. Summary of the sensor's specifications.

Satellite	Sensor	Bands	Spectral Resolution	Spatial Resolution	Radiometric Resolution
Landsat 5	TM	Blue	0.45 - 0.52 µm	30 m	8 bits
		Green	0.50 - 0.60 µm		
		Red	0.63 - 0.69 µm		
		Near Infrared	0.76 - 0.90 µm		
Landsat 7	ETM+	Blue	0.45 - 0.52 µm		
		Green	0.50 - 0.60 µm		
		Red	0.63 - 0.69 µm		
		Near Infrared	0.76 - 0.90 µm		
		Panchromatic	0.52 - 0.90 µm	15 m	
Landsat 8	OLI	Coastal aerosol	0.43 - 0.45 µm	30 m	16 bits
		Blue	0.45 - 0.51 µm		
		Green	0.53 - 0.59 µm		
		Red	0.64 - 0.67 µm		
		Near Infrared	0.85 - 0.88 µm		
		Panchromatic	0.50 - 0.68 µm	15 m	
Dove	Planet	Blue	0,45 - 0,51 µm	3 m	12 bits
		Green	0,50 - 0,59 µm		
		Red	0,59 -0,67 µm		
		Near Infrared	0,78 - 0,86 µm		

Source: Adapted from Engesat (2020).

3.4 Data mining and image classification

With the advancement of Remote Sensing techniques and the total amount of digital data available, it is important to determine which data and information are crucial for a specific study and research. However, the extraction of the most relevant data is laborious and time-consuming. From that necessity, Knowledge Discovery in Databases (KDD) was developed. According to Fayyad et al. (1996), KDD is a process that extracts essential data from a massive volume of information. The steps are data acquisition, pre-processing, data transformation, data mining, interpretation, and evaluation, resulting in knowledge (Figure 3.3).

The primary step of KDD is Data Mining. This process automatically finds patterns and attributes from large data volumes, clustering then. It can be descriptive, which characterizes the data properties, or predictive, which uses the data information to make forecasts about them (HAN et al., 2012, KÖNIG et al., 2019). Some data mining algorithms use statistical methods, neural networks, fuzzy logic, or decision tree, among others (GOLDSCHMIDT; PASSOS, 2005). The statistical methods are used to resume and describe a group of data, helping in the validation process.

In Remote Sensing applications, the data mining process is used to extract attributes and characteristics (spatial and spectral information) from pixels or objects (regions) present in digital images (NOVO, 2010). An example of a system that uses data mining techniques for digital image analysis is GeoDMA, developed by Körting et al. (2013). GeoDMA has a decision tree, Self-Organizing Maps (SOM), and neural networks as algorithm options.

The software WEKA provides the C4.5 algorithm to perform data mining, as presented in Novack (2009), Carvalho (2011), Pinho, et al. (2012), and Bento (2016) studies. Moreover, the eCognition platform uses the Classification and Regression Trees (CART) algorithm for the data mining process (BENTO, 2016; KÖNIG, 2018; KÖNIG et al., 2019), among others.

Figure 3.3. Steps of the KDD process.

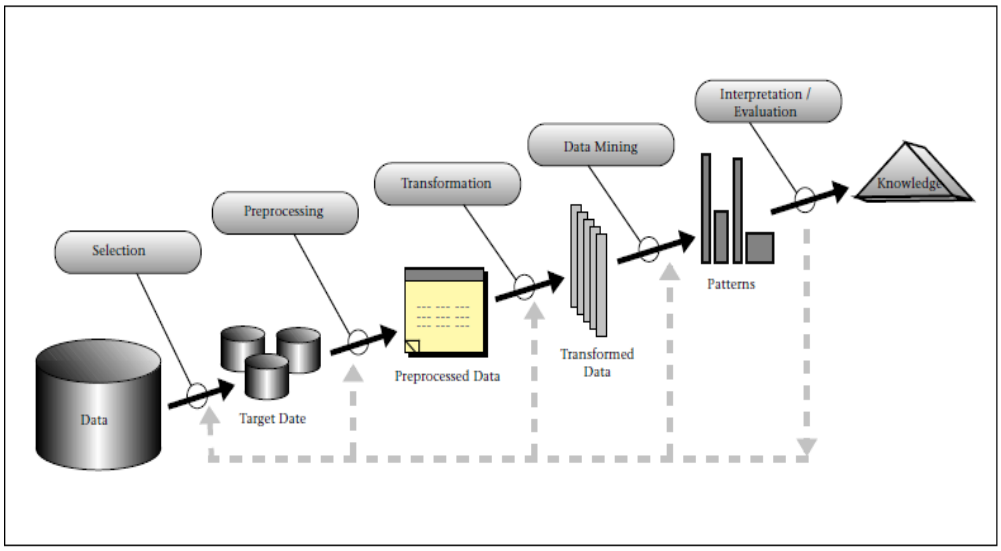

Source: Adapted from Fayyad et al. (1996).

Once the data mining process is finished, and the data are clustered according to specific attributes (spectral, texture, form, color), the image classification process starts. The Object-based Image Analysis (OBIA) paradigm is frequently used for high spatial resolutions images classification. The OBIA paradigm extracts information from satellite images in a semi-supervised way. It clusters similar objects, considering the pixel information and its neighbors. The advantage of this paradigm is to segment the image objects, which makes the interpretation easier (HAY; CASTILLA, 2006; PINHO et al., 2012; DRONOVA, 2015; CHEN et al., 2018; KÖNIG et al., 2019).

3.5 TRIGRS mathematical model

Baum et al. (2008) developed the mathematical model TRIGRS (Transient Rainfall Infiltration and Grid-based Regional Slope Stability Model) to calculate variations in the Factor of Safety (FS) due to changes in the transient pore-water pressure (pressure exerted by water in the soil pores) and soil moisture (soil water content) during a rainfall infiltration. The Factor of Safety is the ratio of the shear strength to the shear stress acting on the soil, meant to determine the slope stability. A FS equal to or higher than 1 means stability, and lower values (FS< 1) indicate unstable slopes (AHRENDT, 2005).

This model, written in FORTRAN, associates the hydrological model based on Iverson

(2000), who linearized the one-dimensional analytical solutions of Richards Equation (Equation 3.1) and a stability model based on the equilibrium limit principle, giving rise to its final formulation (Equation 3.2). It represents the vertical rainfall infiltration within homogeneous isotropic materials (BAUM et al., 2008).

$$\left(\frac{\partial \theta}{\partial t}\right) = \left(\frac{\partial}{\partial z}\right)\left[\mathbf{K}(\boldsymbol{\psi})\left(\frac{1}{\cos^2 \delta}\frac{\partial \Psi}{\partial z} - \mathbf{1}\right)\right] \quad (3.1)$$

where θ is the soil volumetric moisture content (dimensionless), t is the rainfall time duration (s), z is the soil depth (m), $K(\Psi)$ is the hydraulic conductivity (m/s kPa) in the z-direction, and Ψ is the groundwater pressure head (kPa).

$$\mathbf{FS} = \left(\frac{\tan \phi}{\tan \alpha}\right) + \left[\left(\frac{c - \Psi(Z,t)\Upsilon_w \tan \emptyset}{\Upsilon_s Z \sin \alpha \cos \alpha}\right)\right] \quad (3.2)$$

where c is the cohesion (kPa), ϕ is the internal friction angle (deg.), Υ_w is the unit weight of groundwater (kN/m³), Υ_s is the soil-specific weight (kN/m³), Z is the layer depth (m), α is the slope angle ($0^o < \alpha < 90^o$), and t is the time (s).

The TRIGRS input data are the geotechnical parameters (cohesion, soil specific weight, hydraulic conductivity, and internal friction angle), hydrological data (initial infiltration rate and initial groundwater table depth), and rainfall duration and intensity. The model allows for the variation of input values, such as soil properties cell by cell, because it considers horizontal heterogeneity. It is possible to have more than one type of soil in the same area, with specific physical properties. This is called horizontal heterogeneity. According to Baum et al. (2008, p.2), "the model results are very sensitive to the initial conditions, particularly the steady component of the flow field and initial groundwater table depth". Figure 3.4 represents the components of the TRIGRS model in which, during a rainfall event, infiltration and surface run-off happen simultaneously. There is an increase in the groundwater table and, consequently, an increase in pore-water pressure.

Figure 3.4. Representation of how the TRIGRS model calculates the variation of the Factor of Safety, based on the rainfall infiltration in soil layers and the groundwater table variation.

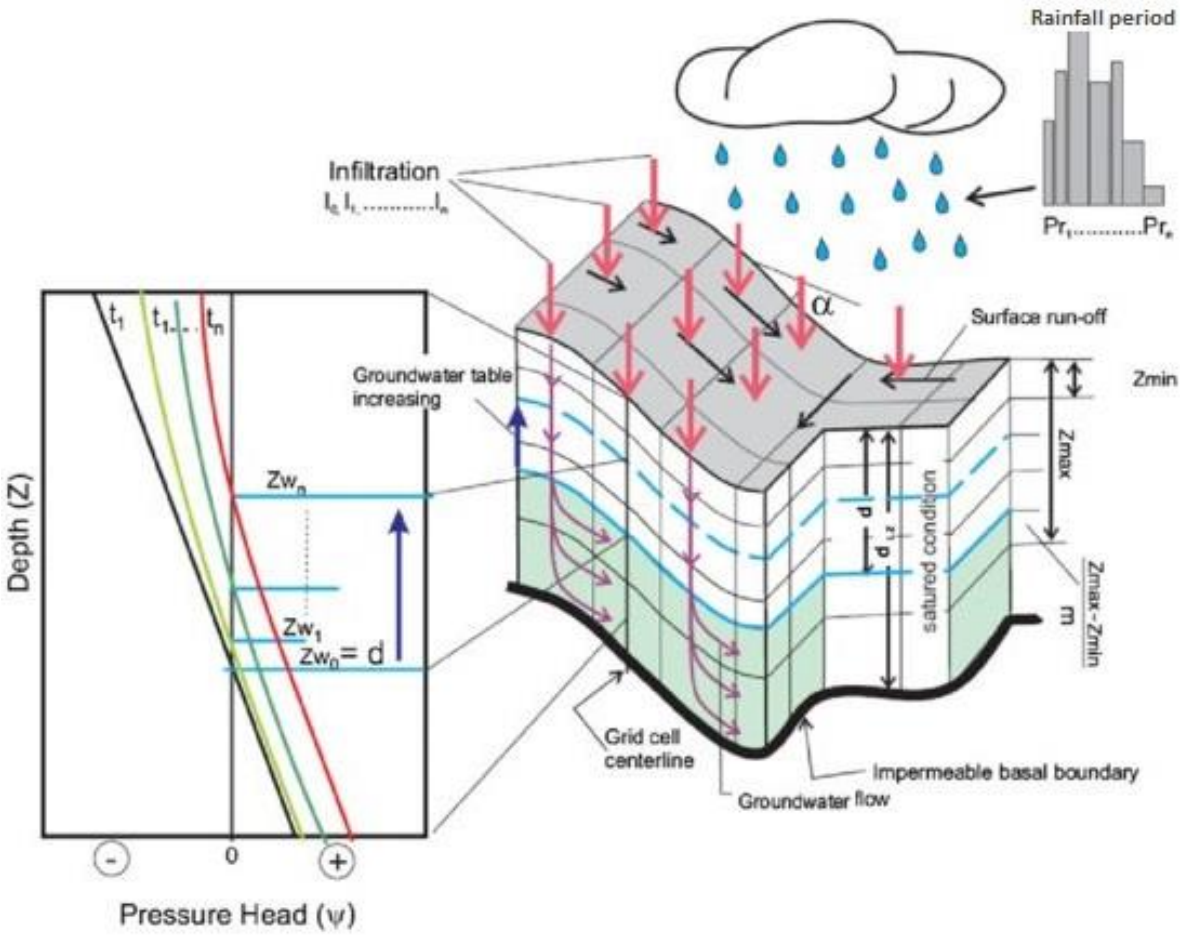

Source: Adapted from Grelle et al. (2014).

3.6 SINMAP

Sinmap is a probabilistic model based upon the steady-state hydrologic concepts with the infinite slope stability model, "that balances the destabilizing components of gravity and the restoring components of friction and cohesion on failures plane parallel to the ground surface" (PACK et al., 1998, p. 1). The approach is appropriated to determine slope instability due to shallow translational landsliding phenomena.

It obtains the input information, such as slope and specific catchment area, from a digital elevation model (DEM). According to Pack et. al., (1998) the soil thickness is constant

and measured perpendicular to the slope. The transmissivity is also constant. This model considers the real uncertainties about the estimation of the other input parameters. It accepts values for upper and lower bounds, using a uniform distribution. Therefore, the model requires the calibration regions, which are sub-samples of the study area based on the difference between soil, vegetation, or geological data (PACK, 1998; MEISINA; SCARABELLI, 2007; MICHEL; et. al., 2012, 2014; ZIZIOLI et al., 2013; THIEBES et al., 2016; CARDOZO; et. al., 2018).

The input parameters are the lower and upper bound of T/R (ratio of transmissivity to the effective recharge), cohesion, and internal friction angle. The output of Sinmap is a Stability Index (SI) defined as the probability of the location being stable, ranging from 0, most unstable, to 1, stable, as presented in Table 3.4.

The term "Lower threshold" refers to regions with a failure probability above 50%, while "Upper threshold" means the probability of failure below 50%. The "Defended slope zone" refers to areas where, according to SINMAP, are unstable no matter the parameter range specified, or the model is unable to compute stability. An example is bedrock outcrop areas and deep-seated instability such as earth flows and rotational slumps.

According to the Sinmap approach, the Factor of Safety (FS) is calculated when the most conservative set of parameters still results in stable areas, and they are usually represented by values greater than 1. Equation 3.3 presents the FS formula.

$$\boldsymbol{FS} = \frac{\{\boldsymbol{Cr}+\boldsymbol{Cs}+\boldsymbol{cos2\theta}[\boldsymbol{\rho_s}\ \boldsymbol{g}(\boldsymbol{D}-\boldsymbol{Dw})+(\boldsymbol{\rho_s}\ \boldsymbol{g}-\boldsymbol{\rho_w}\ \boldsymbol{g})\boldsymbol{Dw}]\boldsymbol{tan\phi}\}}{\boldsymbol{D}\ \boldsymbol{\rho_s}\ \boldsymbol{g}\ \boldsymbol{sin\theta cos\theta}} \tag{3.3}$$

Where *Cr* is root cohesion [N/m²]; *Cs* is soil cohesion [N/m²]; θ is slope angle; *ρs* is wet soil density [kg/m³]; *ρw* is the density of water [kg/m³]; *g* is gravitational acceleration [9.81 m/s²]; *D* the vertical soil depth [m]; *Dw* the vertical height of the water table within the soil layer [m] and; ϕ the internal friction angle of the soil [degrees]. The slope angle θ is the arc tangent of the slope; S is expressed as a decimal drop per unit of horizontal distance (PACK et. al., 1998). The model computes the slope and wetness at each grid point assuming the constant distribution of parameters over the study area.

Table 3.4. Sinmap Stability Index.

Condition	Predicted state	Parameter range	The possible influence of factors not modeled
SI > 1.5	Stable slope zone	The range cannot model instability	Significant destabilizing factors are required for instability
1.5 > SI > 1.25	Moderately stable zone	The range cannot model instability	Moderate destabilizing factors are required for instability
1.25 > SI > 1.0	Quasi-stable slope zone	The range cannot model instability	Minor destabilizing factors could lead to instability
1.0 > SI > 0.5	Lower threshold slope zone	Pessimistic half of the range required for instability	Destabilizing factors are not required for instability
0.5 > SI > 0.0	Upper threshold slope zone	Optimistic half of range required for stability	Stabilizing factors may be responsible for the stability
0.0 > SI	Defended slope zone	The range cannot model stability	Stabilizing factors are required for stability

Source: Pack et. al. (1998).

3.7 Literature review

3.7.1 SINMAP

The probabilistic model SINMAP has been widely used to identify landslide-prone areas. Cardozo; et al., (2018) used the Sinmap to study the municipality of Nova Friburgo, Brazil, located in the mountainous area of Serra do Mar. It is a steep slope area with a declivity ranging from 15º to more than 35º degrees. The data consisted of a 10-meter DEM, a landslide scars inventory produced based on GeoEye-1 satellite data, and soil parameters acquired from the literature. Considering the geotechnical parameters' uncertainty, the authors simulated three scenarios, changing the range of the cohesion and internal friction angle. As a result, the model provides excellent results and successfully identified 90% of the landslides (55% within the unstable zones, and 35% in areas with critical conditions for soil rupture). However, the authors claim that geotechnical and hydraulic parameters performed in situ and tested in laboratories would provide more accurate results.

A similar approach was applied by Pechincha and Zaidan (2015). The authors determined the landslide-prone areas in the Córrego Matirumbide watershed, Juiz de Fora, Brazil. The

area has clayish soils, an annual average rainfall of 1300 mm, and unauthorized human settlement on steep slope areas. A DEM with 1 meter of spatial resolution, extracted from LiDAR images, was used as input. The geotechnical data were acquired from the literature, and a landslide scars inventory was prepared during the field survey. As a result, the instability area identified by SINMAP was validated with the presence of landslide scars. The authors verified a correlation between most of the unstable areas and their location in the steepest slope areas, with human settlement. The model proved its efficacy for the identification of landslide-prone areas.

Similar results were acquired by Nery and Vieira (2015), which used the SINMAP model to identify the unstable areas in the Ultrafertil watershed, in Cubatão, Brazil. The area, located in the Serra do Mar mountains, has declivities ranging from 30º to 50º degrees. Input data were geotechnical and hydrological parameters acquired from the literature. A 2-meter of spatial resolution Digital Terrain Model was used. The landslide inventory was elaborated based on aerial orthophotos from 1985, the year when more than a thousand landslides were registered. Three scenarios were proposed to analyze the sensitivity of each parameter in slope stability. The model correctly identified 90% of the landslides in unstable areas. The authors concluded that hydraulic parameters are the most sensitive ones regarding slope stability.

The SINMAP model proved to correctly identify landslide-prone areas when applied on different terrains and lithologies. Thiebes et al., (2016) applied the SINMAP model in two different study areas: Swabian Alb, Germany, and Wudu County, China. The lithology of the area in Germany is characterized by clay soil underlying marl and limestone. The slopes are covered by debris from previous landslides, usually triggered by rainfall, snow melting, and earthquakes. A small town, named Eningen, is in the study area. The input data were a DEM with 1 meter of spatial resolution, geotechnical parameters acquired from the literature, a landslide inventory extracted from LiDAR images, and field mapping. As a result, 8% of the study areas were classified as unstable, and the model correctly identified 80% of the landslides. The high quality of topographic data led to excellent results.

The lithology from the Chinese study area is characterized by slates, schist, and loess deposits, and it is predominantly used for agriculture. The landslides are usually triggered

by rainfall, especially during summer, and by tectonic activity. The input data used was a 30-meters spatial resolution DEM, geotechnical parameters acquired from laboratory tests, and a landslide inventory prepared from optical remote sensing data. As a result, 22.6% of the area was classified as unstable, and 67.5% of landslides were correctly mapped. The low resolution of topographic data justified the relatively poor results for Wudu.

A volcanic area usually suffers from landslides and monitoring the slope stability helps disaster management. Therefore, Deb and El-Kadi, (2009) applied the SINMAP model in Oahu – Hawaii, USA. The geology of the study area is the result of volcanism. It has steep slopes areas with declivities above 80º and a colluvial layer on the slopes formed from weathered basalt. The annual precipitation ranges from 650 mm to 700 mm (DEB; EL-KADI, 2009). The topographic characteristics of the study area might generate flash floods. A landslide inventory was prepared using aerial photography, hydrological and geotechnical parameters were acquired from the Soil Survey Geographic (SSURGO) database and literature. A 10-meter DEM was used as input da-ta. Four calibration regions were chosen, according to geological, geomorphological, and land-cover characteristics. As a result, the SINMAP correctly identified all the landslides within the most unstable classes. The model classified 18% of the study area as very high susceptibility, and 21% as high susceptibility. The authors also compare the SINMAP results with the debris-flow-hazards maps and realized that the model can be used as a tool to identify both hazard types.

Pack et. al. (1998) applied the SINMAP in the Kimpala drainage, British Columbia, Canada. The soils are characterized by coarse granular tills and colluvium derived from basaltic bedrock. They used a DEM with 10-meters of spatial resolution and a landslide inventory acquired from the government. The model correctly identified 69.2% of the landslides. The authors agree that the combination of aerial photos and field mapping would improve the model results.

The previous studies show that the probabilistic model acquired good results to identify landslide-prone areas in regions with different geological characteristics. Moreover, the quality of input data has a significant impact on the SINMAP results. A summary of studies using SINMAP is presented in Table 3.5.

Table 3.5**.** Summary of SINMAP literature review.

Author	Study Area	Triggered Mechanism	Acquisition data	Validation	Results
(CARDOZO; LOPES; MONTEIRO, 2018)	Nova Friburgo, Brazil	Rainfall	Literature	Landslides inventory	55% landslides in unstable areas
(PECHINCHA; ZAIDAN, 2015)	Juiz de Fora, Brazil	Rainfall	Literature	Landslides inventory and Susceptibility maps	78,5%landslides in unstable areas
(NERY; VIEIRA, 2015)	Cubatão, Brazil	Rainfall	Literature	Landslides inventory	90% landslides in unstable areas
(THIEBES et al., 2016)	Swabian Alb, Germany	Rainfall, Snow melting, Earthquakes	Literature	Sensitivity analysis	80% landslides in unstable areas
	Wudu county, China	Rainfall and Earthquakes	Laboratory tests	Sensitivity analysis	67,5% landslides in unstable areas
(DEB; EL-KADI, 2009)	Oahu, Hawaii, USA	Rainfall and Volcanism	Literature	Landslides inventory and Susceptibility maps	92% landslides in unstable areas
PACK et al., (1998)	British Columbia, Canada	Rainfall	Literature	Landslides inventory	69.2% landslides in unstable areas

3.7.2 TRIGRS

Several studies have used TRIGRS to identify slope stability. Godt et al. (2008) applied the TRIGRS model in the steep coastal bluff of Puget Lowland, north of Seattle, USA. The hydraulic and geotechnical data were collected in situ and tested in a laboratory, and the landslide inventory was prepared from aerial photography. As a result, the model tends to underpredict the spatial extent of landslides for this study area.

On the other hand, Chien-Yuan et al. (2005) had excellent results applying the TRIGRS model in Tenliao Mountain, the northern part of Taipei County, Taiwan. The geotechnical and hydrological parameters were acquired during fieldwork. Soil samples were collected and analyzed in a laboratory to provide the input parameters. However, the analysis's initial condition consists of saturated soil due to more than 500 mm of rain in the previous days. The rainfall infiltration and the soil moisture had a significant impact on triggering landslides and debris flow.

Tan et al. (2008) investigated the landslide-prone areas in the Ta-Chia River watershed, in Taiwan. Due to the difficulty in acquiring soil samples, this research assumed that the soil´s geotechnical properties are strongly related to geology and used these values as input to the TRIGRS model. As a result, the model underestimated the unstable zone compared with the landslide occurrences. The results might be related to the initial conditions: differences in the initial groundwater table and the soil layer´s shear strength. These results show how the model results can be very sensitive to the initial conditions (BAUM; et. al., 2008).

The quality and accuracy of the input parameters allowed TRIGRS to provide better results. Listo and Vieira (2015) compared the TRIGRS performance in two scenarios: first using geotechnical and hydrological parameters collected in situ, and in the second scenario, data were acquired from the literature. The study area was the Guaxinduba River watershed, in the municipality of Caraguatatuba, Brazil. The results were validated using landslides inventory and statistical analysis, such as Scar Concentration (SC), Landslide Potential (LP), and Probability of Detection – POD. The authors concluded that the first scenario had better results than the second one.

Related results are presented in the research conducted by Park et al. (2013), who applied the TRIGRS model in Woomyeon Mountain, South Korea. Geological investigations were conducted by governmental institutions, providing accurate geotechnical and hydrological parameters for the area. This data was used as input, and the results corroborated the reality: TRIGRS classified the areas with landslide scars as unstable. The input parameter's accuracy contributed to TRIGRS's excellent results.

The most typical application of TRIGRS models is to identify landslide-prone areas and validate the results using a landslide inventory. Statistical analysis, such as the Receiver Operating Curve (ROC) analysis, quantitative indexes (Scar Concentration – SC and Landslides Potential – LP; Probability of Detection – POD, False Alarm Ratio - FAR, Critical Success Index – CSI, and Success-Error index (SI and EI) also help to assess the performance and reliability of the model.

To exemplify, Paul et al. (2018) identified the landslide-prone areas in Rio do Sul, Brazil, using the TRIGRS model. The geotechnical and hydrological parameters were acquired in situ. A rainfall series of 2011 events were used as input. Statistical indexes, such as

Success Index (SI) and Error Index (EI), were used to validate the results. Past landslide events have been used to evaluate the model's efficiency, and the results were accurate. Related studies were presented by Listo (2016); Schwarz and Michel (2016); Marín et al. (2018); García-Aristizábal et al. (2019) and Ciurleo et. al. (2019).

The mathematical model has proven to be an appropriate tool to identify landslide-prone areas, and Listo et al. (2018) decided to analyze the models' capability to identify the surface rupture depth. TRIGRS was applied in Caraguatatuba, Brazil, to analyze the FS variation in different soil depths. The geotechnical and hydrological parameters were acquired in situ, and a landslide inventory from the 1967 event was prepared to validate the results. Statistical analysis, such as Scar Concentration (SC), Landslide Potential (LP), and Probability of Detection – POD, was used to validate the results. The model identified areas between 2 and 2,5 m depth with FS<1, which corroborate the surface ruptures from the 1967 landslides. Therefore, the TRIGRS model correctly identified the most unstable areas and the depth of surface rupture.

Marín and Salas (2017) evaluated the influence of vegetation in landslide susceptibility analysis. They applied a model for the prediction of rainfall interception in forest canopies. The results of real rainfall infiltration were used in TRIGRS as initial soil moisture input to calculate the FS. The results show that areas without vegetation tend to be more unstable than those with arboreal cover. However, the authors agreed that tree roots and specific weight might have more influence on slope stability than rainfall interception, thus, future studies are necessary.

Some studies evaluate how TRIGRS predicted slope stability during rainfall events, as shown in Liao et al. (2011). This study tested if the TRIGRS model could predict the most unstable areas during hurricane Ivan. The geotechnical parameters were extracted from the State Soil Geographic, which mapped the soil in the USA, and the River Forecast Center provided hourly rainfall data from Ivan'. The initial conditions of analysis consisted of a saturated soil layer due to the passage of hurricane Frances a week earlier. As a result, the model could predict almost 98% of the landslides, proving to be a useful tool for early warning systems of landslides events. The input parameters were very accurate, which provide even more precise results.

Similar results were presented by Zhuang et al. (2017), which analyzed the TRIGRS performance during a 24-hour rainfall in Yan'an, China. As a result, the model generates four slope stability maps, corresponding to 6:00, 12:00, 18:00, and 24:00 hours. TRIGRS predicted how the total amount of unstable areas (FS<1) scaled with increased rainfall duration. At the beginning of rainfall (6:00), the areas with FS< 1 represented just 0.2% of the total area. As time passed, the area increased to 3.3%, 3.8%, and 5.1%, respectively. A summary of studies using TRIGRS is presented in Table 3.6.

Table 3.6. Summary of research on TRIGRS.

Authors	**Study Area**	**Triggered Mechanism**	**Acquisition data**	**Validation**	**Results**
Godt et al., (2008)	Seattle - USA	Rainfall	Laboratory tests	ROC analysis	80% landslides in unstable areas
Chien-Yuan et al., (2005)	Taipei County -Taiwan	Rainfall	Laboratory tests	Landslides inventory and Variation of pore-water pressure	Variation of pore-water pressure changes the soil rupture mechanism
Tan et al., (2008)	Tai Chi - Taiwan	Rainfall and Typhoon	Literature	Landslides inventory and Typhoon data	Landslides and unstable areas agree with typhoon trajectory
Liao et al., (2011)	Macon County, North Carolina, USA	Rainfall and Hurricane	Literature	POD/FAR/CSI	98% landslides in unstable areas
Park et al., (2013)	Woomyeon Mountain, Seoul - South Korea	Rainfall	Literature and Laboratory tests	ROC analysis, SI/EI, SC/LP, POD/FAR/CSI	33% landslides in unstable areas
Zhuang et al., (2017)	Yan'an - China	Rainfall	Literature and Laboratory tests	Landslides inventory and ROC analysis	Several landslides registered in areas with FS<1
Listo and Vieira (2015)	Caraguatatuba - Brazil	Rainfall	Literature and Laboratory tests	Landslides inventory SC/LP/ POD	The parameters collected in situ have a better result

continue

Table 3.6. Conclusion.

Authors	Study Area	Triggered Mechanism	Acquisition data	Validation	Results
Listo (2016)	Caraguatatuba - Brazil	Rainfall	Literature and Laboratory tests	Landslides inventory SC/LP/ POD	70% of the study area has FS<1
Listo et al., (2018)	Caraguatatuba - Brazil	Rainfall	Laboratory tests	Landslides inventory SC/LP/ POD	Identification of surface rupture depth
Marín and Salas (2017)	Vale de Aburrá - Colombia	Rainfall and tree interception	Literature	Comparison among different scenarios	The rainfall interception has little influence on slope stability and further analysis are necessary
Paul et al., (2018)	Rio do Sul - Brazil	Rainfall	Laboratory tests	Landslide inventory, SI/EI	80,3% landslides in unstable areas
Marín et al.; (2018)	Copacabana - Colombia	Rainfall	Literature and Laboratory tests	Landslide inventory, ROC analysis	The identification of landslide-prone areas allows the calculation of vulnerability and risk
Schwarz and Michel (2016)	Ibirama - Brazil	Rainfall	Laboratory tests	Landslide inventory, SI/EI	50% of the landslides happened in areas with FS<1
García-Aristizábal et al., (2019)	Envigado - Colombia	Rainfall	Literature	Reliability analysis	1,05% of the area has FS< 1
Ciurleo et al., (2019).	Favazzina - Italy	Rainfall	Literature	Landslide inventory, SI/EI	Accuracy of 80% in the identification of landslide-prone areas

Each studied area had different geological and geomorphological aspects, proving that this model´s application is not limited to specific conditions. Several studies from all over the World were presented, including America (Brazil, Colombia, and EUA), Europe (Italy), and Asia (China, Taiwan, and South Korea). A few similarities should be highlighted: the landslides usually happened in the colluvial soil layer, and the most

unstable areas have declivities above 25º. Some geotechnical data were acquired from the literature, while others were measured in situ. There is an agreement that TRIGRS is very sensitive to the quality of input data, especially those related to the initial soil moisture content.

Notwithstanding, the best results were presented in the studies with the most precise geotechnical and hydrological parameters, which were usually measured in situ. The prevailing validation method used was a landslide inventory. Still, the statistical analyses also supported the results produced by TRIGRS.

Furthermore, the model proved to be a useful tool to identify landslide-prone areas and predict slope stability. Despite the excellent results from Liao et al. (2011) and Zhuang et al. (2017), more studies using TRIGRS as a tool that predicts the most unstable areas during a rainfall event are necessary.

TRIGRS has the potential to become an early warning system, and the use of weather forecasts and soil moisture monitoring sensors might enhance its applicability. Knowing the soil moisture content of the area favors modeling the slope stability with higher accuracy. Furthermore, the weather forecast allows the preparation of slope stability scenarios, identifying the critical areas. Such information is essential for disaster prevention. Therefore, the governments can anticipate the landslide-prone areas related to the actual rainfall event and act in preventive removal of the population at risk.

This project aims to test TRIGRS as a tool for early warning systems, using weather forecasts from the Climatempo website (https://www.Climatempo.com.br/) and sensor-based soil moisture information from CEMADEN. Moreover, a risk alert can be defined based on the variation of FS, which is different from the critical rainfall threshold currently in use for alerts. An early warning system based on FS will be provided using the TRIGRS model. And the landslide-prone map produced will be compared with SINMAP results.

4. STUDY AREA

The study area of this work is the Vila Baiana neighborhood, within the municipality of Guarujá, located within the Brazilian southeastern State of Sao Paulo, as presented in Figure 4.1.

Figure 4.1. Study area location.

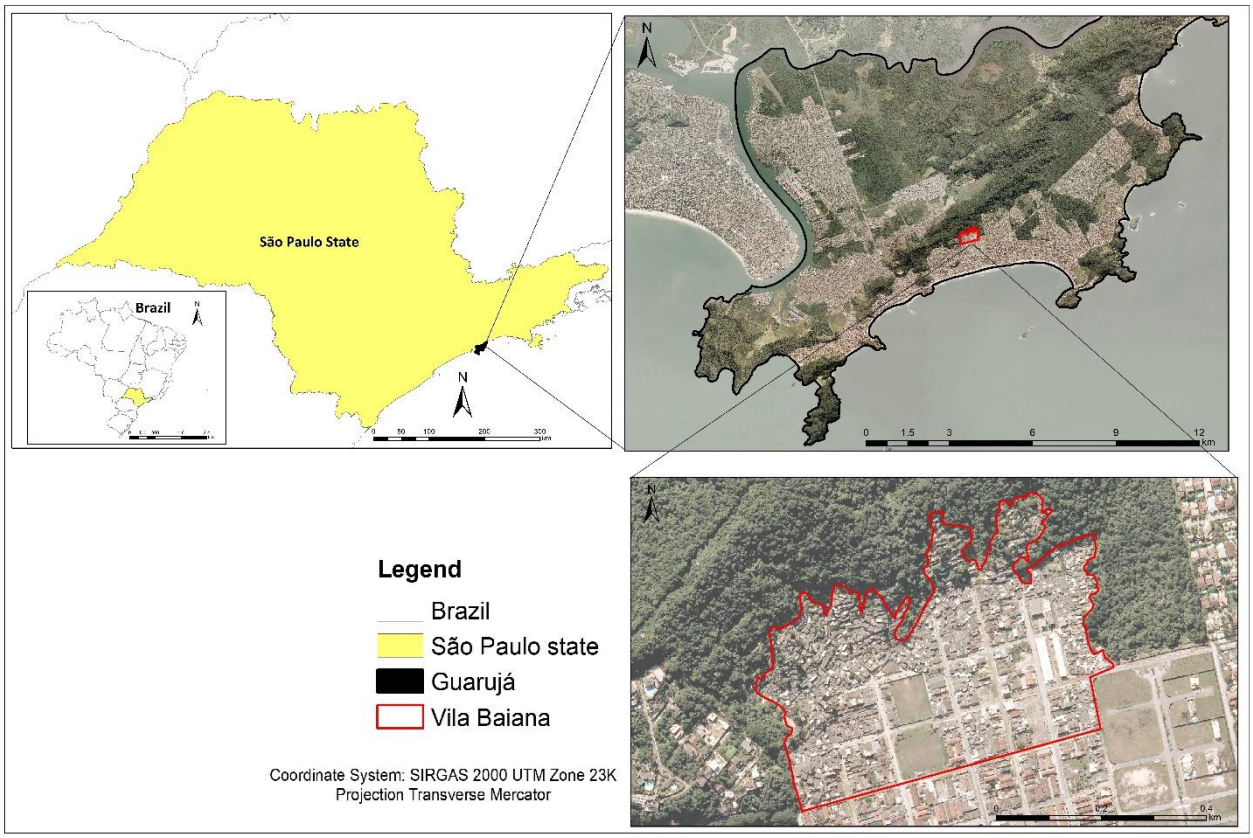

According to IBGE (2019), the municipality has 320,459 inhabitants and a territorial extension of 144,794 km². The mean annual precipitation is 3,000 mm, and the mean annual temperature is 22ºC.

As for its geology, the area is on a crystalline plateau, with gneiss and granite from the Pre-Cambrian period. Tropical forests cover the area, and the coastal plain has quaternary coastal sediments of fluvial-marine origin. In some areas, the crystalline basement becomes apparent. Elevations may reach 150 m, such as Morro do Botelho (ARAKI et

al., 2001). There are four types of soil in Guarujá, classified according to the Brazilian Soil Classification System (SBCS): Haplic Cambisols, Humiluvic Spodosol[1], Gleysols[2], and Lithic Neosoils[3] (EMBRAPA, 2018), as presented in Figure 4.2.

Figure 4.2. Types of soils in Guarujá.

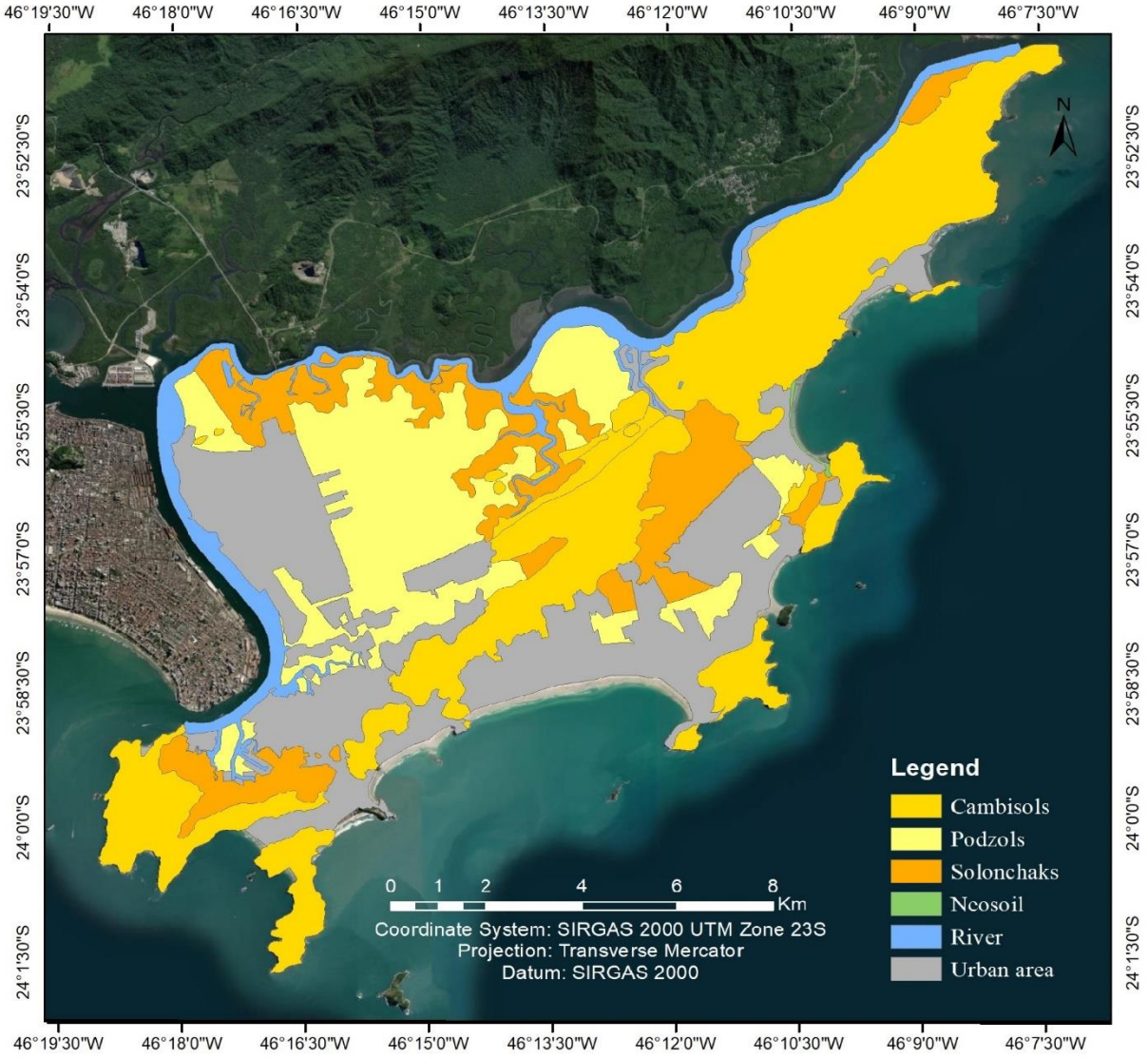

The Haplic Cambisols is a developed soil composed of mineral material and characterized by an incipient B horizon. There is a predominance of clay texture and an aluminic

[1] Humiluvic Spodosols are classified as Podzols by World Reference Base for Soil Resources (WRB), recognized by International Union of Soil Science (IUSS). More information: <<http://www.fao.org/3/a-i3794e.pdf>.
[2] Gleysols are classified as Solonchaks by World Reference Base for Soil Resources (WRB), recognized by International Union of Soil Science (IUSS). More information: <<http://www.fao.org/3/a-i3794e.pdf>.
[3] Lithic Neosoils are classified as Leptosols by World Reference Base for Soil Resources (WRB), recognized by International Union of Soil Science (IUSS). More information: <<http://www.fao.org/3/a-i3794e.pdf>.

qualifier (EMBRAPA, 2018). The Humiluvic Spodosol is soil with mineral compound and a spodic B horizon with 200 cm depth. Spodic B horizon is a subsurface horizon, with 2,5 cm depth, with the presence of organic matter and aluminum (Al). Iron (Fe) can be found as well (EMBRAPA, 2018). The Gleysols have a "Gley" horizon in the upper 50 cm. A Gley horizon is a mineral layer, characterized by the losses of Iron (Fe) due to the presence of water; is a saturated soil horizon (EMBRAPA, 2018). The Lithic Neosoils are characterized as poorly developed soils (20 cm thick), without a B horizon. It is composed of mineral or organic material. The A horizon is directly in contact with the C horizon or the rock and presents coarse fragments such as quartz gravel bed, gravel, pebbles, and boulders (EMBRAPA, 2018).

The urban occupation started in flat and mangrove areas. However, the city has experienced considerable population growth since the 1950s, intensified in the 1970s, with the economic development due to industries, port-related activities, civil constructions, and tourism. Consequently, the price of land increased sharply, and people with low income started to build their houses in steep areas, on cheap but improper terrain (ARAKI et al., 2001). Figure 4.3 presents the population growth from 1980 to 2020.

Figure 4.3. Population growth from 1980 to 2020.

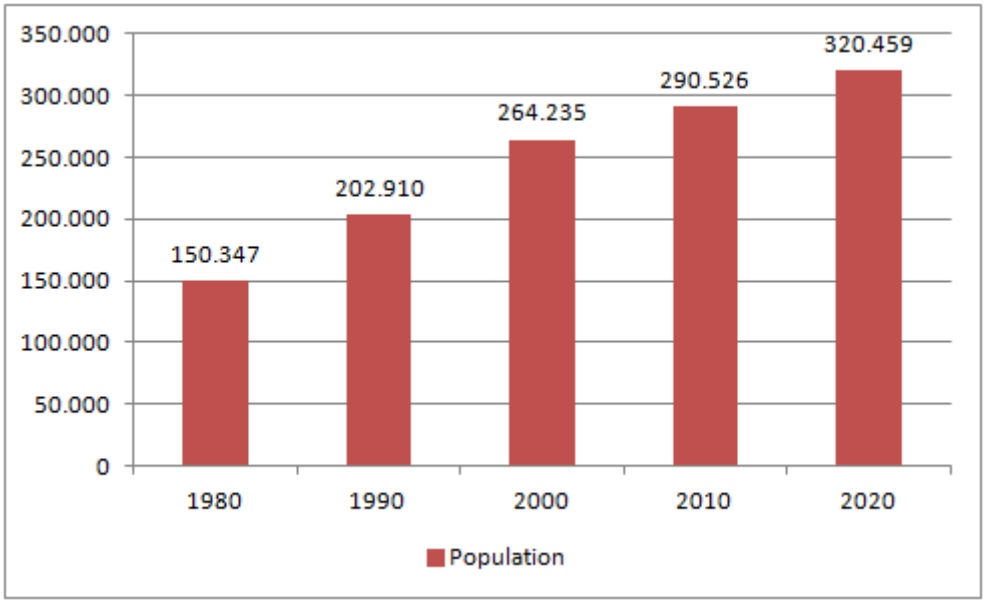

Source: Adapted from SEADE (2020).

The Guarujá municipality presents several registered landslide occurrences. According to COMPDEC-Guarujá data, from 1991 to 2019, February is the month with the most landslide records, totalizing 292 events.

Vila Baiana neighborhood is one of the most landslide-susceptible areas, followed by Morro da Cachoeira and Morro do Engenho (COMPDEC-Guarujá). Table 4.1 presents the number of landslides per area, from 1991 to 2019.

Table 4.1. Landslide occurrences per risk area, from 1991 to 2019.

Risk areas	**Total number of occurrences (1991-2019)**
Vila Baiana	331
M. da Cachoeira	172
M. do Engenho	127
V. da Morte	62
M. Bela Vista	70

Source: Adapted from COMPDEC (2019).

Vila Baiana has a population of 10,835 inhabitants, equivalent to 3,7% of the Guarujá municipality population. The demographic density is 6442,88 inh./km², and on average there are 3,5 people per household (IBGE 2019). This population density in a landslide-prone area tends to enhance the order of magnitude of disasters in the area.

On March 3rd of 2020 after heavy rainfall, several landslides were registered. The most affected areas were Vila Baiana, Morro do Engenho, and Morro do Macaco Molhado. The impacts extended over 140 houses, causing structural damages and 33 deaths. The accumulated rainfall expected for that month was 263 mm. However, 320 mm of rainfall was recorded in 24 hours. The total amount of precipitation registered in only 24 hours was more than the expected volume for March (CEMADEN, 2020).

The recurrent disasters triggered by landslide events, associated with a large population density in risk areas, justify choosing Vila Baiana as the study area for this project.

5. MATERIALS AND METHODS

The materials used in this work were four Landsat satellite images of the study area, one orthophoto with a 1-meter resolution for the image classification of the Vila Baiana neighborhood, soil geotechnical parameters for modeling with TRIGRS and SINMAP, IPT susceptibility map, the landslide inventory from Guarujá Civil Defense, historical rainfall data acquired from DAEE, CEMADEN and weather forecast from Climatempo website. The software's used were ArcGIS, eCognition, and ENVI. Figure 5.1 presents the methodological workflow. The methods applied are further detailed.

The first part of the work is an investigation of the urban sprawl from Guarujá city, analyzing its influence on the increase of landslide-prone areas and disasters. Therefore, four images of Landsat satellites from the years 1990 (Landsat 5), 2013 (Landsat 8), 2020 (Landsat 8), and 2021 (Landsat 8) were acquired and preprocessed. To improve the understanding of land use and occupation and how they influenced landslide disasters, a detailed classification of Vila Baiana, which frequently suffers from landslides, was provided. Using an orthophoto with 1-meter of spatial resolution and eCognition software, the Vila Baiana neighborhood was classified accordingly to the types of soil covers (ceramic roof, concrete roof, vegetation).

The satellite images were pre-processed, which consisted of two steps: pansharpening and orthorectification. Both processes were performed using ArcGIS and ENVI software. The orthorectification corrects distortions in the images caused by topographical variation between the terrain and the sensor's position. It was carried out using the 2021 image from Landsat 8 as a reference. The pansharpening operation provided an image with the best spatial resolution from the panchromatic band while retaining the spectral content from the multispectral bands. This study used imagens from both Landsat 5 and 8, however, Landsat 5 images do not have a panchromatic band, therefore, the pansharpening process was only performed for Landsat 8 images. To better understand the pansharpening procedure, an example is presented in Figure 5.2.

Figure 5.1. Methodological workflow.

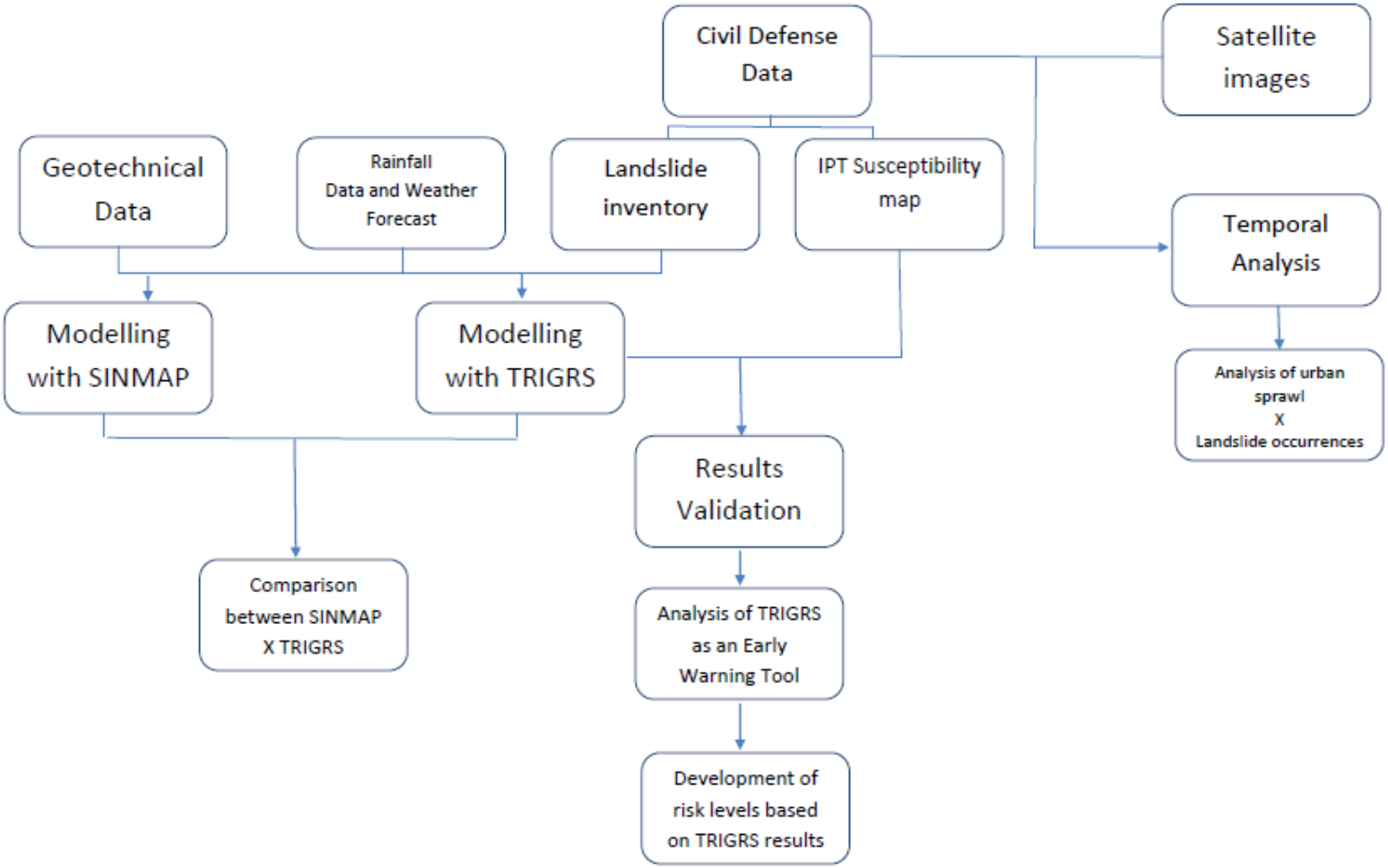

Figure 5.2. Example of pansharpening procedure using Gram-Schmidt method with IKONOS image: a) panchromatic band, b) multispectral band and c) pansharpened image.

Source: Adapted from König (2018).

Figure 5.2 presents the panchromatic and multispectral bands from the IKONOS sensor and the pansharpening result using the Gram-Schmidt method. Figure 5.2a represents the panchromatic band, which has the best spatial resolution. The multispectral bands, presented in Figure 5.2b, have the best spectral resolution. The pansharpening process was performed using the Gram-Schmidt method, and the result is shown in Figure 5.2c.

The next step consisted of the segmentation procedure (Figure 5.3), which helps the classifier algorithm to better discriminate the boundaries of targets (also known as objects) (e.g., vegetation, houses, buildings, roads, rivers, among others).

Figure 5.3a presents the pansharpened image, and Figure 5.3b shows the segmentation procedure. The segments divided the image into adjacent regions, named Objects, such as roads and trees. Object samples are then collected from the segmented image (Figure

5.4). The samples were input to data mining algorithms and based on the available attributes, automatically identified patterns from these large data volumes.

Figure 5.3. Example of Segmentation procedure.

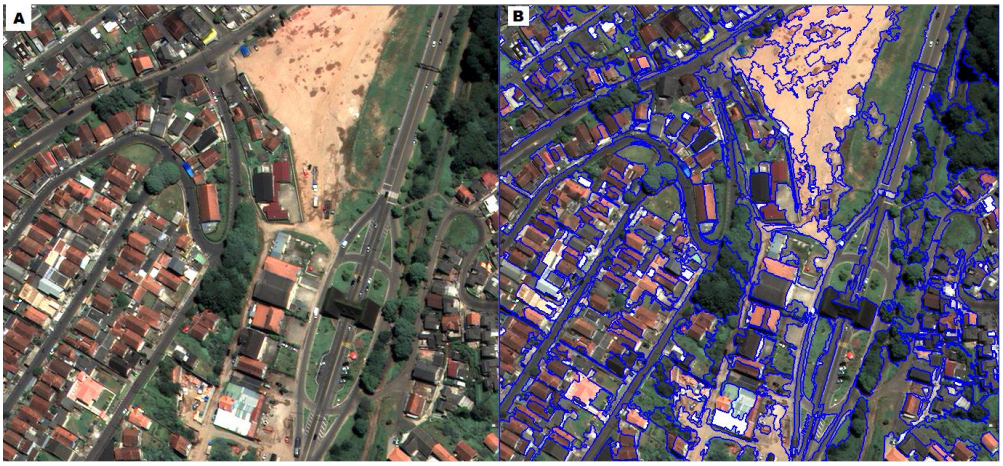

Source: Adapted from König (2018).

Figure 5.4. Representation of sample collection.

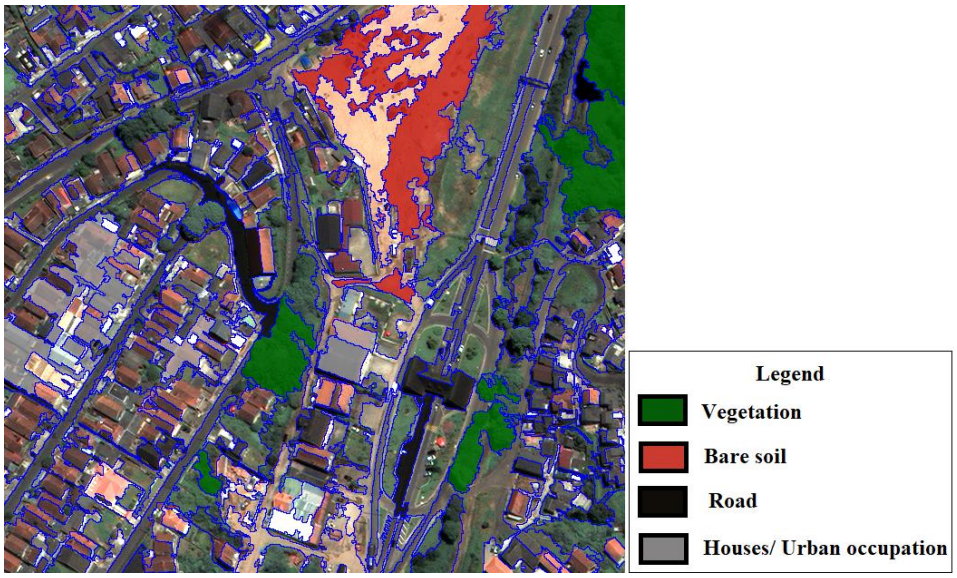

Source: Adapted from König (2018).

The algorithm Classification and Regression Trees - CART, implemented by the eCognition software, was used to extract the most relevant attributes, generating a

decision tree. Based on this decision tree, the images were classified using the Object-based Image Analysis (OBIA) paradigm (KÖNIG et al., 2019). The OBIA paradigm extracts semi-supervised information from satellite images. It clusters similar objects, considering the pixel information and its neighbors (HAY; CASTILLA, 2006; DRONOVA, 2015). The error matrix was calculated to assess the classification accuracy, and to determine the global accuracy. Notwithstanding, the NDVI (Normalized Difference Vegetation Index) was calculated, to determine the environmental degradation.

A temporal study was conducted to verify how the urban expansion from 1990 to 2020 affected the area, comparing the four satellite image classifications. The central queries solved were: Was there an increase in the number of people living in steep slope areas? Did the number of landslides also increase in these areas? Is it possible to link urban sprawl and landslide disasters? Is there a correlation between the irregular occupation of slope areas, precipitation, and landslide events?

This study compared the urban sprawl with the number of landslide events from 1990 to 2020 and analyzed if anthropic changes in steep slope areas have been fostering landslides, or otherwise if there was an increase in extreme rainfall events.

Historical rainfall data from 1991 to 2020, acquired from DAEE, were used to determine if there was a correlation between rainfall events and landslide occurrences. The analysis of topographic and lithological aspects correlated with landslides was conducted to verify how Guarujá geology influences the landslide distribution. Such analysis helps to identify the most critical landslide-triggering factors to support decision-making for urban planning and management.

The next step consisted in modelling the landslide-prone areas using the mathematical models TRIGRS and SINMAP. These data are the input for modelling landslide-prone areas.

The historical rainfall data was acquired from the DAEE website and applied to determine the correlation between rainfall events and landslide occurrences. Using rainfall data from March 3^{rd,} 2020, and July 1^{st,} 2022, the model TRIGRS was calibrated, and its applicability was verified. As a result, the model generates a landslide-prone map of Vila Baiana. The validation was based on the landslides inventory, prepared with satellite

images and landslides documented by the Guarujá Civil Defense, and comparing the unstable areas from TRIGRS with the IPT susceptibility map.

Furthermore, an automated early warning system was developed using the TRIGRS model as its engine. After the geotechnical parameters were established, a Python script acquired the rainfall data (weather forecast) from Climatempo's public API (Application Programming Interface) and simulated the stability scenarios using TRIGRS. The rain values from Climatempo are shown in millimeters per hour (mm/h), while TRIGRS uses meters per second as a unit. Therefore, the rainfall values are converted to the units used in the mathematical model. The following step is to define and set TRIGRS configuration parameters for 3 days of rain forecast. The model is executed, creating the three maps of FS for 24h, 48h, and 72h. To quantify the FS variation, the program calculates the sum of the FS values of the area for each timeframe. An alert was displayed based on the variation of the Factor of Safety (FS). This product is relevant for Civil Defenses, which predicts the most unstable areas for the preventive removal of the affected population.

The same input data used in TRIGRS was used in the SINMAP model to produce another susceptibility map. The distinct methodologies might generate different results. The reliability of both models was evaluated through the Contingency table, Success and Error Index (SI/EI index). Therefore, a discussion about these approaches and their influence on the susceptibility maps was conducted in this work.

This study generated landslide-prone maps of Vila Baiana and Guarujá, produced using the mathematical model TRIGRS, with a thorough analysis of the landslide-triggering factors. Furthermore, an early warning system was developed, helping the Civil Defense to quickly identify unstable areas and act preventively to remove and safeguard the population at risk.

6. RESULTS AND DISCUSSIONS

6.1 Temporal analysis of urban expansion from 1990 to 2021

6.1.1 Pan-sharpening process

A pansharpening procedure was performed to acquire the best spectral and spatial characteristics. The Gram-Schmidt method was chosen because it provides the best distinction of objects (vegetation, urban area, sand/bare soil, water) in the scene for the Principal Components Analysis (PESCK; DISPERATI, 2011; POLIZEL et al., 2011; PU; LANDRY, 2012; MENEGHETTI; KUX, 2014). Figure 6.1, Figure 6.2, and Figure 6.3 present the results of the pansharpening process for the years 2013, 2020, and 2021.

Figure 6.1. Pansharpening process for 2013 image: a) multispectral band, b) panchromatic band, c) result of pansharpening.

Figure 6.2. Pansharpening process for 2020 image: a) multispectral band, b) panchromatic band, c) result of pansharpening.

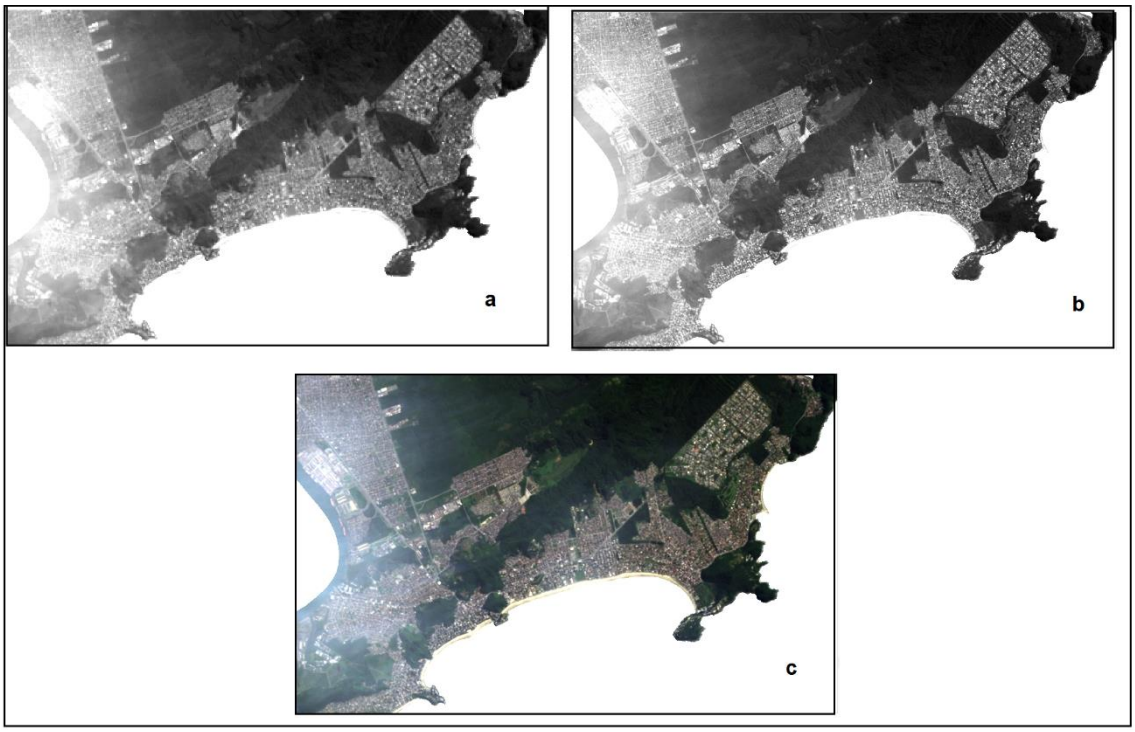

Figure 6.3. Pansharpening process for 2021 image: a) multispectral band, b) panchromatic band, c) result of pansharpening.

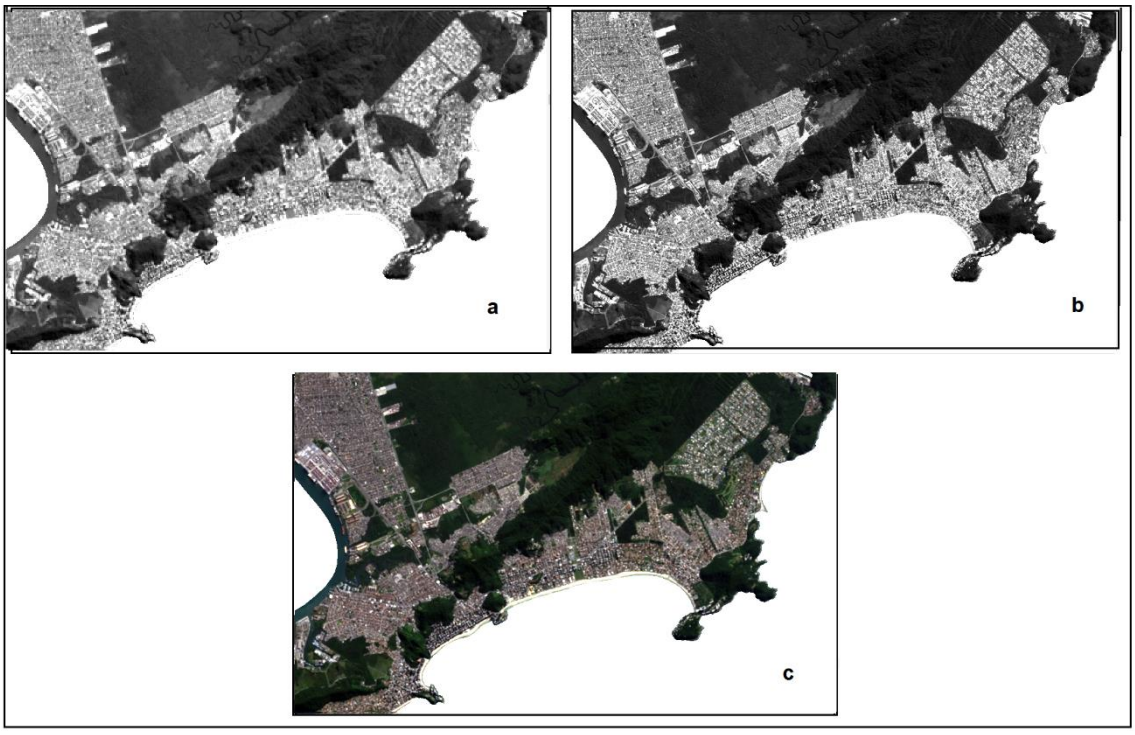

6.1.2 Segmentation, samples acquisition, and data mining

The image segmentation and the sample acquisition were performed using the eCognition software. The multiresolution segmentation was applied. The parameters used in the multiresolution segmentation procedure of the Landsat images are presented in Table 6.1. It is important to highlight that the values of shape and compactness vary from 0 to 1, indicating each parameter's weight in the segmentation process.

Table 6.1. Segmentation parameters applied in the satellite images.

Year	Satellite/Sensor	Scale	Shape	Compactness
1990	Landsat-5/ TM	50	0.1	0.5
2013	Landsat-8/OLI	350	0.1	0.5
2020	Landsat-8/OLI	300	0.1	0.5
2021	Landsat-8/OLI	300	0.1	0.5

The results of the segmentation process and sample acquisition for each satellite image are presented in Figure 6.4, Figure 6.5, Figure 6-6, and Figure 6.7.

Figure 6.4. Segmentation (a) and samples acquisition (b) from 1990 satellite images of Landsat-5.

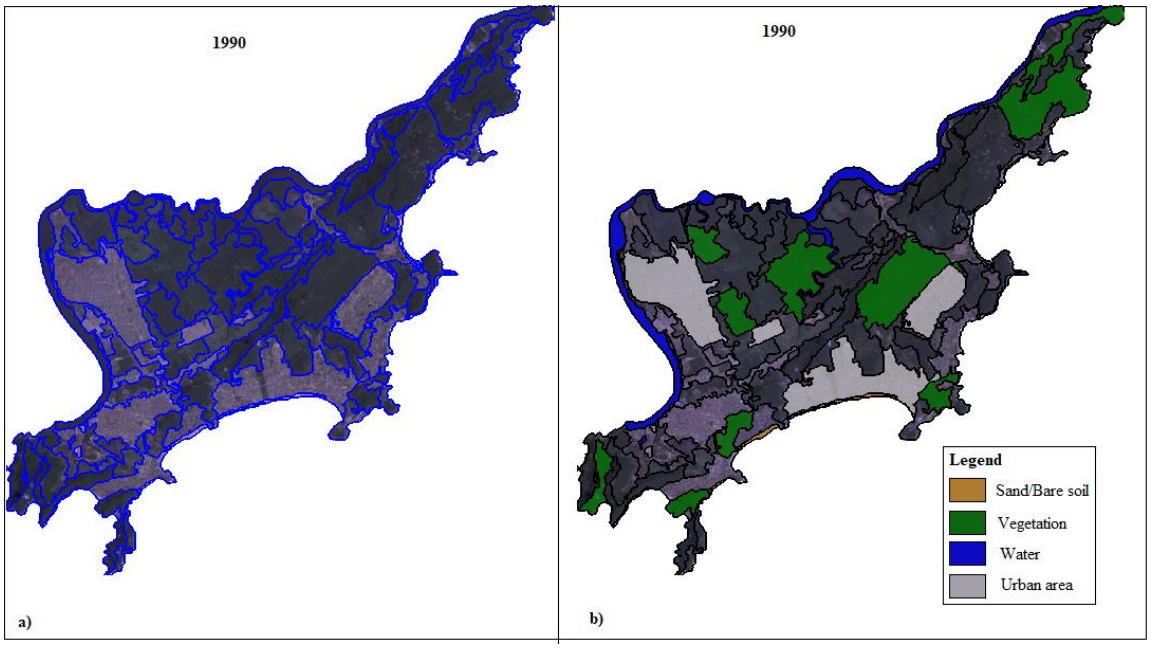

Figure 6.5. Segmentation (a) and samples acquisition (b) from 2013 satellite images of Landsat-8.

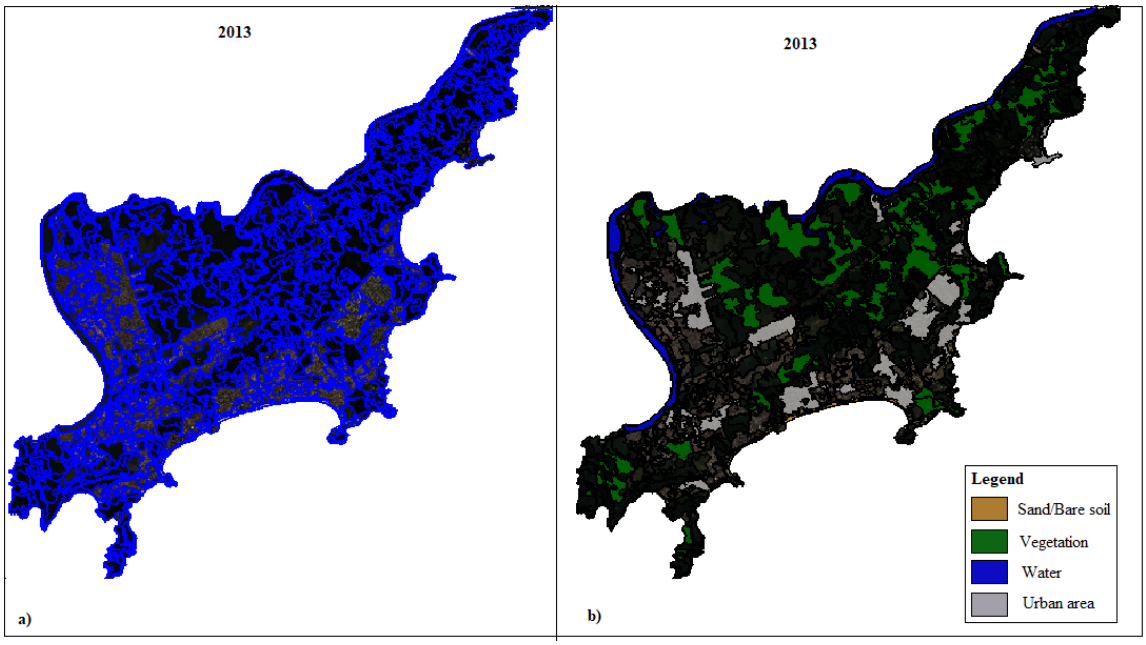

Figure 6.6. Segmentation (a) and samples acquisition (b) from 2020 satellite images of Landsat-8.

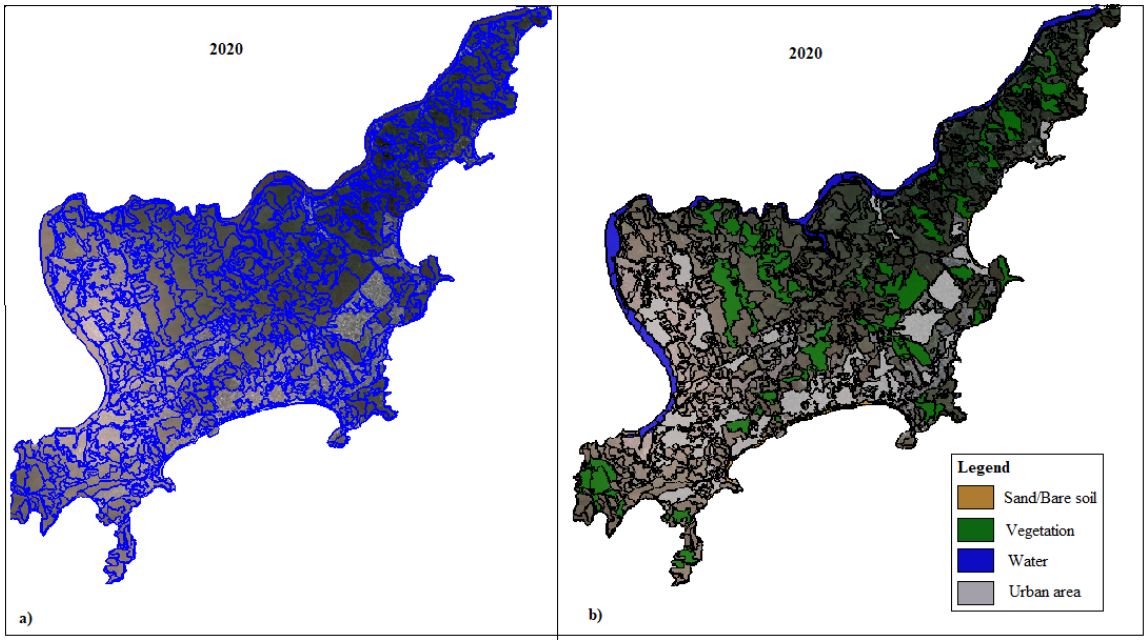

Figure 6.7. Segmentation (a) and samples acquisition (b) from 2021 satellite images of Landsat-8.

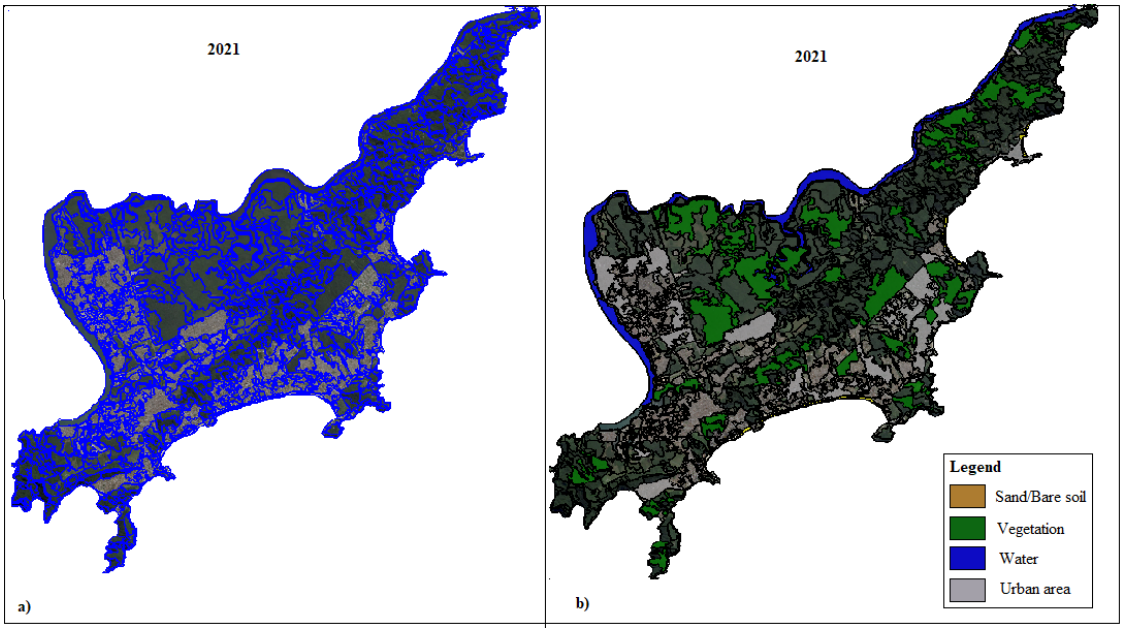

The Vila Baiana classification is characterized by different land covers, such as variable types of roofs, roads, and vegetation. An orthophoto with 1-meter of spatial resolution was used. Due to the different sizes of the objects in the scene, two segmentation levels were applied: level 1 to discriminate larger objects, such as blocks and streets, and level 2 to identify the types of roofs and vegetation cover. The first level consisted of the distinction between blocks and streets. A multiresolution segmentation was performed using a thematic layer considering the following parameters: scale 500, shape 0.9, and compactness 0.5 (Figure 6.8).

Figure 6.8. Segmentation (a) level 1 and classification (b) of blocks and roads.

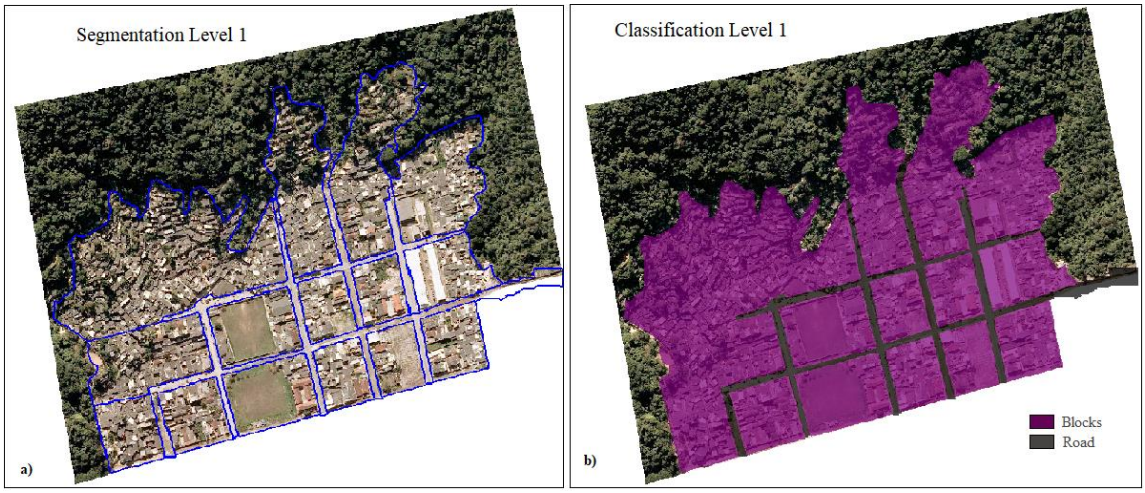

Following, the “elliptic fit” attribute was performed to identify if an object fits in an elliptic with similar proportions, in which 0 means that the object does not fit, and 1 that it fits. The block objects range from 0.6 to 0.8. Afterward, using the “assign class” algorithm, two threshold conditions were defined: objects >= 0.6 are assigned as blocks, and objects <= 0.1 are assigned as roads.

The second segmentation level is performed to identify smaller objects, such as types of roofs and vegetation cover. In segmentation level 2, the class Blocks was used as a filter, meaning that the segmentation procedure occurs only within the blocks. The multiresolution segmentation algorithm was applied, using the following parameters: scale 30, shape 0.1, and compactness 0.5. (Figure 6.9).

Figure 6.9. Multiresolution segmentation Level 2.

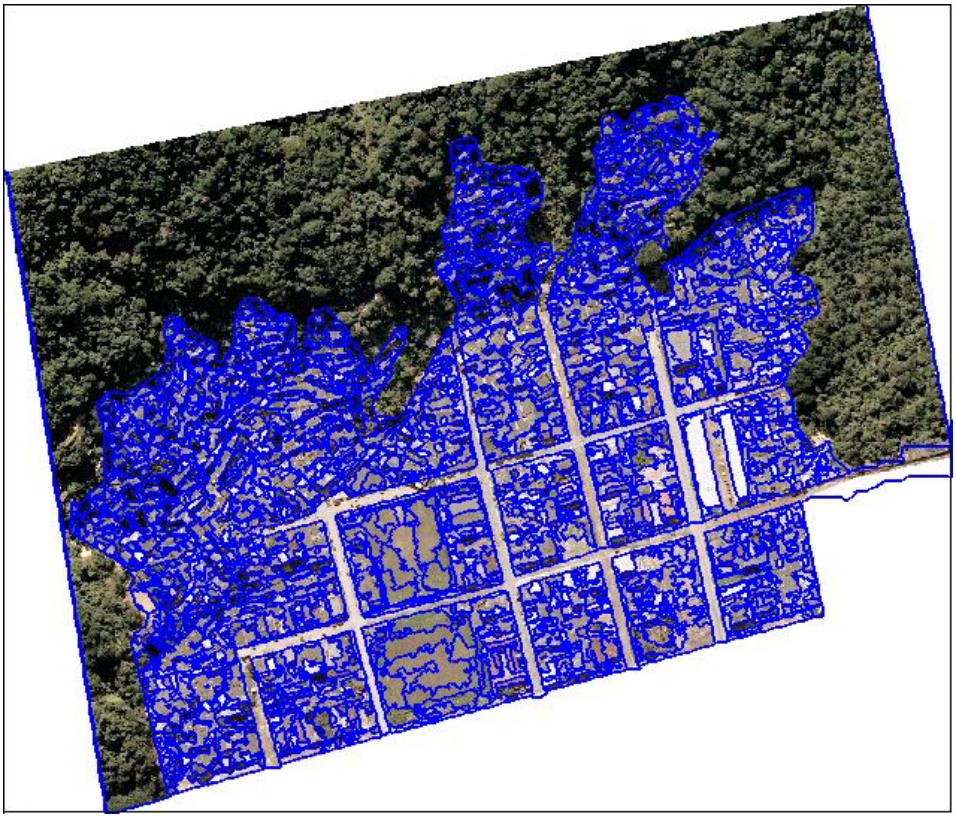

The last step before the classification was the sample acquisition. It consists of the selection of image features that correctly represent the class objects. Five classes were described: ceramic roofs, concrete roofs, roofs with different materials (named “other roofs”), arboreal vegetation, and grass vegetation. Figure 6.10 presents the sample selection in Vila Baiana orthophoto.

Figure 6.10. Samples acquisition in Vila Baiana orthophoto.

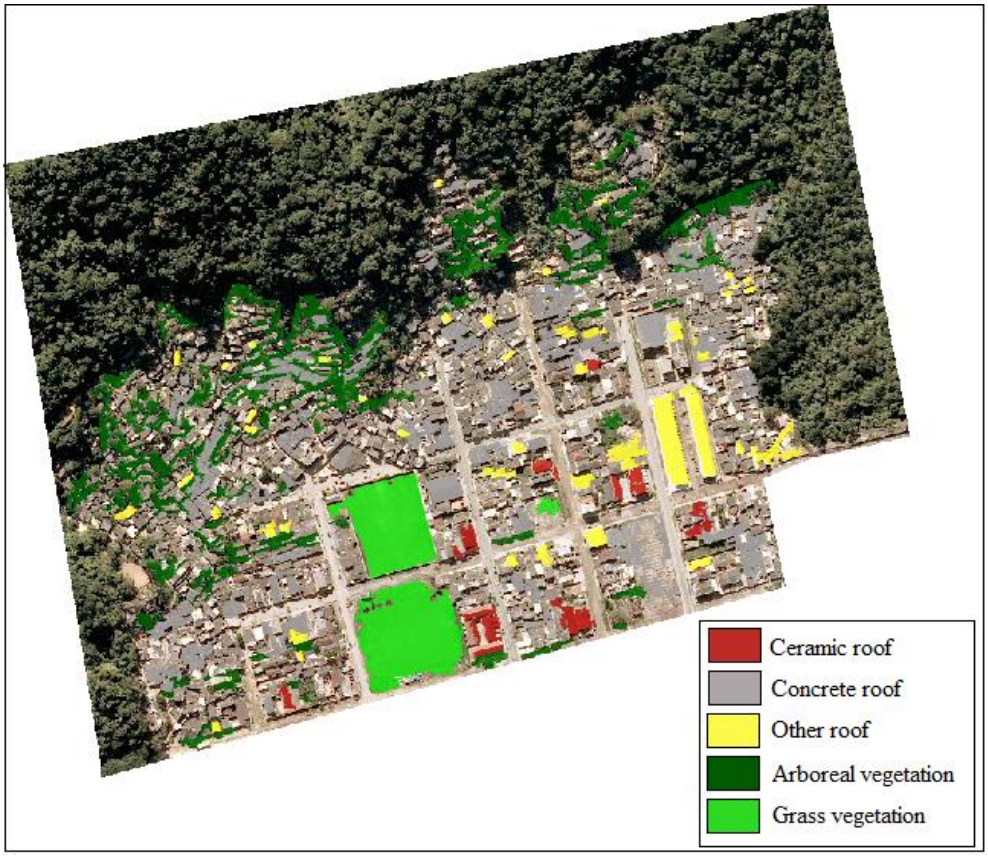

Data mining is important to determine the most relevant attributes to classify the image. This study used the CART algorithm, available on the eCognition platform. The process was carried out in three stages: training operation (Train), analysis operation (Query), and application of data mining results (Apply). The first step consists of generating a file with the statistics information from the objects selected (the samples). This statistical information is based on selected attributes and parameters set by the user. It results in a decision tree containing the variables and determining thresholds for the identification and separation of each class. The analysis operation (Query) allows the visualization and analysis of the decision tree (Appendix A) generated in the Train operation. And the last step consists of the application of thresholds and variables to classify the image.

6.1.3 Image classification, NDVI index, and discussion

The urban sprawl is a direct consequence of population growth and the development of Guarujá municipality. During the past 31 years (1990-2021), deforestation of native

vegetation increased to open space for urbanization. Figure 6.11 presents the temporal analysis of urban sprawl for 1990, 2013, 2020, and 2021.

Figure 6.11. Urban sprawl from 1990, 2013, 2020, and 2021.

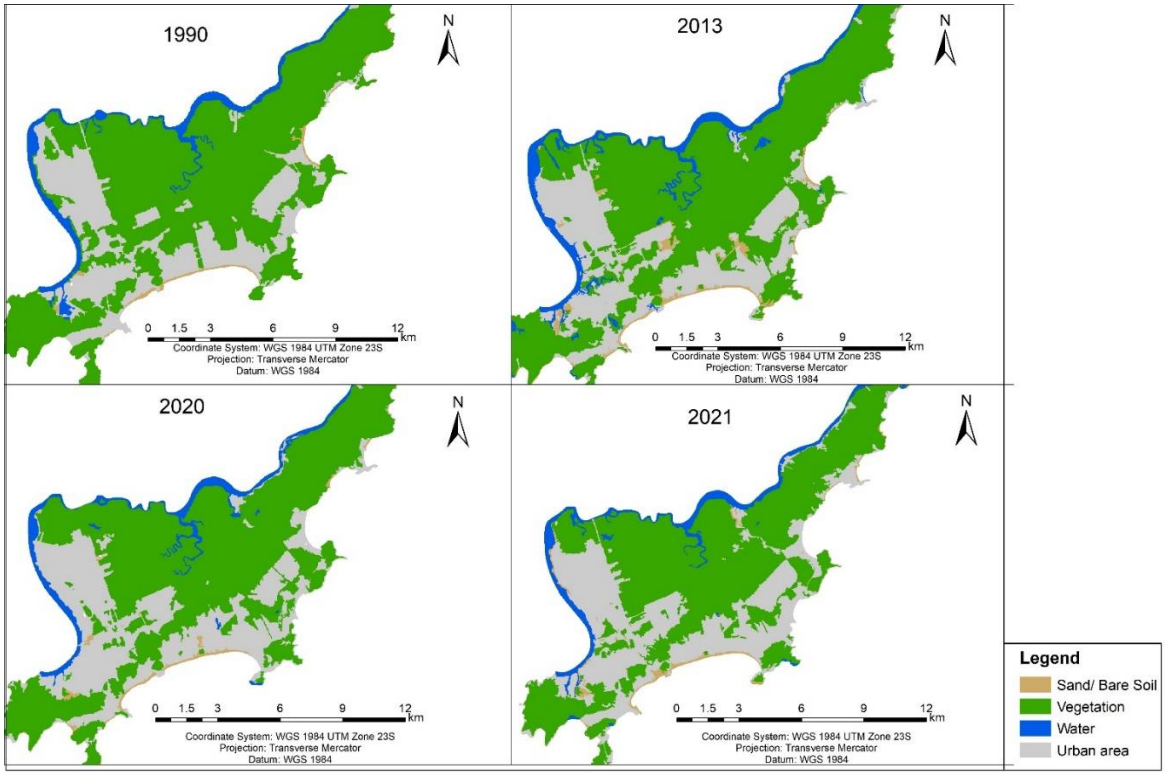

Analyzing Figure 6.11, it is possible to verify an intense increase in the urban area from 1990 to 2021, represented in gray. Moreover, the urban sprawl continues to intensify rapidly since, in 2021, the increase was 7,9% above the amount in 2020. Furthermore, the removal of natural vegetation continues, giving space to the city's expansion. Table 6.2 shows the built-up area occupied by the town and the vegetation cover for the years 1990, 20213, 2020, and 2021. Appendix B shows the urban sprawl from 2013 to 2021.

Table 6.2. Variation of urban and vegetation area (km²) from 1990 to 2021.

Year	Urban area (km²)	Vegetation (km²)
1990	36.252	96.003
2013	37.618	89.912
2020	43.764	88.734
2021	47.252	84.252

Table 6.2 shows a correlation between the increase in urban areas and the decrease in vegetation-covered areas. From 1990 to 2021, the urbanization process increased by 30%, while the vegetation area suffered a 12% reduction.

An error matrix was calculated to assess the classification accuracy, as presented in Table 6.3, Table 6.4, Table 6.5, and Table 6.6. The diagonal values, highlighted in yellow, represent the count of correctly classified polygons, and the columns show the number of polygons classified in each class. The producer's reliability is the percentage of a reference polygon to have been correctly classified, and the user's accuracy is the percentage of the classified polygon being in the correct class. Values closer to or equal to 1 indicate the best results (NAGAMANI et al., 2015).

Table 6.3. Error matrix of 1990 classification.

1990							
		Reference polygon					
		Water	Urban area	Sand/bare soil	Vegetation	Total	User's accuracy
Classified polygon	Water	10	0	0	1	11	0.91
	Urban area	0	54	3	1	58	0.93
	Sand/bare soil	0	1	10	1	12	0.83
	Vegetation	2	3	0	129	134	0.96
	Total	12	58	13	132	215	
	Producer's accuracy	0.83	0.93	0.77	0.98		
	Global accuracy	0.94					

Table 6.4. Error matrix of 2013 classification.

2013							
		Reference polygon					
		Water	Urban area	Sand/bare soil	Vegetation	Total	User's accuracy
Classified polygon	Water	40	0	0	3	43	0.93
	Urban area	0	157	1	2	160	0.98
	Sand/bare soil	0	1	57	1	59	0.97
	Vegetation	2	4	0	315	321	0.98
	Total	42	162	58	321	583	
	Producer's accuracy	0.95	0.97	0.98	0.98		
	Global accuracy	0.98					

Table 6.5. Error matrix of 2020 classification.

2020							
		Reference polygon					
		Water	Urban area	Sand/bare soil	Vegetation	Total	User's accuracy
Classified polygon	Water	24	0	0	2	26	0.92
	Urban area	0	124	1	3	128	0.97
	Sand/bare soil	0	1	24	1	26	0.92
	Vegetation	1	2	0	255	258	0.99
	Total	25	127	25	261	438	
	Producer's accuracy	0.96	0.98	0.96	0.98		
	Global accuracy	0.97					

Table 6.6. Error matrix of 2021 classification.

2021							
		Reference polygon					
Classified polygon		Water	Urban area	Sand/bare soil	Vegetation	Total	User's accuracy
	Water	21	0	0	2	23	0.91
	Urban area	0	174	1	4	179	0.97
	Sand/bare soil	0	2	37	1	40	0.93
	Vegetation	3	2	0	259	264	0.98
	Total	24	178	38	266	506	
	Producer's accuracy	0.88	0.98	0.97	0.97		
	Global accuracy	0.97					

All the classification's error matrices presented a global accuracy higher than 0.9. However, there is spectral confusion between vegetation and urban areas. The probable cause is the proximity of some constructions to the forest canopy in Guarujá.

The development of urban areas destroys vegetation. To improve the distinction between the urban area and the vegetation, the Normalized Difference Vegetation Index (NDVI) was calculated. The NDVI is used to differentiate the vegetation areas from the non-vegetation areas. The leaves have a strong reflectance in the near-infrared band, while chlorophyll and other leaf pigments have a weak reflectance in the visible wave band red (LÜDEKE; et. al., 1996; MENG; et. al., 2013). The NDVI formula is presented in Equation 6.1, and the temporal analysis of vegetation changes using NDVI is shown in Figure 6.12.

$$\boldsymbol{NDVI} = \frac{(\boldsymbol{NIR}-\boldsymbol{Red})}{\boldsymbol{NIR}+\boldsymbol{Red}} \quad (6.1)$$

Figure 6.12. Temporal analysis of variation in NDVI for 1990, 2013, 2020, and 2021.

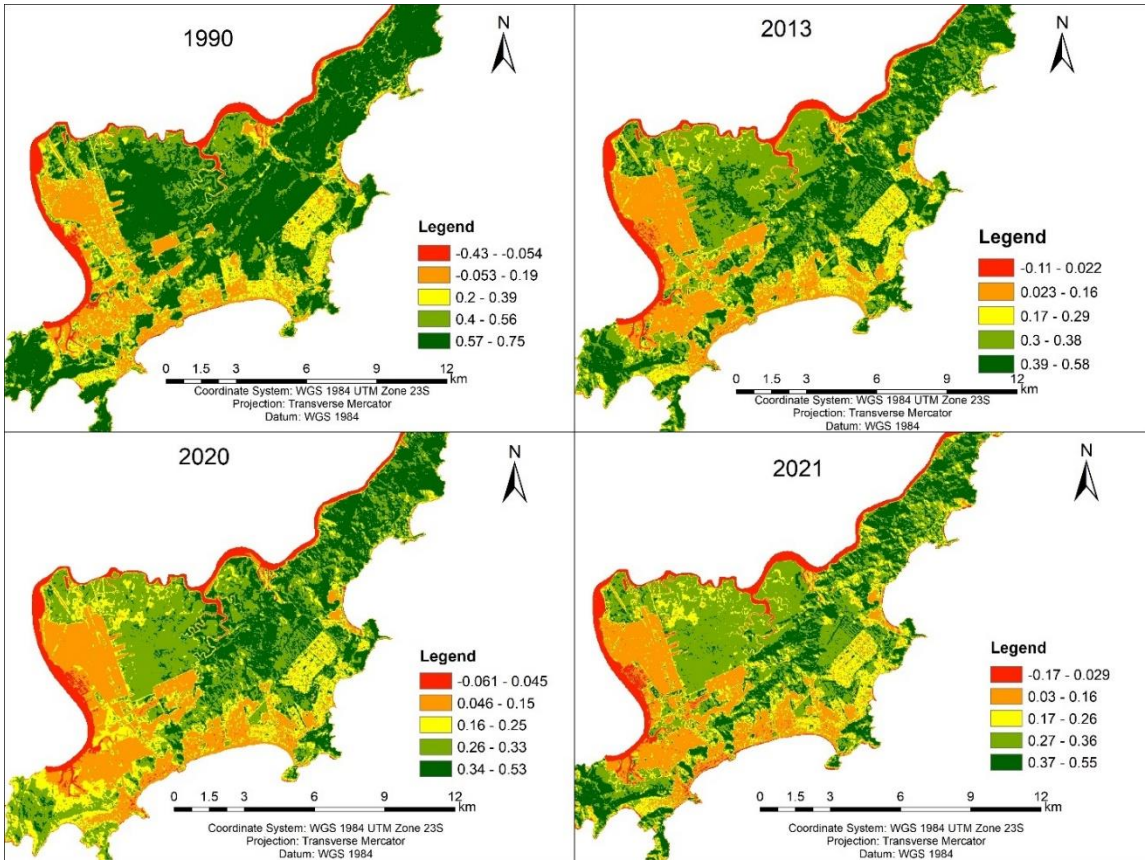

The analysis of Figure 6.12 shows the vegetation changes in the past 31 years. The water, represented in red, has low reflectance and, consequently, lower values of NDVI. The colors orange and yellow characterized the urban areas according to the degree of urbanization (high level of urbanization and medium level, respectively). The vegetation is represented by green: the light green areas have lower biomass than those in dark green. In the 1990 classification, it was observed that the vegetation cover is denser and spreads over most of Guarujá municipality. Dark green is the predominant color, meaning that most forest areas were preserved. However, in 2021, a reduction of the vegetation-covered areas and the green-leaf density is perceptible. Few forest areas were maintained, and the leaf-area density decreased.

There is a strong annual building activity due to the city's development. Land prices increased sharply, and low-income people made their homes in steep areas on cheap but improper terrain (ARAKI et al., 2001), as presented in Figure 6.13. Moreover, the deforestation processes are directly related to the construction on steep slope areas. In

Figure 6.13, it is possible to identify steep slope areas overlapping urban areas. These are landslide-prone areas, and people living there are at risk; they can lose their houses and lives.

Figure 6.13. Overlap between slope and the classification of urban areas for 2021.

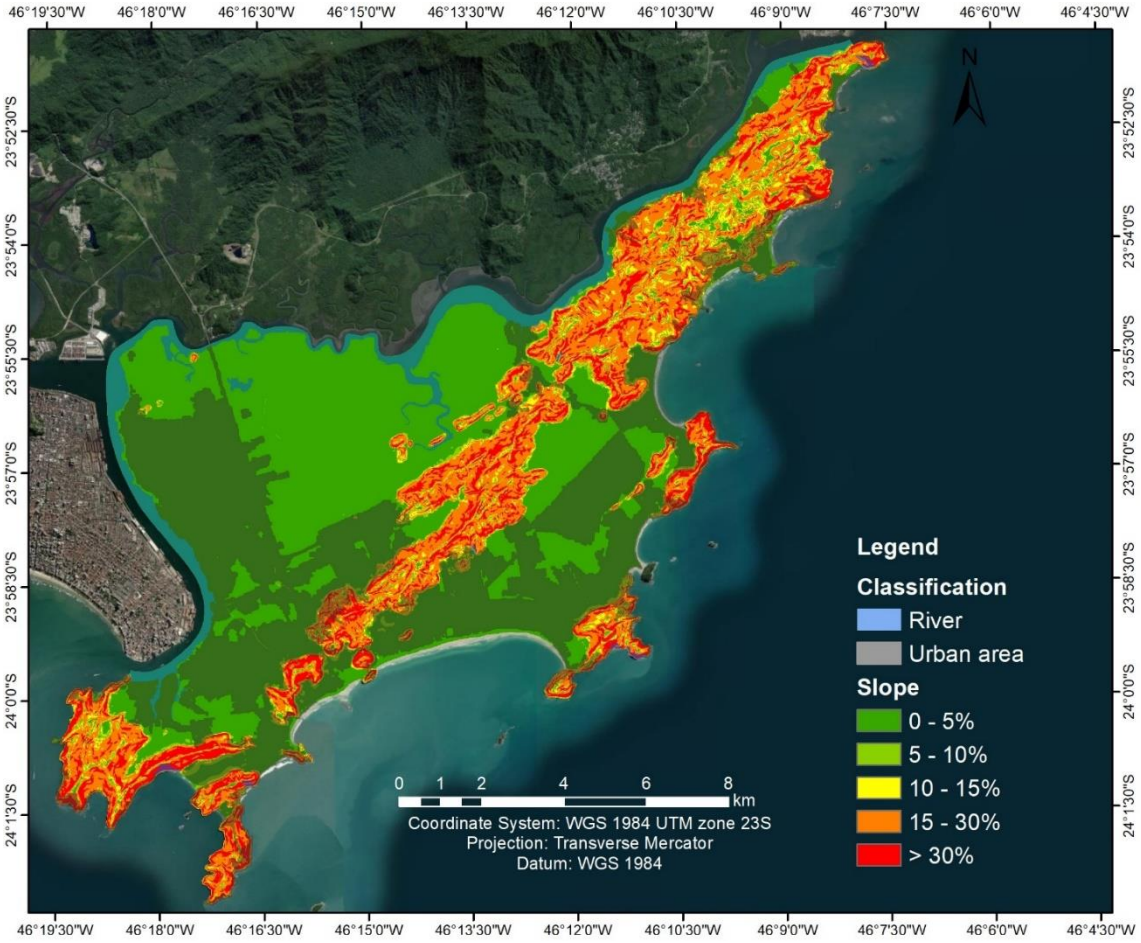

Those people who cannot afford a house or land in the central part of Guarujá start to build their houses on the slopes, favoring deforestation (MODENESI-GAUTTIERI; HIRUMA, 2004; KÖNIG et. al., 2019). To build houses under such conditions, the vegetation is destroyed and vertical cuts in the slope are made without retaining walls. Most of these constructions have low building standards, which decrease the slope stability, and increase the risk of accidents to the population (MENDES et al., 2018b; KÖNIG et. al, 2020).

The weight of several constructions on steep slope areas, associated with improper water drainage and deforestation, could change the soil moisture and thus, any amount of rain can trigger landslides. Vila Baiana neighborhood is one of these areas, where several houses were improperly constructed in slope areas, which are commonly affected by landslides.

Therefore, to identify and distinguish the types of construction in Vila Baiana, a classification of the orthophotos was performed, as presented in Figure 6.14.

Figure 6.14. Classification of Vila Baiana.

Figure 6.14 identifies several constructions built on the edge of the arboreal vegetation, especially in steep slope areas. Generally, these constructions have a low building standard, and most have a concrete roof.

Moreover, the roads are well delimited in the flat land but not on the upper slopes. There is any pavemented street in high declivity areas, becoming difficult to access the area.

Furthermore, the government did not authorize construction in these areas. Besides that, sanitation and garbage collection are nonexistent.

Areas with high declivities are susceptible to landslides, and the inappropriate ways of land use and occupation can induce landslides, putting at risk everyone living there (AHRENDTH, 2005; MENDES et. al., 2018a). Table 6.7 presents the values of the area and the perimeter of each class related to the classification of Vila Baiana.

Table 6.7. Values of area and perimeter by class.

Class	**Area (m²)**	**Perimeter (m)**
Roads	25.136	5.764
Ceramic roof	8.254	5.958
Concrete roof	74.340	48.348
Other roofs	22.930	17.154
Arboreal vegetation	240.684	73.172
Grass vegetation	26.719	16.518

Table 6.7 shows a predominance of constructions with concrete roofs in Vila Baiana, totaling 74.340 m². The houses localized on slope sections, meaning on the edge of arboreal vegetation, have mostly concrete roofs, and just a few present different types of roofs ("other roofs" in the classification). In these slope areas, it is not possible to identify roads, but many houses are observed in a small area.

Notwithstanding, the ceramic roof class is the less representative roof type, with only 8.254 m² of constructed area. They occur in places where it is still possible to determine the blocks and the roads, meaning that these areas are part of the urban planning of Guarujá municipality.

The grass vegetation predominates in two blocks, and both are soccer fields. The arboreal vegetation occurs mostly in steep slope areas, with only a few polygons mixed with the constructions.

The error matrix was calculated to assess the classification accuracy, as presented in Table 6.8. It shows that the class "Road" was correctly classified because a thematic layer with all the street vectors was used in the segmentation and classification process. However,

there is a spectral confusion between the classes “Other roof” and “Concrete roof.” Analyzing the orthophoto, it is observed that some concrete roofs are lighter than others. The material used in these constructions probably has a similar composition to those used by the class “Other roof,” justifying the confusion in the classification process.

Table 6.8. Error Matrix of Vila Baiana classification.

Classified polygon \ Reference polygon	Roads	Ceramic roof	Concrete roof	Other roofs	Arboreal Vegetation	Grass Vegetation	Total	User's accuracy
Roads	2	0	0	0	0	0	2	1.00
Ceramic roof	0	64	1	1	0	0	66	0.95
Concrete roof	0	0	369	8	2	1	380	0.97
Other roofs	0	1	11	325	3	2	342	0.95
Arboreal vegetation	0	0	2	1	728	15	746	0.98
Grass vegetation	0	0	7	1	3	76	87	0.87
Total	2	64	386	337	740	94	1623	
Producer's accuracy	1.00	0.98	0.96	0.96	0.98	0.81		
Global accuracy	0.96							

Moreover, there is spectral confusion between the grass vegetation and the concrete roof. Most polygons wrongly classified as grass vegetation are in the areas with high declivity because these sections were covered with forest, and to build houses, the trees were removed, and the grass is regrowth. Therefore, a grass pixel in a polygon that can confound the algorithm, classifying it incorrectly. Due to the spectral similarity, the classes “Arboreal vegetation” and “Grass vegetation” also presented some misclassification.

Despite some incorrectly classified polygons, the global accuracy is 0.96, meaning a good accuracy of the classification processes. Visualizing the classified map, it is possible to affirm that several constructions in slope areas contributed to deforestation. Furthermore,

the high density of houses, close to each other, increases the soil weight, making it more fragile and susceptible to suffer fractures and landslides (MENDES et al., 2018a, 2018b).

6.1.4 Correlation between urban sprawl and landslide occurrences

Analyzing the populational growth and the landslide occurrences, it is possible to verify that from 1990-2000, the population went from 202.910 in 1990 to 264.235 in 2000 (see Figure 4.3). There was an increase of 30.22% in the population of Guarujá within ten years.

Therefore, during this period, more than 60 thousand people settled and built houses all over the municipality. The area suffers from environmental degradation and an increase in the weight of the new constructions, justifying the 482 landslide occurrences. Notwithstanding, from 2000-2010 the population increased by 9.95% when compared with the previous decade, and 473 landslides were documented. Table 6.2 shows, in 2013, a decrease of 6.34% in vegetation cover.

Furthermore, from 2010-2020, the populational growth increases by 10.30%, totalizing 320.459 people. Consequently, the vegetation-covered area was reduced by 5.05%, and the urban area was incremented by 7.97%. Therefore, the environmental degradation caused by population growth and urban sprawl has consequences in soil changes and induces landslides.

Moreover, from the 336 landslides documented during 2010-2020, 138 happened due to an extreme climatic event on March 3rd, 2020. Most landslides in Brazil are triggered by rainfall, thus the correlation between heavy rainfalls and phenomena like El-Niño and La-Niña is important to the identification and monitoring of landslides-prone areas.

6.2 Correlation between landslides and rainfall

According to the Civil Defense of Guarujá, from 1991-2020, 1319 landslides were recorded, as presented in Figure 6.15. The years with higher landslide occurrences were: 1991, 1993, 2005, 2009, 2010, and 2020.

Figure 6.15. Landslides Occurrences in Guarujá from 1991 to 2020.

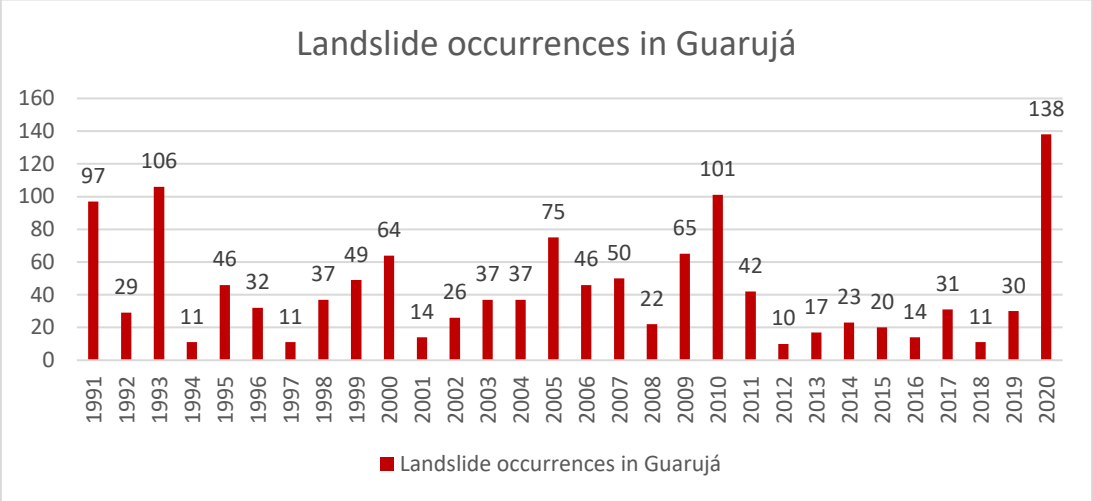

The Vila Baiana neighborhood is one of the most affected areas, followed by Morro da Cachoeira, Morro do Engenho, Morro Bela Vista, and Vale da Morte (COMPDEC – Guarujá). During 1991 - 2020, more than 338 landslides happened in Vila Baiana. Figure 6.16 presents the distribution of landslides over the years.

Figure 6.16. Landslide occurrences in Vila Baiana during 1991-2020.

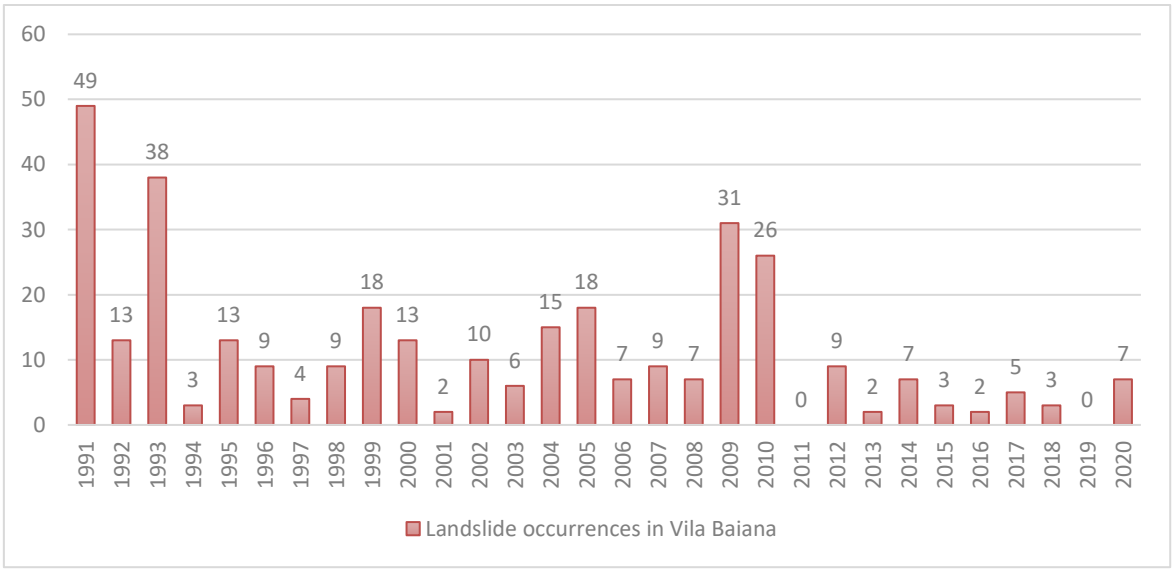

As we can see, the years with higher landslide occurrences in Guarujá (1991, 1993, 2009, and 2010) had more landslides in Vila Baiana as well. The landslide occurrences corroborate with the annual average rainfall, shown in Figure 6.17.

Figure 6.17. Comparison between annual average rainfall and landslide occurrences in Guarujá.

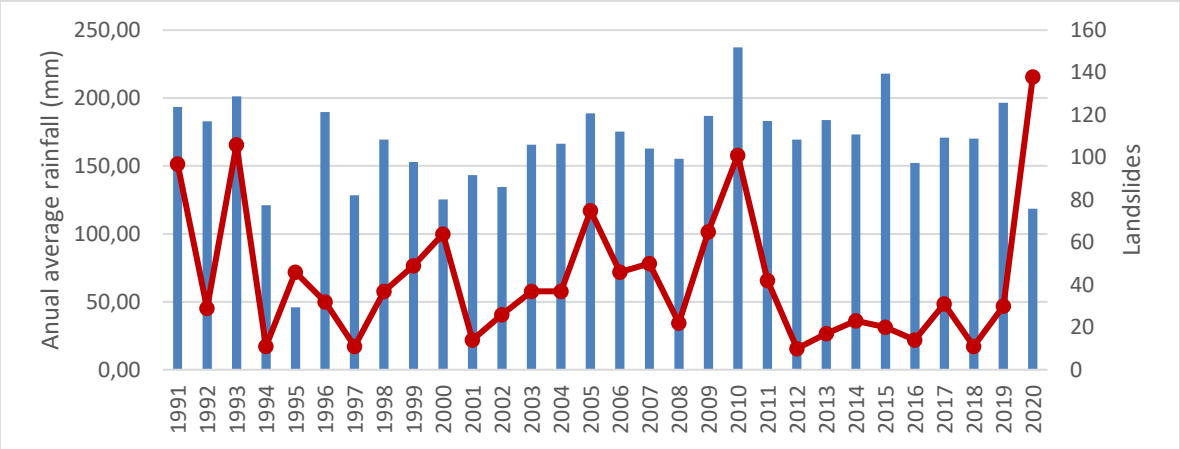

Figure 6.17 shows a correlation between the annual average rainfall and landslide occurrences. There is a tendency for more landslides during the rainy years, such as in 1991, 1993, 2005, 2009, and 2010. However, in 1996 the annual rainfall average was 189,6 mm, but the number of landslides was only 32 when compared with the year 2005, which had 75 landslides and a yearly rainfall average of 188,8 mm. A similar result happened in 2015 when only 20 landslides were documented, but the annual rainfall average was 218.05 mm. It is also important to notice that 46 landslides were registered in 1995, the year with the lowest rainfall annual average (46,0 mm). Notwithstanding, during the year 2020, 138 landslides were documented, and the annual rainfall average was 118.54 mm. This means that the annual rainfall average was lower than in other years, such as 1993 and 2010, but more landslides occurred.

Therefore, it is important to determine if an extreme rainfall phenomenon happened and might have triggered those landslides. It is considered an extreme rainfall event when 20% or more of the total amount of rain expected for a month, falls in one day (LIEBMANN et. al., 2001; CARVALHO et. al., 2002). The Civil Defense of Guarujá determined a threshold of > 70,0 mm in 24h as a heavy rainfall event (COMPDEC –

Guarujá). Table 6.9 presents statistical values of landslides triggered by heavy rainfall events. The years selected represents those with higher annual rainfall averages and with documented landslides triggered by heavy rainfall both in Guarujá and Vila Baiana.

Table 6.9. Heavy Rainfall events with a threshold >70 mm in 24h.

Year	Location	Total Landslide	Landslides triggered by heavy rainfall > 70 mm in 24h	(%) Landslides triggered by heavy rainfall > 70 mm in 24h
1991	Guarujá	97	21	21.65
	Vila Baiana	49	10	20.41
1993	Guarujá	106	68	64.15
	Vila Baiana	38	22	57.89
2009	Guarujá	65	47	72.31
	Vila Baiana	31	20	64.52
2010	Guarujá	101	57	56.44
	Vila Baiana	26	20	76.92
2013	Guarujá	17	14	82.35
	Vila Baiana	2	2	100
2015	Guarujá	20	12	60
	Vila Baiana	3	3	100
2020	Guarujá	138	138	100
	Vila Baiana	7	7	100

The analysis of Table 6.9 shows an increase in landslides triggered by heavy rainfall, from 1991 to 2010, in Vila Baiana. Moreover, in 2013, 2015, and 2020, 100% of the landslides in Vila Baiana were triggered by rainfall with a threshold of >70mm in 24h. Furthermore, these results corroborate the years with a higher annual rainfall average in Guarujá, as presented in Figure 6.18. The years in navy blue are those with a higher yearly standard.

Figure 6.18. Annual rainfall average (mm) in Guarujá.

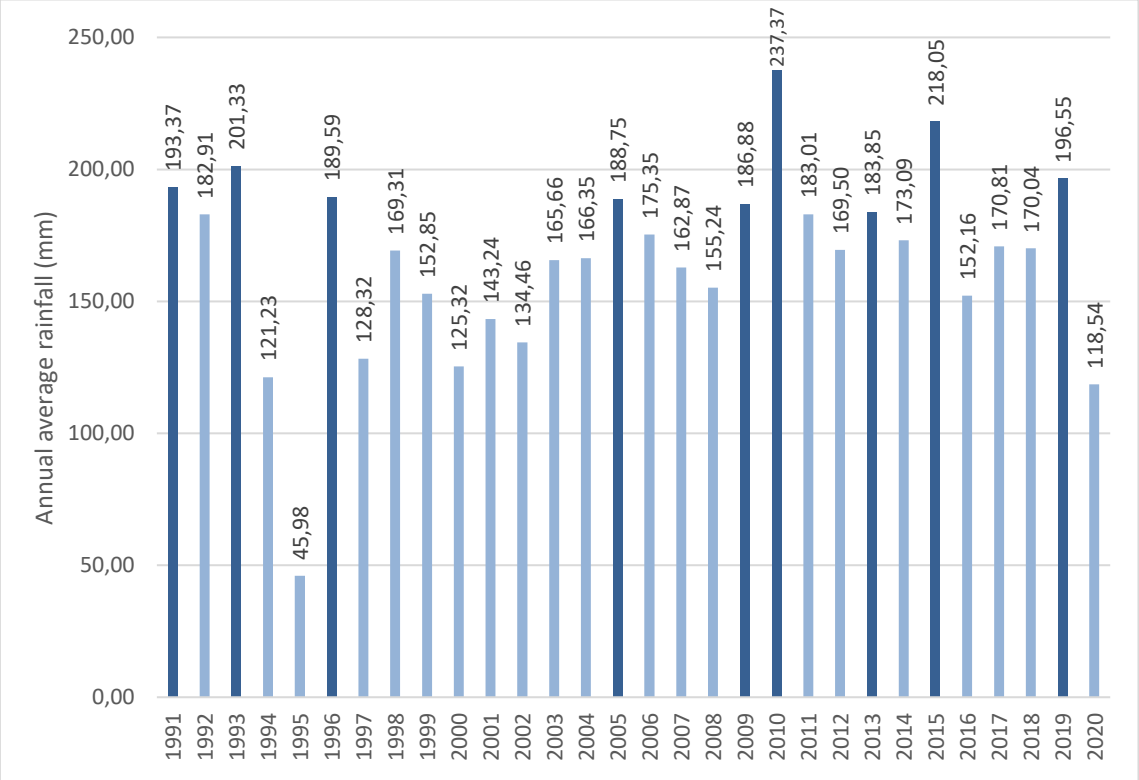

Source: Adapted from DAEE (2021).

Analyzing Figure 6.18, it is possible to identify that those years with higher annual averages are the same with most landslides triggered by heavy rainfall. The exception is in 1996 because, despite an average of 189,6 mm, only 46,88% of documented landslides in Guarujá (and 44,44% in Vila Baiana) were triggered by rainfall with a threshold >70 mm. In 2019, the rainfall average was 196,6 mm, and only 30 landslides were recorded in Guarujá (none in Vila Baiana). The year 2020 is interesting, because the annual rainfall is 118.54 mm, but presented more landslide occurrences. This case is further discussed, because extreme rainfall happened, triggering 138 landslides in 24h.

Since Vila Baiana is the study area, further analysis will examine the relationship between some landslides and rainfall events. Figure 6.19, Figure 6.20, Figure 6.21, and Figure 6.22, are presented the accumulated volume of rainfall for 24h and 72 hours on the same days of the landslides occurrences.

Figure 6.19. Accumulated rainfall (mm) for 24h and 72h in Vila Baiana in 1991.

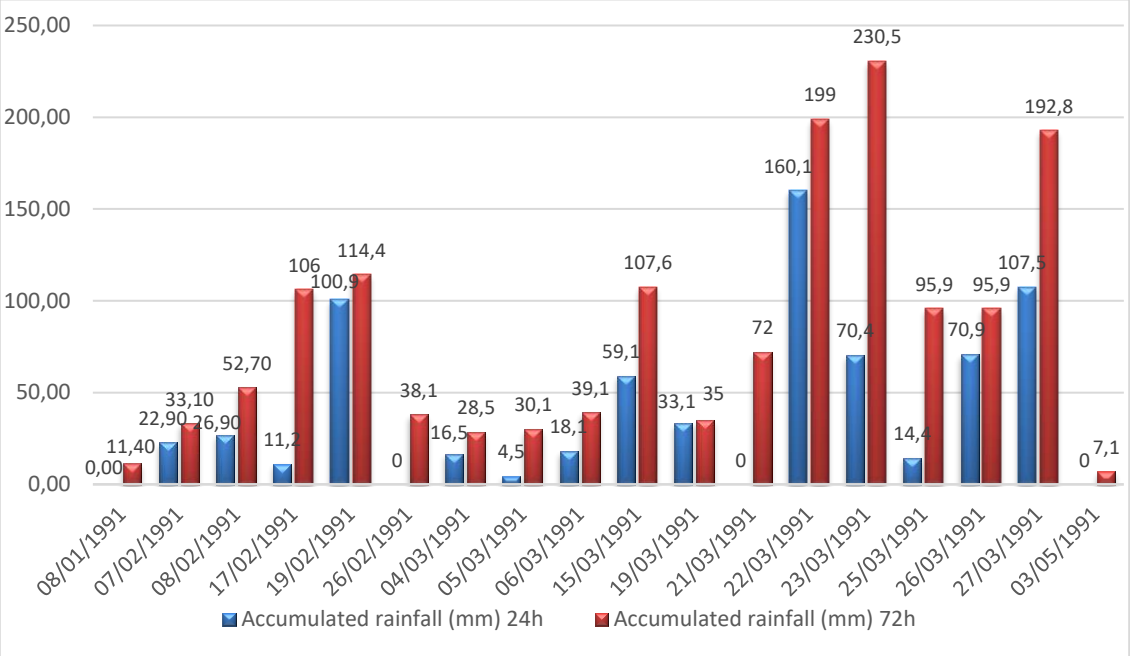

Source: Adapted from DAEE (1991).

In 1991, 97 landslides were recorded in Guarujá, of which 47 happened in Vila Baiana. The PPDC (Preventive Plan of Civil Defense – in Portuguese) determined that 80 mm is the threshold of accumulated rainfall during 72h. Values above 80 mm/72h indicate that landslides might happen. Analyzing Figure 6.19, it´s possible to observe that since March 21st, the areas have been affected by several rainfalls, justifying the higher values of accumulated rain in 72h. Furthermore, on March 25th, with 95,9 mm of accumulated precipitation, 12 landslides were registered in Vila Baiana (COMPDEC – Guarujá). However, 9 landslides occurred with a threshold < 80 mm, indicating that anthropic changes and human influence might have contributed to triggering some landslides.

In 1993 (Figure 6.20), 38 landslides happened in Vila Baiana. On February 18th, after a heavy rainfall of 74,5 mm in 24h (90,0 mm in 72h), 60 landslides were recorded in Guarujá, and 19 of them occurred in Vila Baiana (COMPDEC – Guarujá). Although several landslides were triggered by heavy rainfall, 6 of them happened with a threshold < 80,0 mm. That´s the case on February 11th, when a landslide occurred with accumulated precipitation for 24h and 72h of 2,9 mm and 3,3 mm, respectively. Another landslide was

reported on April 6th, despite the lowest rainfall values (0,0 mm in 24h and 2,9 mm in 72h) (COMPDEC – Guarujá).

Figure 6.20. Accumulated rainfall for 24h and 72h in Vila Baiana in 1993.

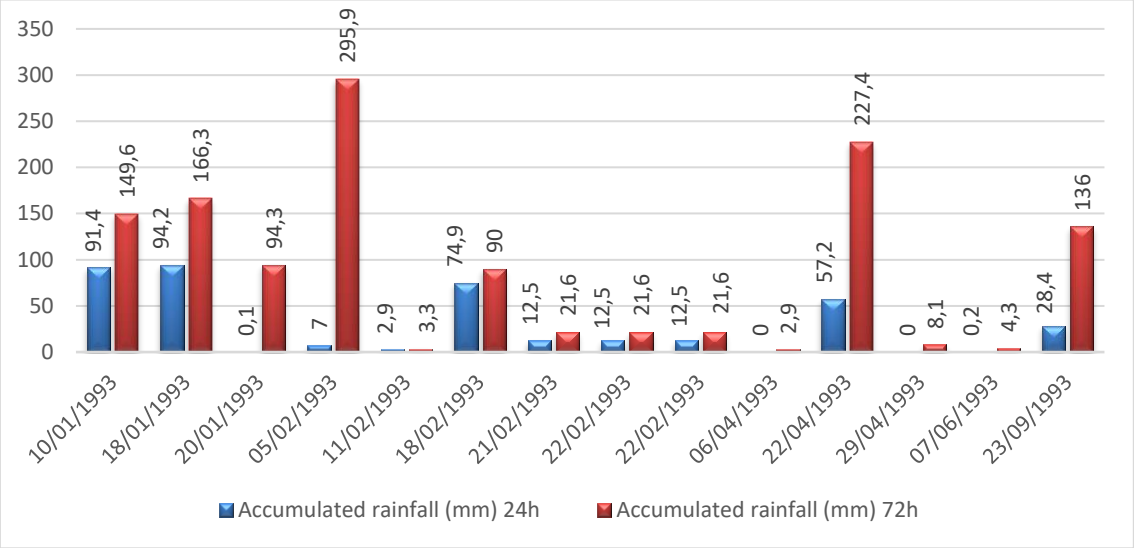

Source: Adapted from DAEE (1993).

In 2009, 31 landslides were documented in Vila Baiana, and only 3 of them happened with a threshold < 80,0 mm. It is interesting to enhance that on May 13th, a landslide occurred, but it wasn´t triggered by rainfall (0 mm was registered for both 24h and 72h) (COMPDEC – Guarujá). This disaster probably has anthropic influence.

Figure 6.21. Accumulated rainfall for 24h and 72h in Vila Baiana in 2009.

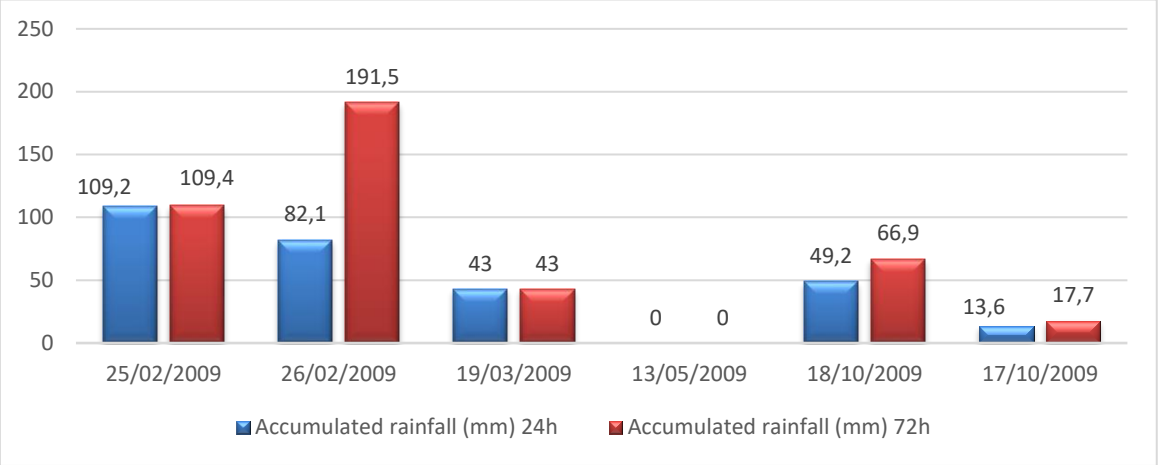

Source: Adapted from DAEE (2009).

Similar results were founded in 2010 when 26 landslides were documented in Vila Baiana, and 6 of them were triggered with a threshold < 80,0 mm. A landslide happened on April 14th, despite the absence of rain for 72h (COMPDEC – Guarujá). These cases foment the idea of anthropic contribution to trigger landslides.

Figure 6.22. Accumulated rainfall for 24h and 72h in Vila Baiana in 2010.

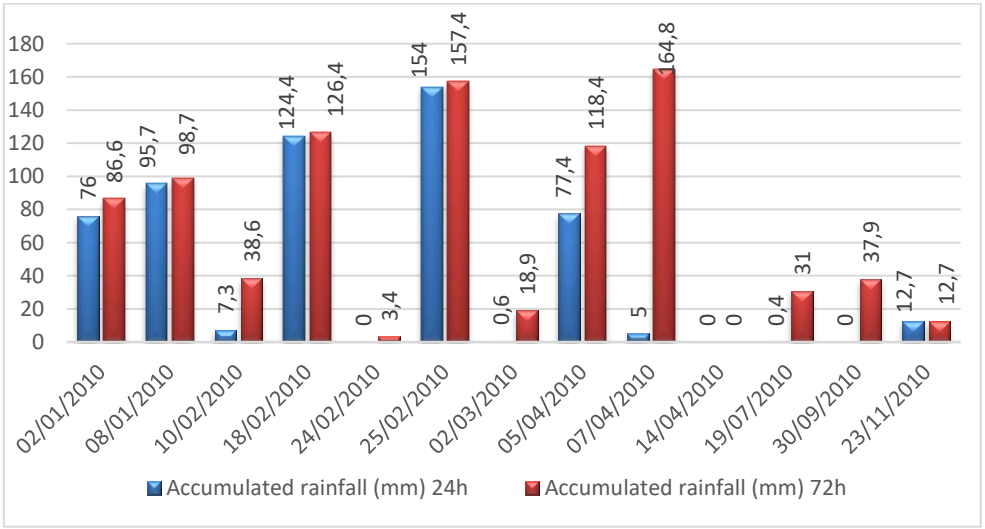

Source: Adapted from DAEE (2010).

In 2020 (Figure 6.23), extremely heavy rainfall occurred, triggering 138 landslides in Guarujá municipality, of which 7 of them were at Vila Baiana. Despite the several days with constant rainfall, on March 3rd more than 320 mm of rainfall were registered by rain gauges and PCDs in 24h.

Figure 6.23. Accumulated rainfall for 24h and 72h in Vila Baiana in 2020.

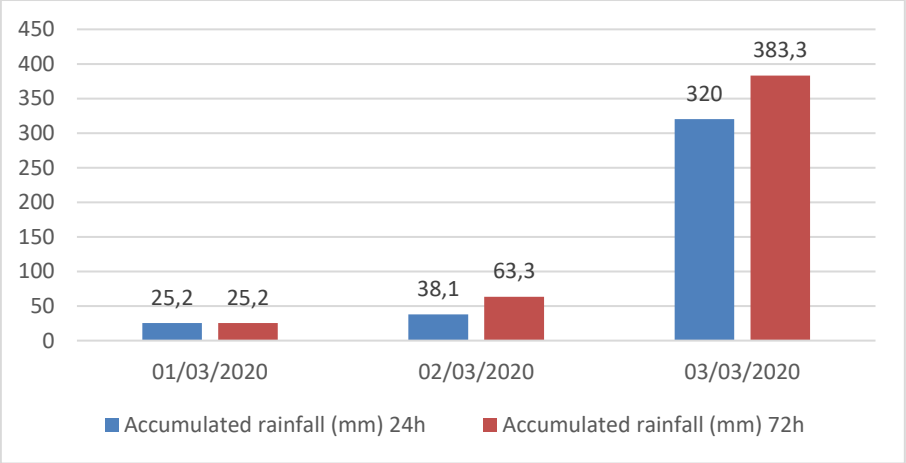

Source: Adapted from DAEE (2020).

Most landslides happen during the summer (December to March), but January, February, and March are the months with higher landslide records. From 1991 to 2020, March was the month with more landslide events, followed by February (COMPDEC – Guarujá), as presented in Figure 6.24.

Figure 6.24. Total landslide events per month from 1991-2020

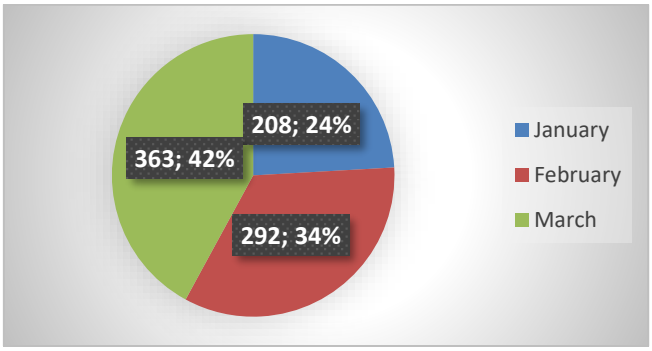

Source: Adapted from COMPDEC (2021).

Therefore, the analysis of the rainfall average is essential to determine if the mentioned months had experienced extreme climatic events, such as heavy rainfalls. The DAEE (Water and Electrical Energy Department of São Paulo State - in Portuguese: "Department Departamento de Águas e Energia Elétrica do Estado de SP") provides rainfall data since 1937; thus, Figure 6.25 presents the monthly average rainfall for the years 1991, 1993, 2009, 2010 and the global average (timeframe 1937-2020).

Figure 6.25. Monthly average rainfall (mm).

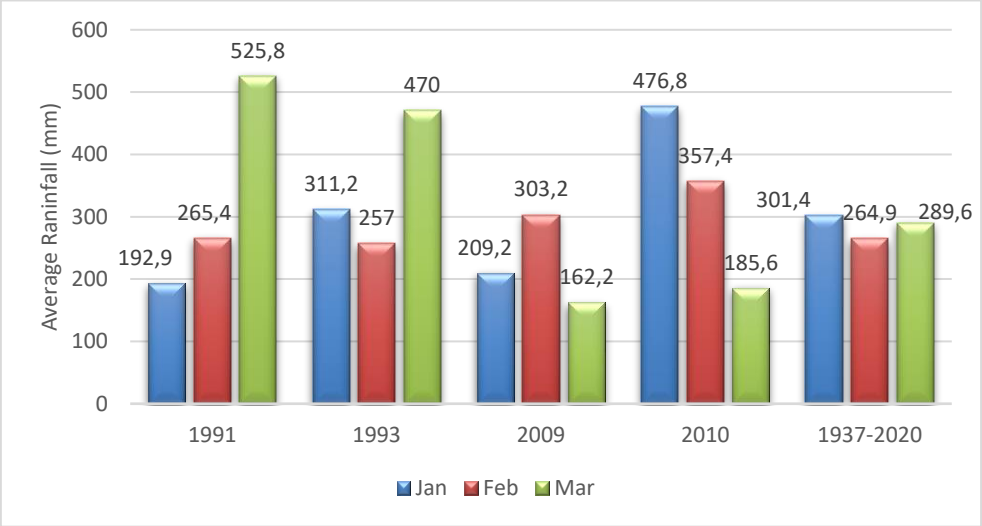

Source: Adapted from DAEE (2021).

Figure 6.25 shows that both years 1991 and 1993 had higher rainfall values during March. In 2009, the month with the highest rainfall average was February and March was the month with the lowest volume of rain. Similarly, March of 2010 registered lower values of rainfall. However, January was the month with the most rainfall events.

Furthermore, Figure 6.26 compares the variation of monthly rainfall for the mentioned year with the global average.

Figure 6.26. Comparison among rainfall variation.

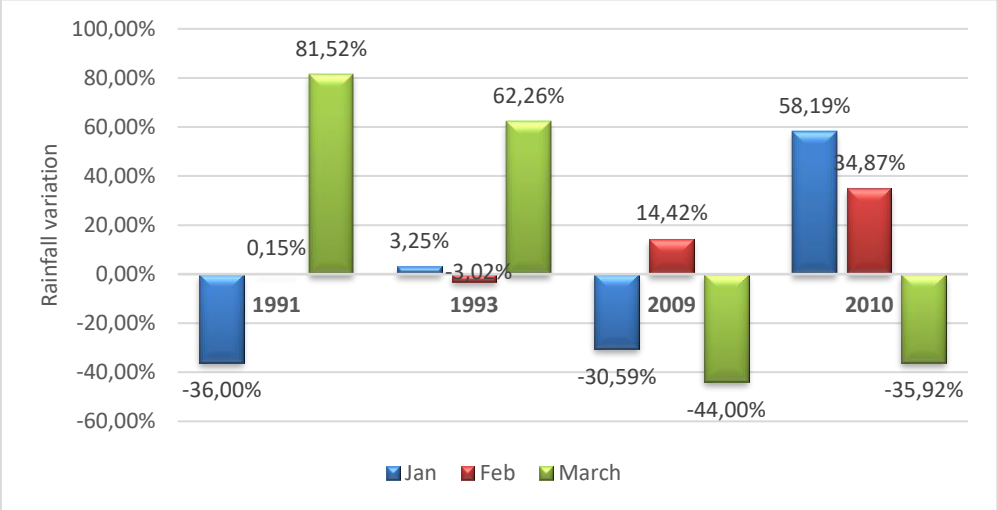

Figure 6.26 shows that in January 1991, the total amount of rainfall was 36% lower than the global rainfall (1937-2020). However, February and March presented an increase of 0,15% and 81,52%, respectively, compared with the worldwide average. In 1993, February registered a rainfall value of 3,02% lower than the global one. But during January and March, the registered rainfall was higher than the global (3,25% and 62,26%, respectively).

In 2009, the month with the highest precipitation values was February, with 14,42% more rain than globally expected. In January, the total amount of rain (209,2 mm) was 30,59% below the global average. And March presented 44% less rainfall than expected for this month. The year 2010 registered the highest rainfall values for January, with a total of 476,8 mm, corresponding to 58,19% more rain than expected. February also had higher rainfall values (357,4 mm), meaning an increase of 34,87% of the global average rainfall.

A correlation between the rainy years with El-Niño and La Niña phenomenon was also investigated. The El-Niño South Oscillation (ENOS in Portuguese) and La Niña are natural phenomena related to the abnormal variation of the Sea Surface Temperature (SST). These variations are calculated based on NOAA's National Oceanic and Atmospheric Administration) indicator Ocean Niño Index (ONI). ONI tracks the rolling 3-month average SST in the east-central tropical Pacific. It is considered El-Niño when a positive variation of 0,5 or higher of the SST occurs, meaning a warning in Pacific Ocean

water. La Niña is the opposite when the sea temperature decreases by -0,5 or more. Moreover, these phenomena can be classified by their intensity: weak (variation of SST between 0,5 – 0,9), moderate (1,0- 1,4), Strong (1,5 – 1,9), and very strong (≥ 2,0). Table 6.10 presents the occurrences of both phenomena and their intensity from 1991-2021.

Table 6.10. El-Niño and La Niña events during 1991-2021.

Period	Phenomeno	Intensity
1991-1992	El Niño	Strong
1994-1995	El Niño	Moderate
1995-1996	La Niña	Moderate
1997-1998	El Niño	Very Strong
1998-2000	La Niña	Strong
2002-2003	El Niño	Moderate
2004-2007	El Niño	Weak
2007-2008	La Niña	Strong
2009-2010	El Niño	Moderate
2010-2012	La Niña	Strong
2014-2015	El Niño	Weak
2015-2016	El Niño	Very Strong
2017-2018	La Niña	Weak
2018-2019	El Niño	Weak
2020-Present	La Niña	Moderate

Source: Adapted from Golden Gate Weather Service (2022).

In the southeast Brazilian region, the consequence of El-Niño is an increase in rainfall volume and intensity, while in the northeast region, droughts are common. Meanwhile, the La Niña phenomena generate a dry clime in the southeast region and a rainy season in the northeast of the country.

Analyzing Table 6.10, it is possible to associate the volume of rainfall for 1991, 2009, and 2010 with El-Niño. Moreover, the years 2005 and 2015, both marked by the influence of El-Niño (intensities weak and very strong, respectively), had an average annual rainfall >188,0 mm (Figure 6.18). Notwithstanding, from 1990-2000, the El-Niño phenomenon occurred three times, with intensities varying from Very Strong, Strong, and Moderate, and as mentioned in Section 6.1.4, 482 landslides were documented. From 2000-2010, moderate El-Niño had its influence and was associated with the urban sprawl, inducing

473 landslides. This corroborates the hypothesis that a climatic phenomenon justifies some heavy rainfalls.

However, the exception happened during 1996, which was marked by the influence of La Niña but also had an annual rainfall average of 189,6 mm. During 2010-2020, the La-Niña was more representative, but heavy rainfalls happened and triggered landslides. That is the case of March 3rd, 2020, when a heavy rainfall with almost 320mm of rain, triggered 138 landslides all over the Guarujá municipality.

Heavy rainfalls have been proved to trigger landslides, and the El-Niño impacts the rainy season. Therefore, knowing if the current year under study is influenced by El-Niño helps to determine the probability of more heavy rainfall events and their consequences.

6.3 Analysis of topographic and lithological aspects correlated with landslides

Certain areas are prone to suffer more from landslides than others. Different geology and lithologies might contribute to landslide susceptibility. Therefore, thematic maps (hypsometry, aspect, curvature, slope, and pedology) and tables containing the Frequency of Distribution (Fd) of each class, Scars Concentration (SC), and the Landslides Potential (LP), were prepared to identify which characteristics prevail in landslide-prone areas. The scar concentration (SC) determines the scar distribution in each stability class. It is the ratio between the number of cells (of each class) affected by the landslide with the total cells of that class. The landslide potential (LP) indicates the distribution of the landslides among the stability classes. It is the ratio between the number of cells of each class affected by the landslides with the total cell affected in the study area. And the Frequency of Distribution (Fd) represents the distribution of each stability class, calculated by the ratio of the cell number per class to the total cells in the study area (VIEIRA, 2007; LISTO; VIEIRA, 2015; VIEIRA; RAMOS, 2015; LISTO; et. al., 2018).

The altitude might influence the landslide-prone areas due to the pluviometry variation at different heights, meaning that the orographic rain varies accordingly to the altitude. Observing the hypsometry map, presented in Figure 6.27 and Table 6.11, it is noticed that 91.09% of the landslides happened in elevations ranging between 30-150 m above sea level.

Table 6.11. Percentage distribution of scar concentration, landslide potential, and frequency for each hypsometry class.

Hypsometry			
Class	**Scar Concentration (%)**	**Landslide Potential (%)**	**Frequency Distribution (%)**
0 - 20m	59.11	0.47	72.12
20 - 90m	36.60	0.29	9.92
90 - 150m	3.95	0.03	9.05
150 - 200m	0.33	0.00	6.28
200 - 320m	0.00	0.00	2.63

Figure 6.27. Hypsometry map of Guarujá municipality.

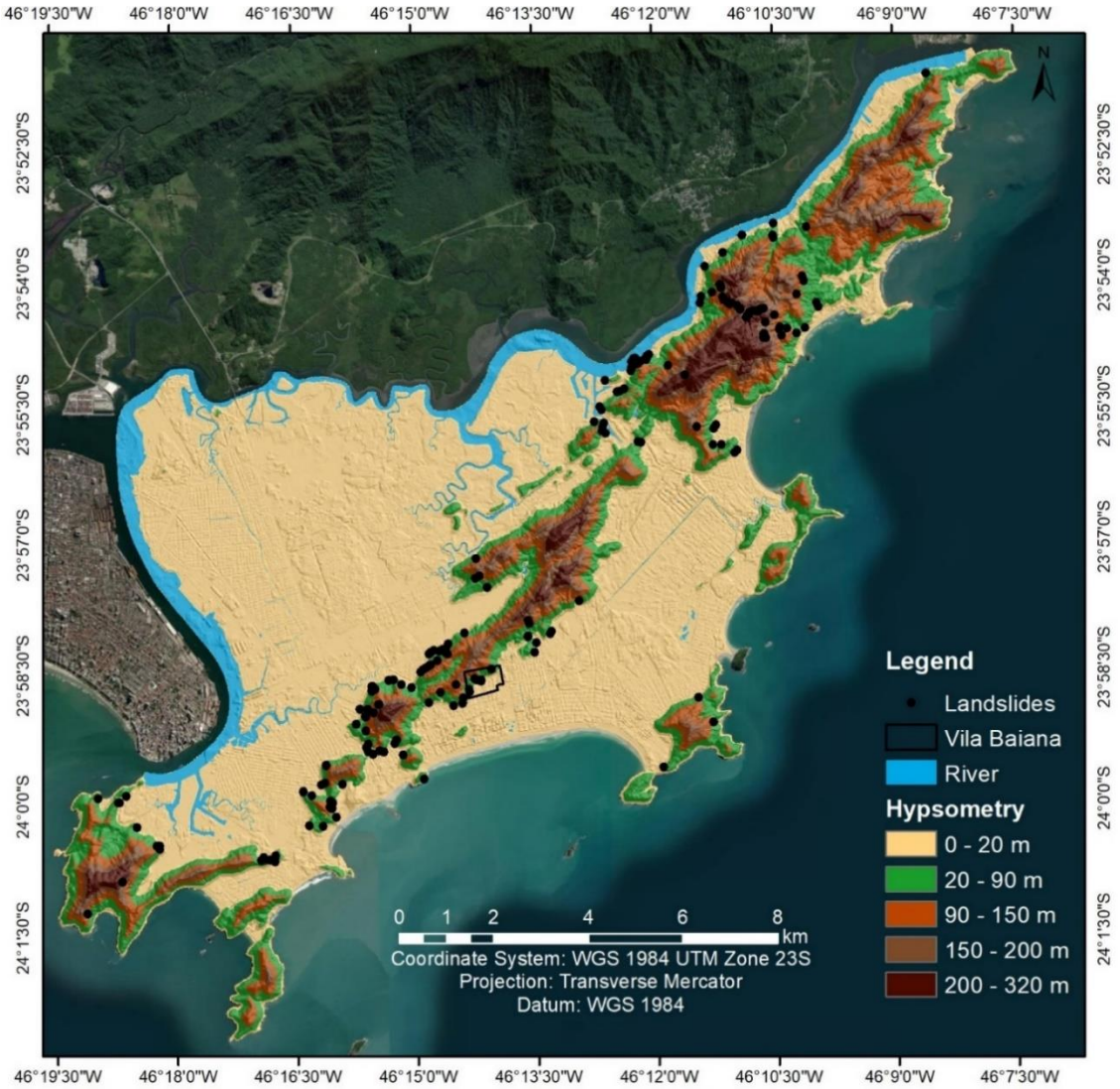

In agreement with the hypsometric map, the declivity map (Figure 6.28), and the distribution of landslides for each slope declivity (Table 6.12), indicates that the landslide scars are concentrated in declivities above 15%. Moreover, in Guarujá municipality, 16.3% of the area has declivities higher than 15%, as presented in the Frequency distribution.

Figure 6.28. Declivity Map of Guarujá Municipality.

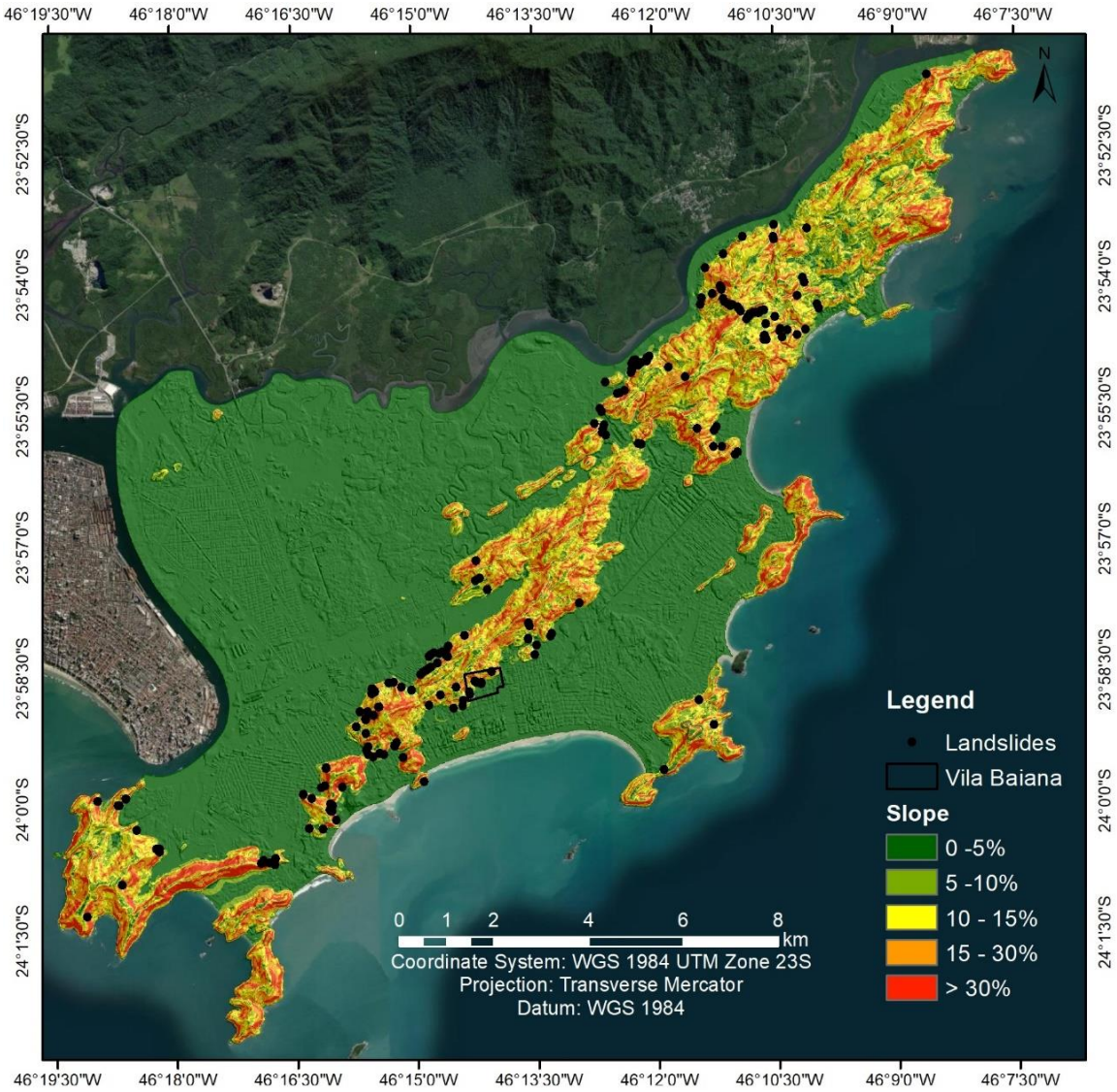

Table 6.12. Percentage distribution of scar concentration, landslide potential, and frequency in each declivity class.

Slope			
Class	**Scar Concentration (%)**	**Landslide Potential (%)**	**Frequency Distribution (%)**
0-5%	17.72	1.60	65.78
5-10%	17.28	1.56	7.73
10-15%	15.78	1.43	10.19
15-30%	25.83	2.34	10.84
>30%	23.39	2.11	5.46

Notwithstanding, these areas suffer from deforestation to open space for several houses in irregular occupations. The urbanization process decreases vegetation in such areas, reducing evapotranspiration. Consequently, soil moisture rapidly increases during rainfall events. When associated with slope overload, leakages, and irregular settlements, the landslides are easily triggered (PRIETO et al., 2017; MENDES et al., 2018a; KÖNIG et al., 2019, 2020, 2022). Similar results were founded by Larsen and Torres-Sanchez (1998). Studying the frequency of landslides in three mountainous areas in Puerto Rico, these authors identified a higher frequency of landslides in the slopes modified by human settlements.

The thematic map of the aspect (Figure 6.29) shows the slope directions. These directions could affect, directly and indirectly, the slope stability, due to the frequency of solar incidence, soil moisture, and vegetation type (VIEIRA, 2007). Table 6.13 presents the distribution of scar concentration, landslide potential, and frequency for each Aspect class.

Table 6.13. Distribution of scar concentration, landslide potential, and frequency in Aspect classes of Guarujá.

Aspect			
Class	**Scar Concentration (%)**	**Landslide Potential (%)**	**Frequency Distribution (%)**
N	25.84	12.87	11.94
NE	5.93	2.95	10.22
E	12.63	6.29	12.27
SE	2.39	1.19	15.27
S	2.36	1.18	11.90
SW	3.10	1.54	10.36
W	10.71	5.33	11.25
NW	37.05	18.45	16.79

Figure 6.29. Aspect map of Guarujá municipality.

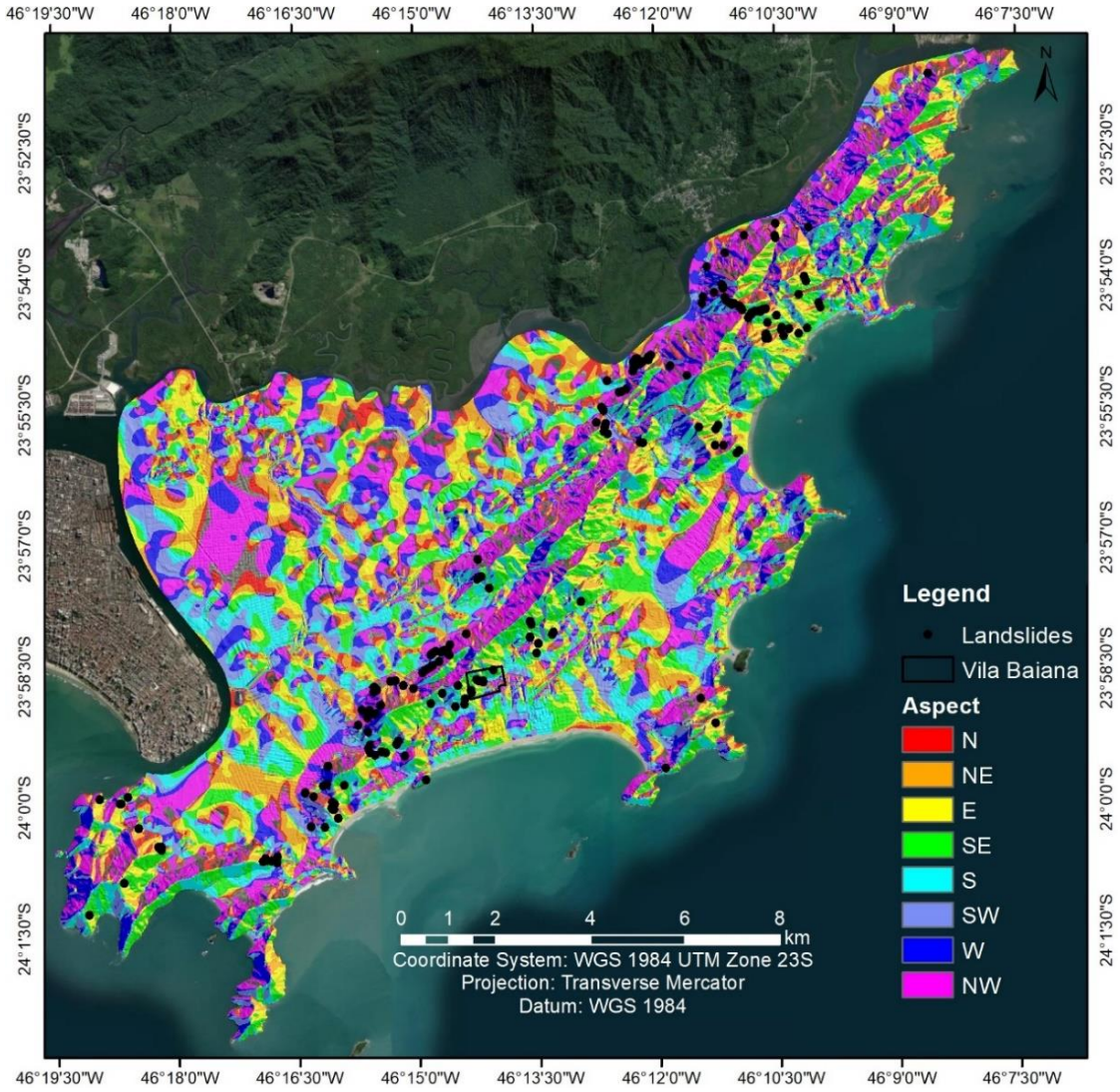

Analyzing Figure 6.29 and Table 6.13, it is observed that most slopes have Northwest (16.79%) and Southeast (15.27%) directions. Additionally, the slopes with a north direction (N, NE, and NW) represent 38.95% of the area, while the south-oriented slopes (S, SE, and SW) occupied 37.53% of the site. Observing the scar concentration, the slopes facing NW present 37.05% of the landslides, and 25.84% happened in the North. Those slopes facing E, NE, and SE sum up 20.94% of the landslides registered, while slopes facing W, SW, and NW sum up 50.86% of documented landslides.

Some studies found a correlation between the slope aspect and landslide susceptibility. For example, both Vieira (2007) and Gao (1993) identified that the most frequent landslides in their respective study areas occur on slopes with a South orientation (S, SE, and SW). However, Guimarães (2000) identified that the susceptibility in the Tijuca watershed is higher on slopes facing NW. A similar result is found in Guarujá; although the frequency of class distribution is similar, the slopes facing NW and N have together 62.89% of the landslide scars. These areas deserve more attention during the rainy season since the landslide susceptibility is higher than in other areas. Further analysis will determine if there is a correlation between landslides with the curvature and pedology.

The curvature map shows if a slope is convex, rectilinear, or concave. The type of curvature is related to the processes of water accumulation and changes in the soil's amount of organic matter and minerals due to gravity. Observing the curvature map (Figure 6.30) and the distribution of frequency, scar concentration, and landslide potential (Table 6.14), it is noticed that 32.63% of Guarujá slopes are concave and 31.19% are convex. The rectilinear areas represented 36.17% of the municipality.

Figure 6.30. Curvature map of Guarujá municipality.

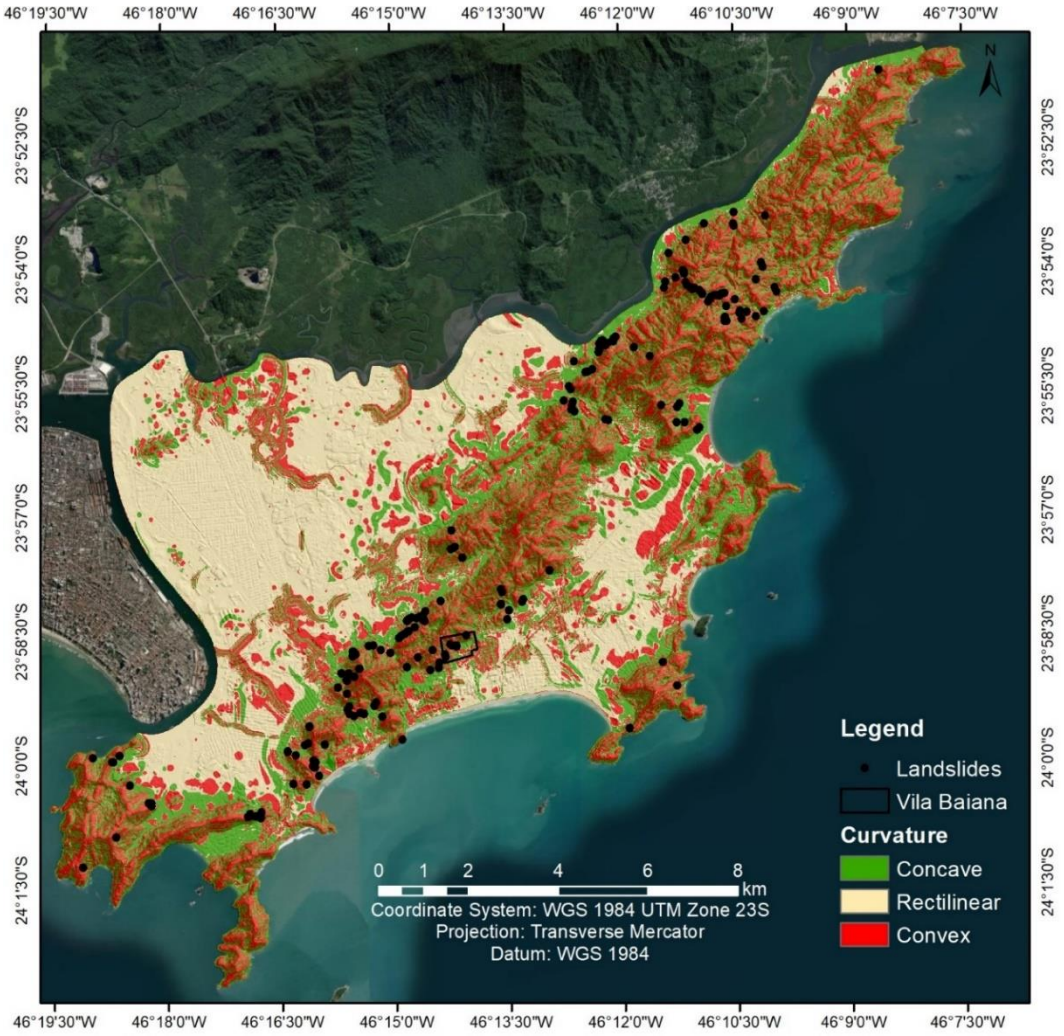

Table 6.14. Distribution of scar concentration, landslide potential, and frequency according to slope's curvature.

Curvature			
Class	**Scar Concentration (%)**	**Landslide Potential (%)**	**Frequency Distribution (%)**
Concave	40.03	0.44	32.63
Rectilinear	0.69	0.01	36.17
Convex	59.28	0.65	31.20

The convex area is usually more susceptible to landslides due to water accumulation and increased soil moisture (CANAVESI et al., 2013). According to IPT (1986 and 1988) and Vieira (2007), the slopes in the Serra do Mar are predominantly rectilinear and steep. In

the mid-slope sectors, the rectilinear and convex profiles alternate, and if associated with declivities above 15%, the landslide susceptibility of the area increases. Analyzing the distribution of the landslide's scars, it is noticed that 59.28% of the landslide happened on a convex slope and 40.03% on a concave one.

Additionally, the landslide susceptibility should be analyzed accordingly to the soil types. Each soil has unique physical properties, and these characteristics change the slope susceptibility. Figure 6.31 shows the correlation map between the landslides and the soils in Guarujá. Table 6.15 presents the landslide scars in each soil class, its distribution, and landslide potential.

Table 6.15. Distribution of scar concentration, landslide potential, and frequency according to pedology classes in Guarujá.

Pedology			
Class	**Scar Concentration (%)**	**Landslide Potential (%)**	**Frequency Distribution (%)**
Urban area	25.44	0.57	26.94
Cambisols	65.12	1.46	34.15
Podzols	0.00	0.00	18.44
Solonchaks	9.43	0.21	13.50
River	0.00	0.00	6.87
Neosoil	0.00	0.00	0.09

Most landslides (65.12%) happened in Cambisols, followed by 9.43% registered in Solonchaks. There is no record of landslides in the Neosoil and Podzol classes. However, 25.44% of the landslides occurred in urban areas on the edge of the Cambisols and steep slopes. Colluvial layers and landfill deposits cover these areas, and as mentioned in item 3.1, this type of soil cover could suffer ruptures and become a landslide (MENDES et al., 2018a). Furthermore, 34.15% of the municipality is covered by Cambisols, and 26.94% is an urban area.

In Guarujá municipality, a combination of geological and physical aspects characterizes the most susceptible areas. Therefore, convex, or rectilinear slopes with altitudes above 30 m, declivities higher than 15%, Cambisols, and urban areas covered by colluvium and landfill deposits are very likely to suffer landslides.

Figure 6.31. Correlation between landslides and pedology in Guarujá.

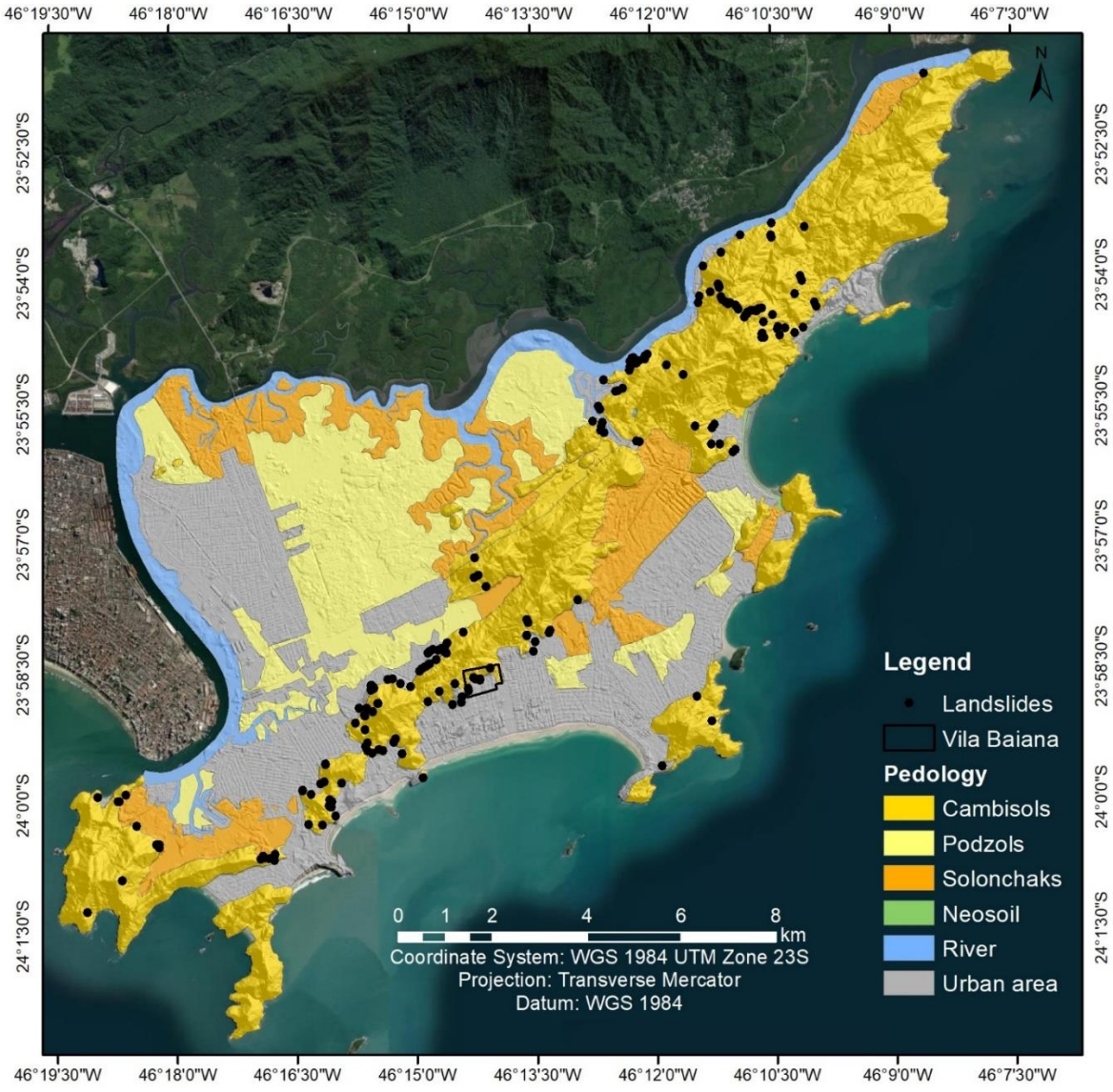

Nonetheless, the soil behavior is modified due to the variation of moisture content, thus, saturated soils can trigger landslides. Further analysis of soil saturation during a landslide event was prepared using the PCD (data acquisition platform) data from CEMADEN.

6.4 Analysis of landslide events and soil moisture

When combined, some geological and physical characteristics increase the probability to develop into a landslide. The knowledge of rainfall intensity and the influence of phenomena such as El-Niño helps to understand the quantity of landslides occurrences, providing a “global” parameter of the situation.

The identification of landslide-prone areas demands more data such as soil moisture. Some landslides happened without rainfall to justify the disaster. In this case, two possible situations could have triggered such events: human influence (anthropic changes in slope) or high soil moisture values. Below it was analyzed the landslides from March 3rd, 2020, and the soil moisture behavior. Soil moisture and pluviometry data were acquired from the CEMADEN PCD, installed in Vila Baiana.

On March 3rd, heavy rainfalls hit Guarujá municipality, and 138 landslides were recorded. According to CEMADEN, the rain gauge registered 320,0 mm in 24 hours, 10% above of what was expected for the entire month (monthly average of 289,66 mm). Figure 6.32 shows the soil moisture and the pluviometry recorded during 72 h (March 1st to March 3rd of 2020) by a PCD installed in Vila Baiana.

Figure 6.32 shows that the accumulated rainfall rapidly increased after 54 hours. An extreme heavy rain occurred in the early morning of March 3rd, increasing the volume of accumulated rainfall. All the sensors indicate that the soil moisture changes agreed with the rainfall intensity. The initial soil moisture (0h) at 0.5m depth was 38.64%, and the sensor's registered the highest value (39.27%) after 60h. The initial soil moisture at the 1.0m depth sensor was 40.94%, with the highest value of 41.49% at 66h. Moreover, the 1.5m sensor depth had minimal variation (0.26%) of soil moisture during the analyzed period. At 0h, this sensor registered soil moisture of 42.92%, and the maximum registered was 43.18% after 66h. At 2m depth, the initial soil moisture was 34.38% and increased to 35.8% after 66 hours. Furthermore, the 2.5m sensor registered initial soil moisture of 46.84%, and after 66h, the sensor indicated an increase of soil moisture to 47.28%. This is the highest soil moisture value documented during this 72 h.

Figure 6.32. Variation of soil moisture and rainfall intensity during 72 h (March 1st to March 3rd of 2020) in Vila Baiana.

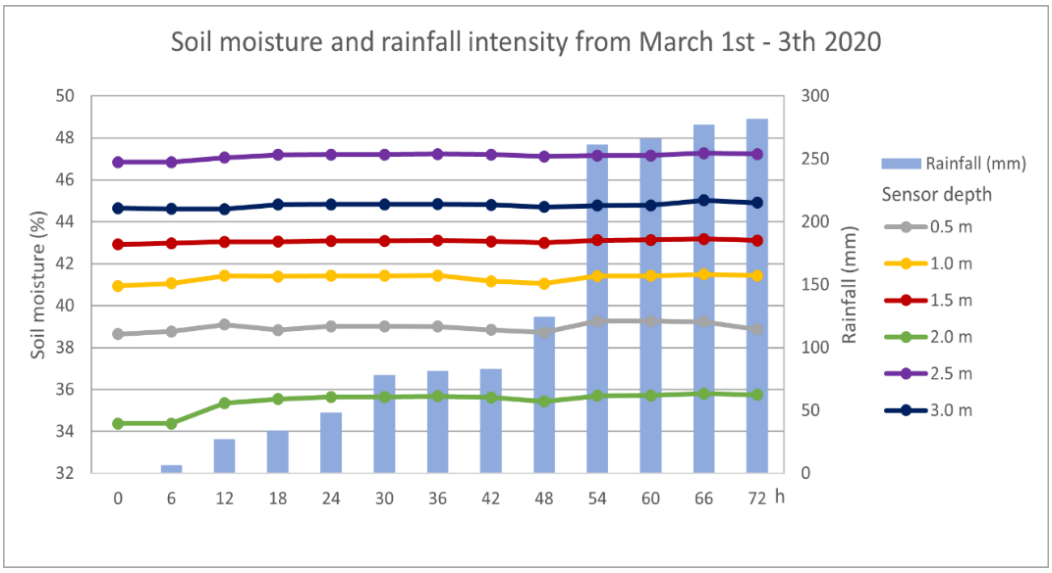

According to CEMADEN (2020), soil moisture of 50% means saturated soil, and with low cohesion between its particles, prone to fractures and landslides. The deepest sensor, at 3m depth, had a different behavior: the initial soil moisture (0h) was 44.65%. During the first 12h, the soil moisture decreases to 44.60%. But due to the rainfall, it increased, reaching 45.02% at 66h.

Despite the soil moisture variation in agreement with the rainfall intensity, it is essential to remind that the initial values of soil moisture at all depths were above 34%, meaning that the soil wasn't very cohesive and had the propensity to fracture and trigger landslides. The soil moisture sensors show lower values on days without rain, as presented in Figure 6.33.

Figure 6.33 represents the soil moisture during 72h, from July 1st to July 3rd, 2022. In July, there are usually fewer rainfall events in Guarujá, with extended drought periods. Therefore, it is possible to compare the soil moisture values during drought and rainfall. Figure 6.33 shows that no rainfall was registered during the 72h considered. The sensor at 0.5m depth indicates a decrease in soil moisture values, from 34.76% at 0h to 34.33 after 72h. Similar behavior is shown at the 1.0m depth sensor: the initial soil moisture (0h) was 38.45% and decreased to 38.35% after 72h. Both sensors at 1.5m and 2.0m depth

presented the minimum variation: initial soil moisture of 40.09% and 30.07%, respectively, with a decrease to 41.02% (at 1.5m) and 29.99% (at 2.0m). A reduction in soil moisture values was also observed at 2.5m depth, yet this sensor had the highest values. At 0h, the soil moisture was 43.86%, and after 72h, the value decreased to 43.74%. At 3.0m depth, the last sensor had initial soil moisture of 38.97% which changed to 38.81% after 72h.

Figure 6.33. Variation of soil moisture and rainfall intensity during 72 h (July 1st to July 3rd of 2022) in Vila Baiana.

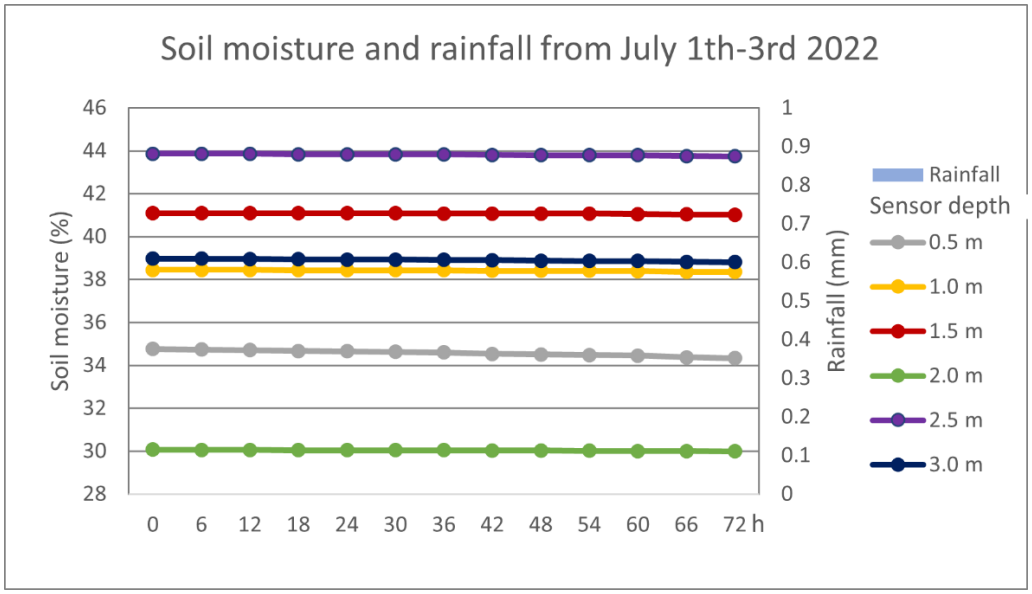

Comparing both soil moisture values presented in Figure 6.32 and Figure 6.33, one verifies that the highest soil moisture values occurred at 2.5m depth. Most of the landslide surface ruptures in Guarujá had depths ranging between 0.5 to 3.0m. During the landslides of March 3rd, 2020, the 2.5m sensor indicated 47.28% of soil moisture. In July of 2022, the lowest soil moisture value registered was 43.74%, meaning that even during periods of drought, the soil moisture at 2.5m is above 40%. Therefore, any rainfall rapidly increases the soil moisture, and this soil layer can be saturated, triggering landslides.

To predict and avoid disasters, the knowledge of the soil's initial conditions, such as soil moisture, besides geotechnical and physical parameters, is necessary.

6.5 Modeling with TRIGRS

The mathematical model TRIGRS was chosen to determine the landslide-prone areas in Guarujá municipality and the Vila Baiana neighborhood. As mentioned in Section 3.4, this model calculates the Factor of Safety (FS) variation using the soil's physical and hydrological parameters.

The geotechnical parameter used to model the landslide-prone areas were acquired from Wolle (1988) and are presented in Table 6.16.

To verify the influence of the soil moisture in the initial conditions for the assessment of slope stability, a comparison between the FS of Vila Baiana and Guarujá between March 3rd, 2020, and July 1st, 2022, was performed using the model TRIGRS.

Table 6.16. Geotechnical parameters used as TRIGRS inputs.

Zones	Depth (m)	Cohesion (kPa)	Internal friction angle (º)	Hydraulic Conductivity (m/s^{-1})	Hydraulic Diffusivity (m/s^{-1})	Specific Weight (kN/m^3)
1	0 - 1m	4.00E+03	39	1.0x10-5	6.0x10-6	1.95E+04
2	1 -2m	1.00E+03	34	1.0x10-5	6.0x10-6	1.71E+04

In March 2020, during the summer and rainy seasons, the soil moisture was higher (as presented in Section 6.4), whereas in July 2022, during the dry winter season, there are lower soil moisture levels. Table 6.17 shows the rainfall values used for both periods. The results of the comparison between the landslide-prone areas from March 1st, 2020, and July 1st, 2022, are presented in Figure 6.34 for Guarujá municipality and Figure 6.35 for Vila Baiana. Black circles in both figures highlight areas with major changes in the FS.

Table 6.17. Rainfall values were used as inputs for March 1st, 2020, and July 1st, 2022.

Date	Rainfall (m/s)
March 1st 2020	5.21x10-7
July 1st 2022	2.31x10-8

Regarding Figure 6.34 and Figure 6.35 it is observed that on March 1st of, 2020, more areas are susceptible to landslides, with FS < 0.5. On July 1st of, 2022, some areas that had

FS< 0.5 in March 2020 now display FS 0.5 – 1.2. The black circle in both images indicates areas with expressive changes in the FS. Table 6.18 presents a comparison with the proportion of areas according to FS.

Table 6.18. Comparison between the proportion of stability classes on March 1st of 2020 and July 1st of 2022 for both Vila Baiana and Guarujá.

	Count (%) class Vila Baiana		**Count (%) class Guarujá**	
	March 1st 2020	**July 1st 2022**	**March 1st 2020**	**July 1st 2022**
FS < 0.5	6.07	3.99	4.05	1.14
0.5 - 1.0	16.58	16.71	14.94	14.06
1.0 - 1.2	21.59	22.40	11.84	14.95
1.2 - 1.5	6.10	7.12	2.58	3.07
FS > 1.5	49.66	49.79	66.60	66.78

Figure 6.34. Comparison between landslide-prone areas from March 1st, 2020, and July 1st, 2022, for Guarujá.

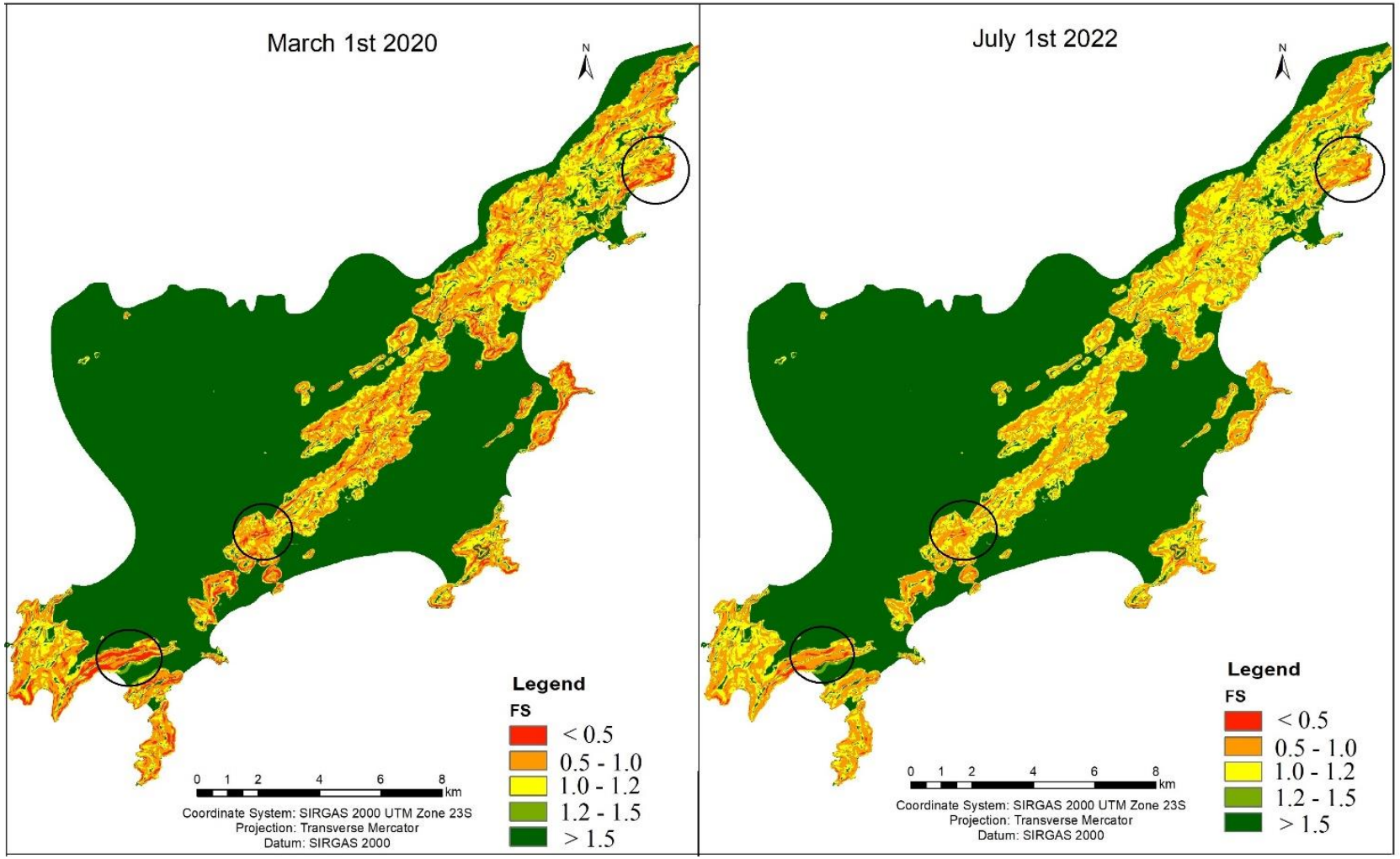

Figure 6.35. Comparison between landslide-prone areas from March 1st, 2020, and July 1st, 2022, for Vila Baiana.

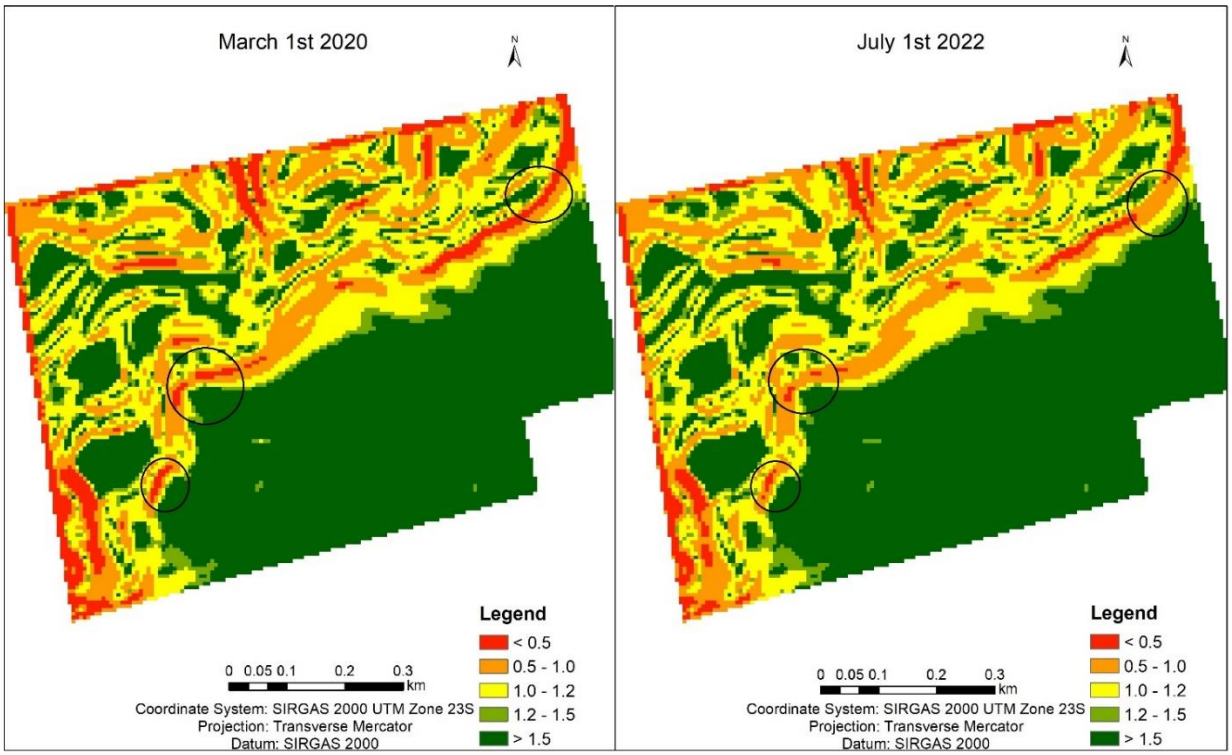

Analyzing Table 6.18, it is noted that in March 2020 at Vila Baiana, 6.07% of the area had FS<0.5, while in July 2022, only 3.99% of the area presented FS lower than 0.5. A similar pattern is observed in Guarujá: 4.05% of the area has FS<0.5 in March 2020, and only 1.14% during July 2022. These results indicate that these areas easily decrease the FS during rain events and, consequently, must be monitored cautiously.

However, even during periods of drought, there are slopes with FS< 0.5, which means that these areas are very unstable and have a high chance of suffering from soil ruptures. Besides that, fewer changes in the proportion of regions with FS between 0.5 -1.0 are noticed. In Vila Baiana, 16.58% of the areas have FS between 0.5 and 1.0 during March, while in July, the proportion is 16.71%. For Guarujá, in 2020, 14.94% of the areas have FS from 0.5 to 1.0, and 14.06 in 2022. These areas are unstable, no matter if it is a rainy or drought season and must be constantly monitored to avoid disasters.

To determine if the model TRIGRS is suitable to become an early warning system, a rainfall period was chosen to analyze how the model calculates the FS variation. From

February 29th to March 3rd, several heavy rainfalls occurred in Guarujá and triggered landslides (CEMADEN, 2020). Table 6.19 shows the precipitation levels used in TRIGRS.

Table 6.19. Rainfall values from February 29th to March 3rd of 2020.

Date	Time (h)	Rainfall (m/s)
Feb 29	24h	1.8x10-7
March 1	48h	5.21x10-7
March 2	72h	8.4x10-7
March 3	96h	1.96x10-6

Modeling 96 hours allows to observe the changes in slope stability. With several consecutive rainy days, the soil moisture increases, and consequently, the slope stability decreases. The variation of the Factor of Safety represents the changes in slope stability, indicating those areas are more susceptible to a soil rupture. Figure 6.36 and Figure 6.37 present the results of the FS variation from February 29th to March 3rd in Guarujá and Figure 6.38 in Vila Baiana.

In Figure 6.36, Figure 6.37, and Figure 6.38, it is noteworthy that the FS changes are in agreement with the rainfall intensity. On February 29th, the volume of rainfall registered was 15.51 mm, and only a few sections had a FS<1 (represented in red). During the next 72h, March 1st and 2nd, the rainfall volume was 45.05 mm and 52.78 mm, respectively. Due to the increase in soil moisture and the constant rainfall, more areas become susceptible to landslides, which is represented by the increase of areas with FS<1. On March 3rd, heavy rainfall in Guarujá triggered several landslides. After 96h and four days of consecutive rainfall, most areas of Vila Baiana have a FS<1, and several landslides were registered in areas with FS<0.5.

The results show that the FS changes agree with the rain intensity and duration. The landslide scars corroborate with the areas computed by TRIGRS as unstable (FS<1), validating the model´s performance. To validate the TRIGRS modeling, a landslide inventory was used. The landslide scars were collected from both satellite images of Google Earth and documents from Guarujá Civil Defense. Moreover, 197 landslides were registered in the landslide inventory from 2019-2020, which were used to validate the TRIGRS results.

Figure 6.36. FS variation from February 29th to March 3rd in Guarujá.

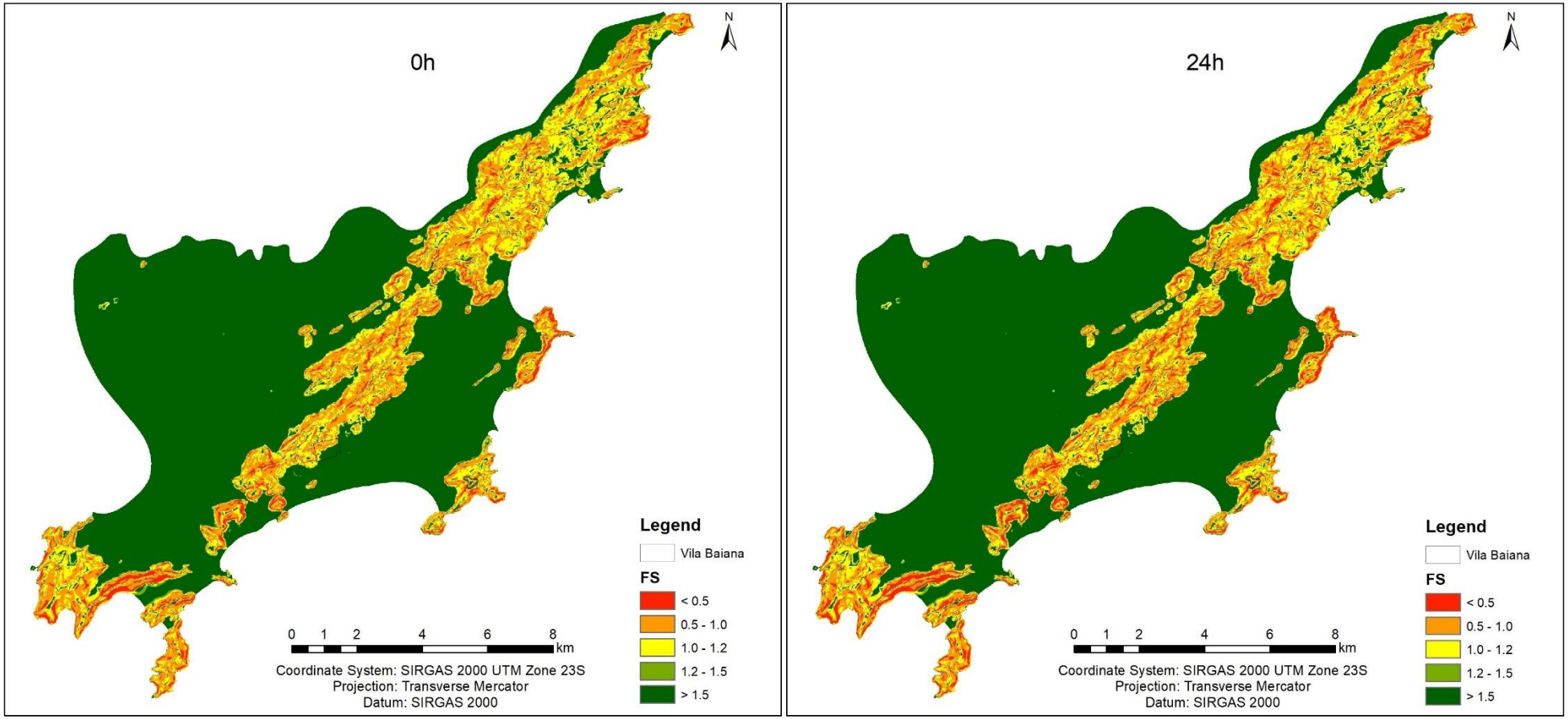

Figure 6.37. FS variation from March 2nd and 3rd in Guarujá.

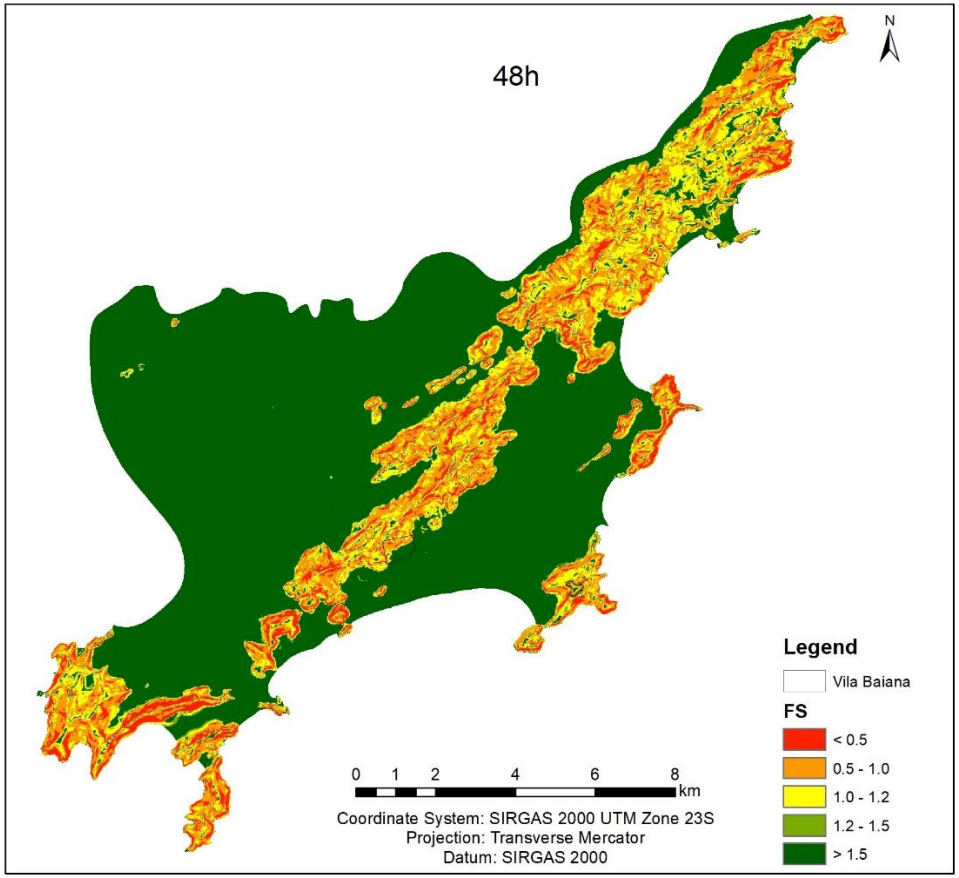

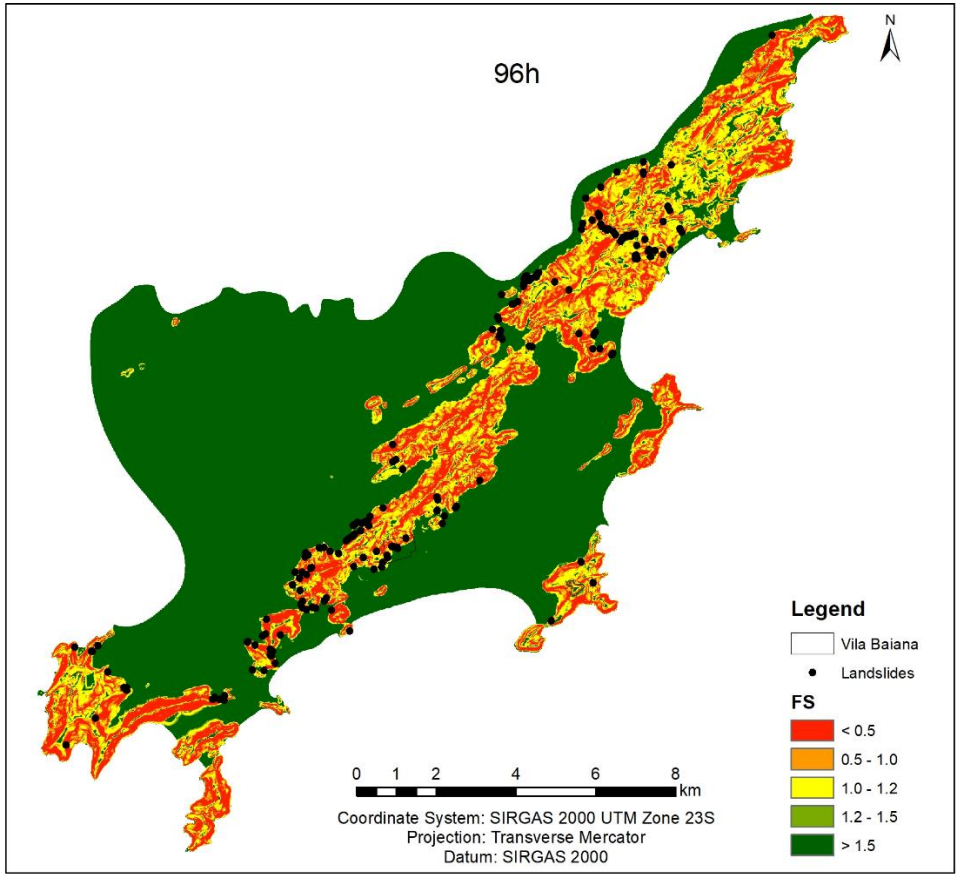

Figure 6.38. FS variation from February 29th to March 3rd in Vila Baiana.

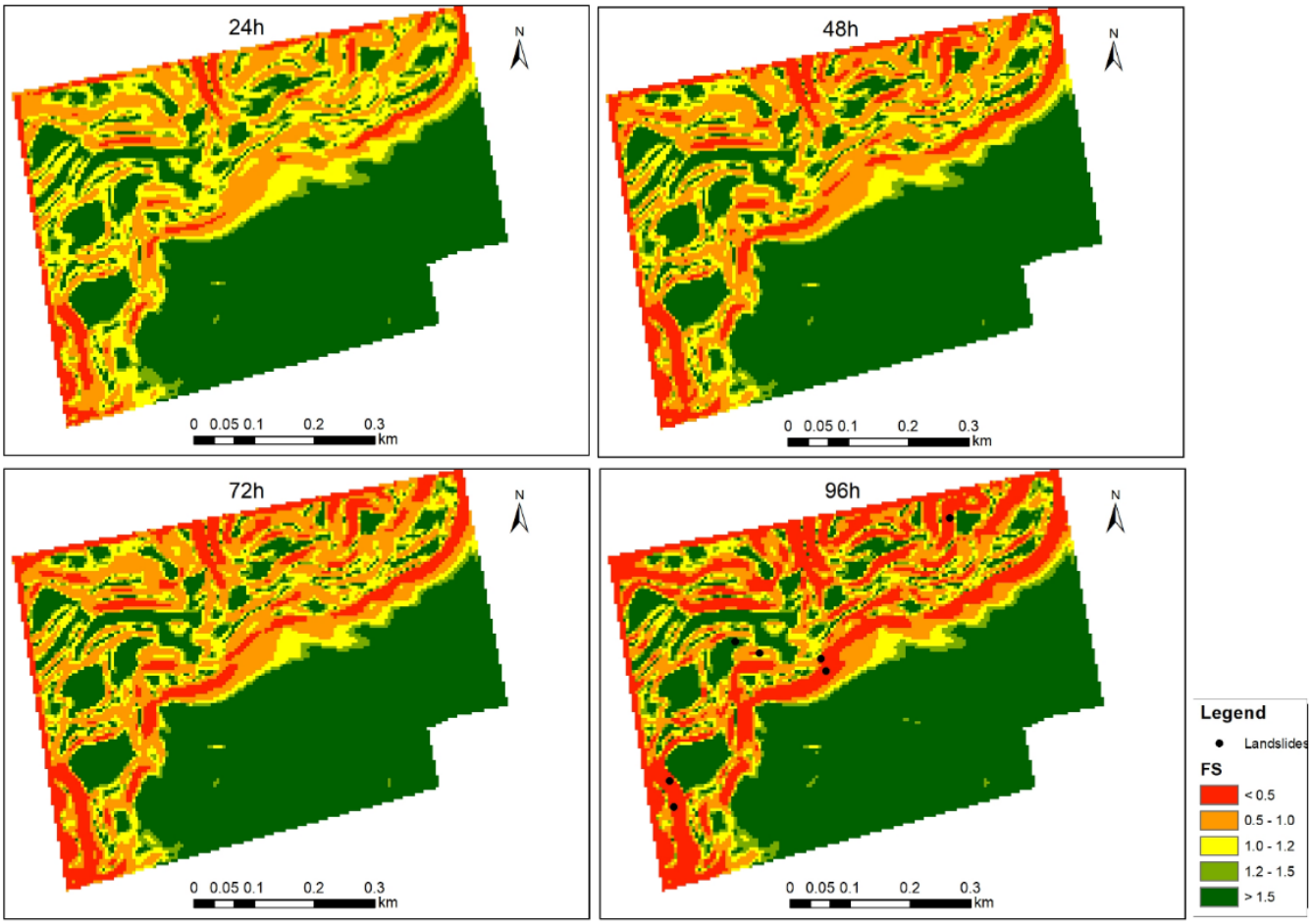

Two statistical indexes were defined to confirm TRIGRS efficiency: the Success Index (SI) and the Error Index (EI). The SI, presented in Equation 6.2, corresponds to the percentage of correctly classified unstable classes, and the EI (Equation 6.3) indicates when the computed unstable class does not correspond to verified landslide scars (SORBINO et al., 2010; SCHWARZ; MICHEL, 2016; PAUL et al., 2018; CIURLEO et al., 2019; KÖNIG et al., 2022).

$$SI = \left(\frac{A_{in}}{A_{uns}}\right) * 100 \tag{6.2}$$

The variable A_{in} is the computed unstable areas within the triggering areas, and A_{uns} are the triggering areas.

$$EI = \left(\frac{A_{out}}{A_{stb}}\right) * 100 \tag{6.3}$$

The variable A_{out} is the computed unstable areas outside the triggering areas, and A_{stb} is the stable area.

This statistical index was calculated only for Guarujá municipality because in Vila Baiana, on March 3rd, 2020, only seven landslides were registered, which is not enough to calculate statistical indexes. Table 6.20 presents the SI and EI index for Guarujá municipality.

Table 6.20. Success and Error index for Guarujá municipality.

Location	Success Index (SI)	Error Index (EI)
Guarujá	54.24 %	17.11%

Analyzing the SI and EI of TRIGRS results, it is observed that the model had a SI of 54.24% and an EI of 17.11%. High values of SI and lower values of EI indicate the model's efficiency in correctly identifying landslide-prone areas and its usefulness as an early warning tool. Notwithstanding, the scar concentration (SC), landslide potential (LP), and Frequency of distribution (Fd) were calculated to improve the validation of the TRIGRS results. These indexes' results are presented in Figure 6.39.

Figure 6.39. Scar concentration, landslide potential, and Frequency of distribution for March 3rd of 2020 in Guarujá.

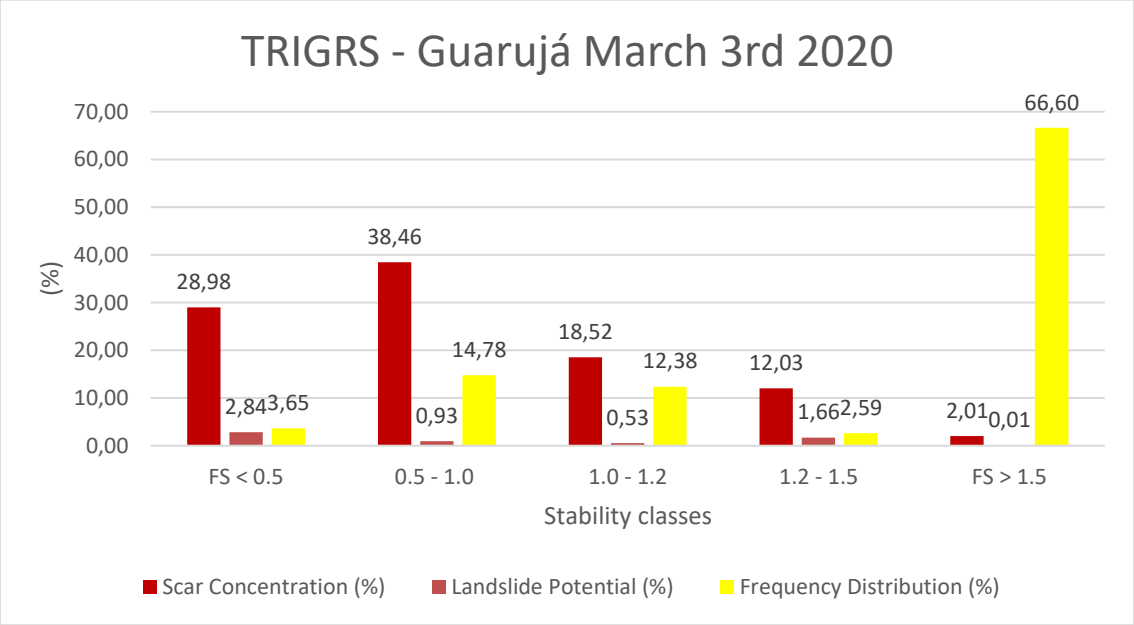

Figure 6.39 shows that 67.44% of the landslide scars are in FS < 1.0, and these classes represent 18.43% of the Guarujá area. The classes considered stable (FS > 1.0) have landslide scars (32.56%), which corroborates the assumption that anthropic influences enhance the chances of soil rupture.

Therefore, it is important to analyze the correlation among the susceptibility map from IPT, the landslide inventory, and TRIGRS results. Figure 6.40 presents the IPT susceptibility map and the landslide occurrences.

Figure 6.40. IPT's susceptibility map of Guarujá and landslide occurrences.

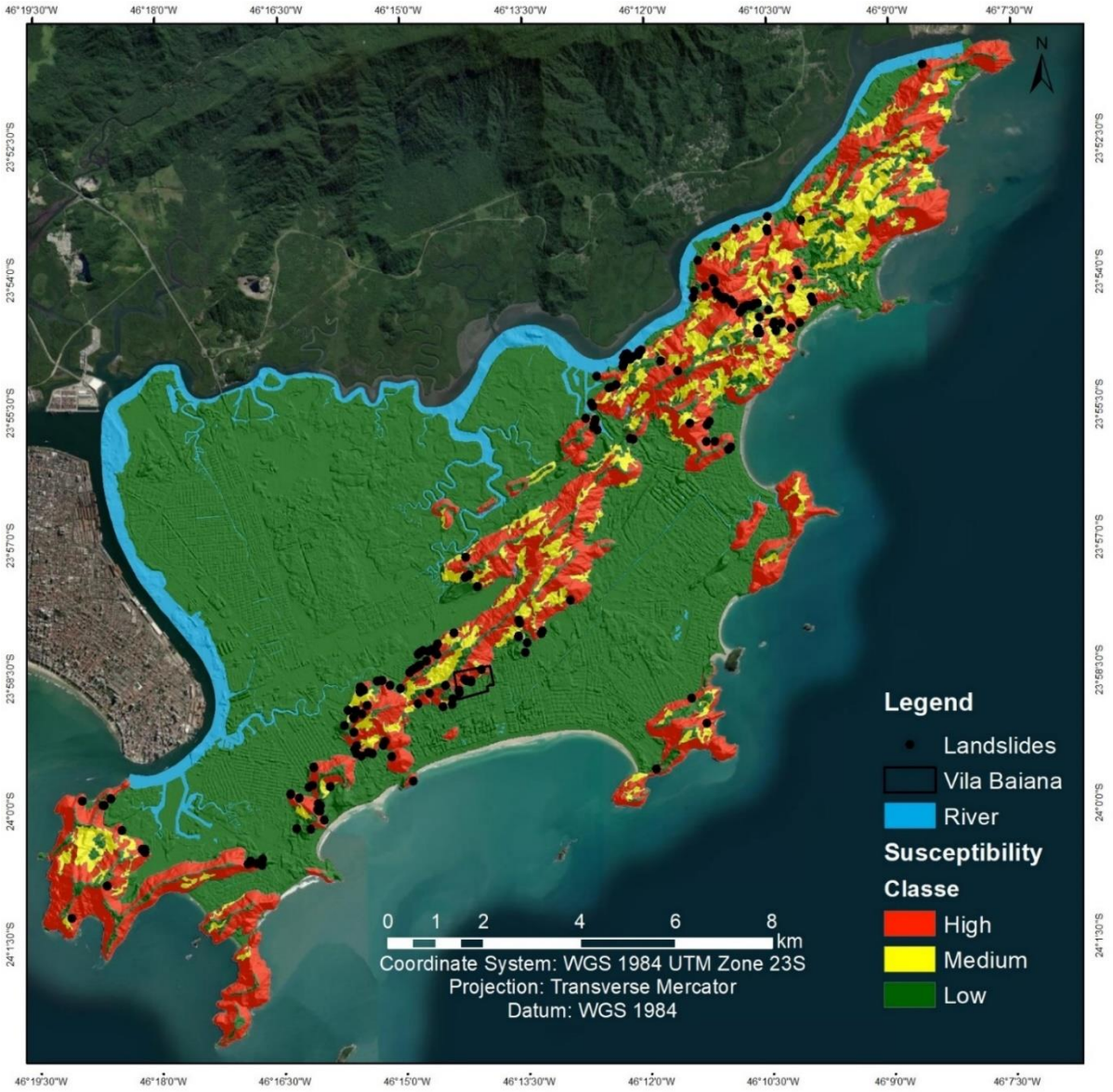

Figure 6.40 shows that most declivity areas have high or medium levels of susceptibility, with several landslides recorded. The areas with a high level of susceptibility registered 83.93% of the landslides. Areas with medium susceptibility levels recorded 7.14% of landslides and 8.93% in classes with a low level of susceptibility.

Figure 6.41 shows the comparison between the instability areas from TRIGRS (FS< 1.0) and the IPT susceptibility map. The red color is usually used to represent the most unstable areas. To differentiate the landslide-prone areas, a light red was applied to indicate TRIGRS unstable areas, and yellow to represent the IPT unstable areas.

Figure 6.41. Comparison between the instability areas from TRIGRS and IPT susceptibility map.

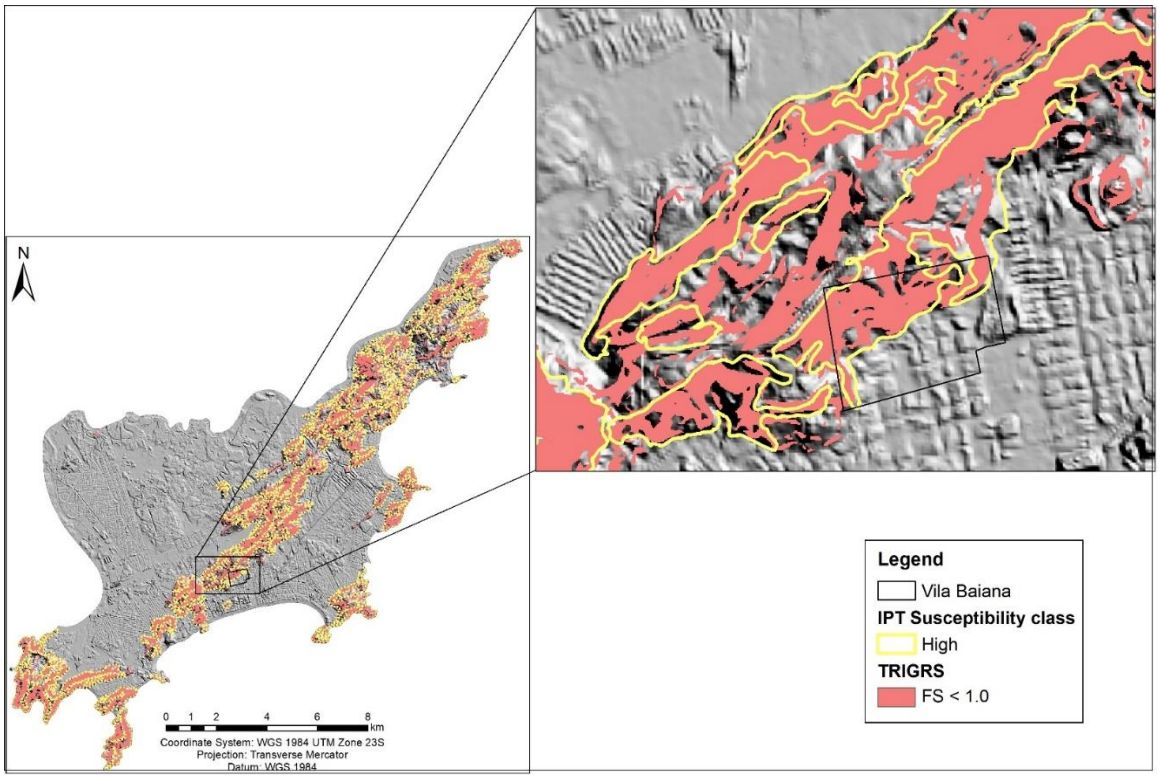

Figure 6.41 shows that TRIGRS unstable areas match the high susceptibility class from the IPT map. The results show the applicability of TRIGRS to identify the landslide-prone areas in Guarujá, and the possibility to be applied as an early warning system for landslides.

6.6 Modeling with SINMAP

With a different approach, the mathematical model SINMAP is a probabilistic model to determine the landslide-prone areas in Guarujá municipality and the Vila Baiana neighborhood. The Stability Index (SI) indicates the most susceptible areas.

The SINMAP uses a range of values (lower and higher values) to determine the landslide-prone areas. Therefore, the range of values is the same parameters used in both scenarios of the TRIGRS model. Table 6.21 presents the geotechnical parameters used in SINMAP, which were acquired from Wolle (1988). Figure 6.42 shows the SINMAP model result for Guarujá municipality, and Figure 6.43 for Vila Baiana.

Table 6.21. Geotechnical parameters used in SINMAP.

	Cohesion (kPa)	**Internal friction angle (º)**	**T/R (m/h)**	**Hydraulic Conductivity (m/ s^{-1})**	**Specific Weight (kN/m^3)**
Lower	4.00E+03	39	46	1.0x10-5	1.71E+04
High	1.00E+03	34	142	1.0x10-5	1.71E+04

Analyzing the results of the landslide-prone areas of Guarujá (Figure 6.42), it is observed that the lower and upper threshold limits encompassed more than 17.11% of the area, characterizing the area as a region with a high probability of landslides. However, the stable class, which represents the flat area of Guarujá, represents 74.05% of the municipality area. Therefore, excluding the stable class, it is observed that 65.92% of the area has high susceptibility to landslides.

For Vila Baiana, the lower and upper threshold limits represent 27.75% of the area. By excluding the stable class, which represents 57.72% of the neighborhood, the landslide-prone area is 65.65%. Moreover, three landslides were registered in the lower threshold limit, two in the Quasi-stable class, and two in the Moderate-stable limit.

To validate the SINMAP results, the Success Index (SI), Error Index (EI), Scar Concentration (SC), Landslide Potential (LP), and Frequency of distribution (Fd) were calculated. The statistical indexes were calculated for Guarujá only, due to the lower value of landslides (only seven) in Vila Baiana. The SI and EI results are presented in Table 6.22.

Table 6.22. SINMAP's Success and Error indexes.

SINMAP	
Success Index (SI)	**Error Index (EI)**
17.48	6.71

The statistical index of SINMAP identified a Success Index of 17.48 and a 6.71 Error Index. The model has lower values of SI and EI, indicating that the model's performance was not satisfactory. To understand the model's SI and EI, it is necessary to analyze the correlation between the landslides and the model's unstable areas.

Figure 6.42. Results of landslide-prone areas with Sinmap model for Guarujá.

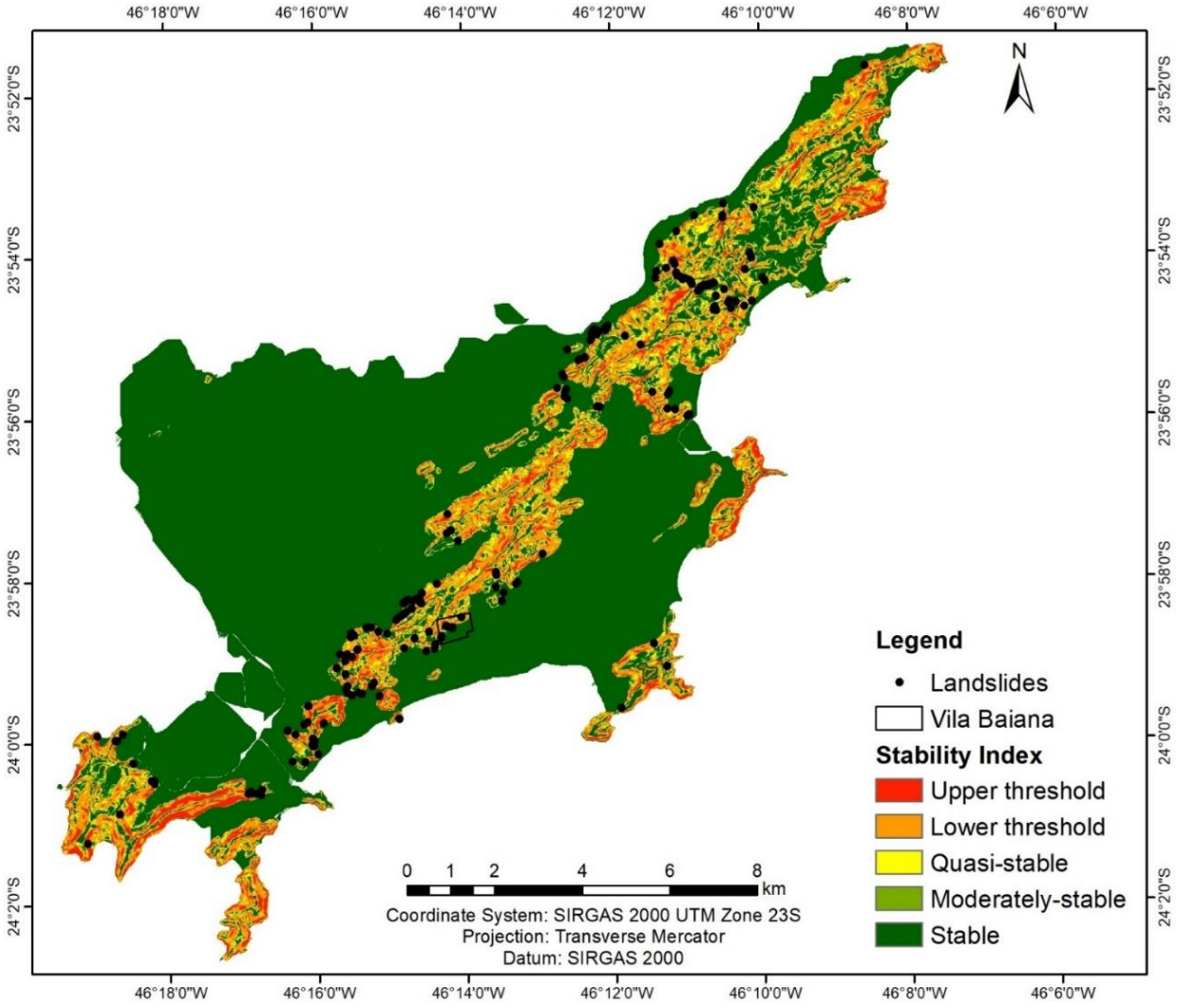

Figure 6.43. Results of landslide-prone areas with Sinmap model for Vila Baiana.

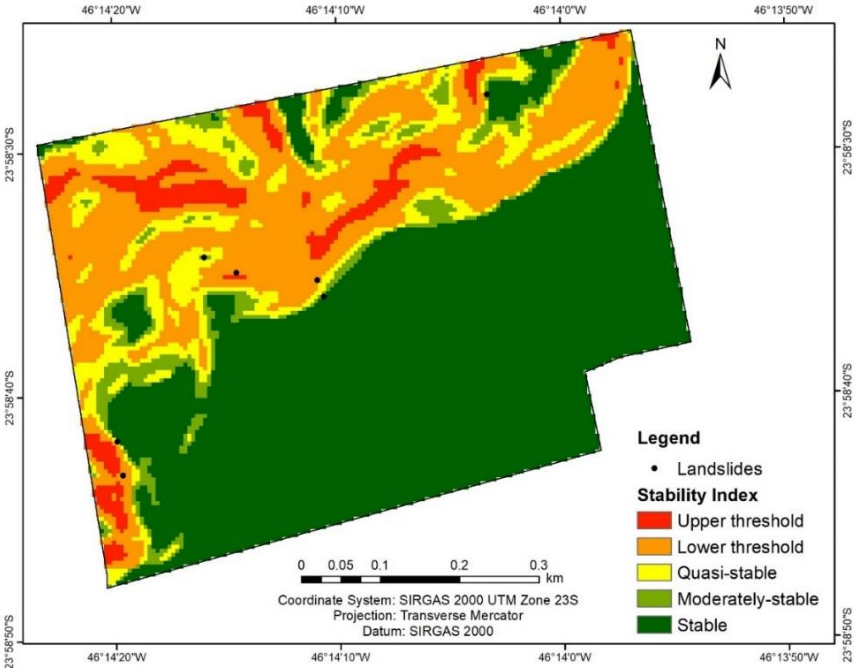

Figure 6.44 shows the values of Scar Concentration, Landslide Potential, and Frequency of distribution.

Figure 6.44. SC, LP and Fd of SINMAP model for Guarujá.

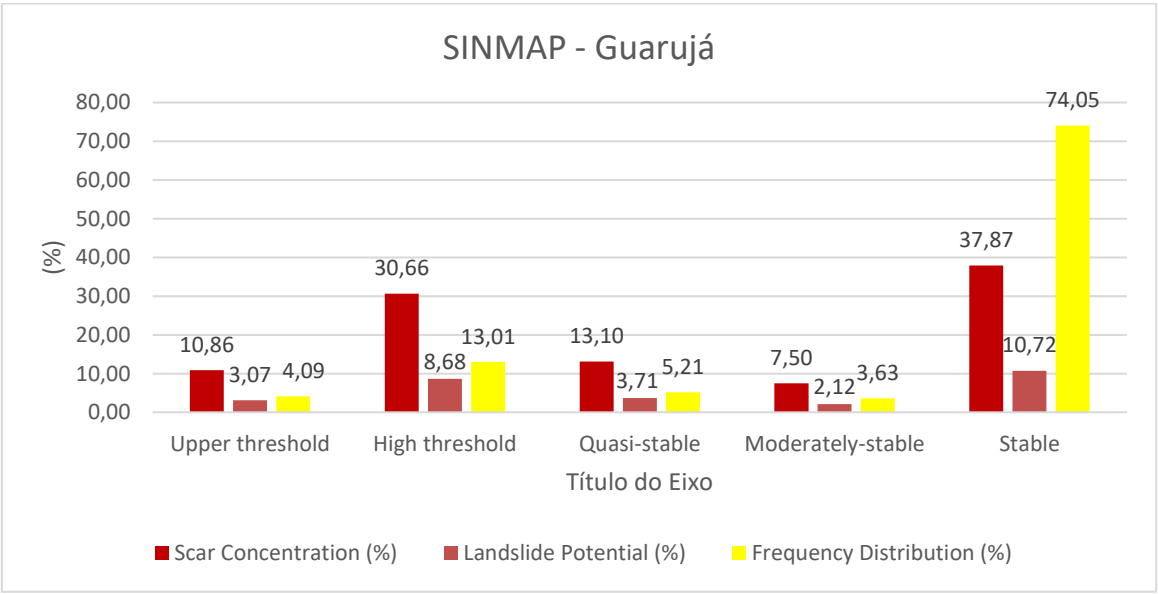

Figure 6.44 identified that 37.87% of the landslide scars happened in the stable class, followed by a high threshold limit (30.66%). The upper threshold limit has 10.86% of the landslide's scars, while the Quasi-stable class has 13.10%. These values corroborate with the Success and Error index (Table 6.22) since several landslides' scars were in areas with medium or low susceptibility.

The SINMAP results were compared with the IPT susceptibility map, as presented in Figure 6.45. The red-light color indicates the unstable classes from the SINMAP (SI < 1.0) and in yellow the high susceptible areas from the IPT map.

Figure 6.45. Comparison between SINMAP unstable areas and IPT susceptibility map.

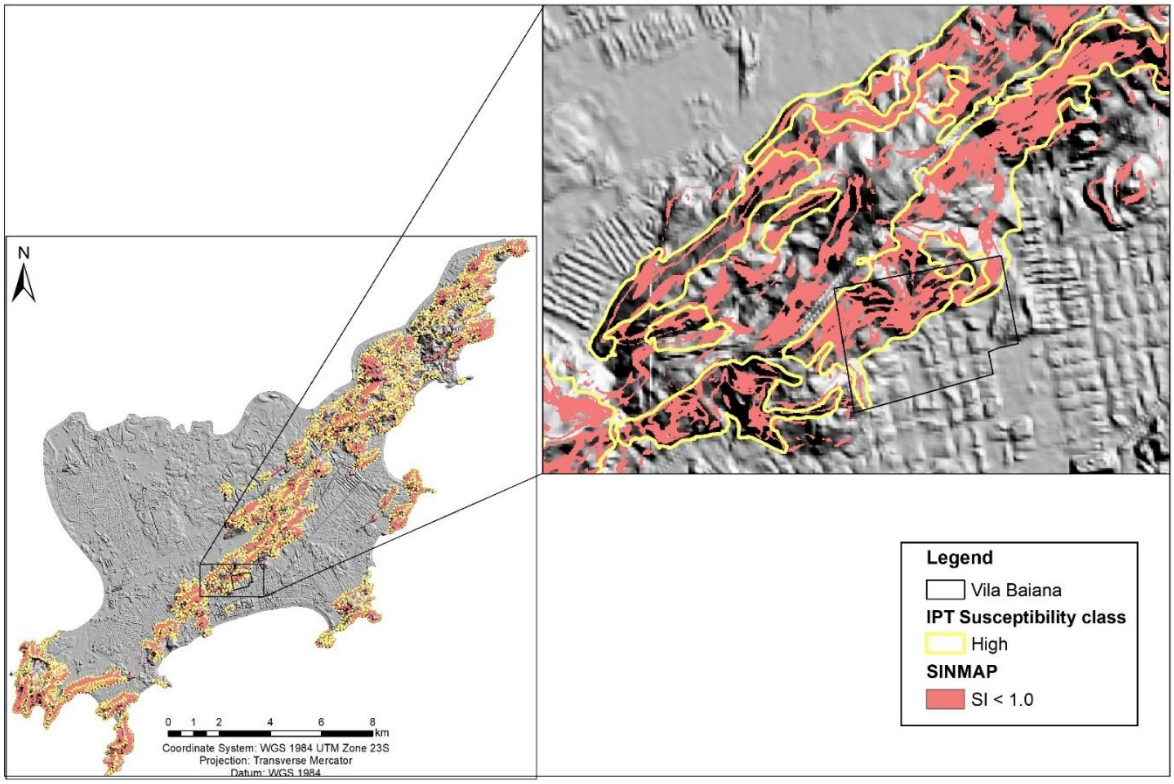

Figure 6.45 shows that the probabilistic model SINMAP classified fewer areas as unstable than the IPT map. This result confirms the lower value for the SI index and explains why several landslides were in areas with medium or low susceptibility. The model underestimates the landslide-prone areas.

6.7 Comparison between TRIGRS and SINMAP results

The two mathematical models TRIGRS and SINMAP were applied to identify the landslide-prone areas. Due to the specificity of each model, the results are different. Their different approach was summarized in Table 6.23.

Table 6.23. Comparison between SINMAP and TRIGRS different approaches.

	SINMAP	**TRIGRS**
Input parameters	Cohesion	Cohesion
	Internal friction angle	Internal friction angle
	R/T	Soil depth
	DEM	DEM
		Hydraulic Conductivity
		Hydraulic Diffusivity
		Rainfall
Data from the study area	Multi-resolution calibration	Parameter cell by cell
Output results	Stability Index (SI)	Factor of Safety (FS)
Output File format	Shapefile	ASCII
Interface	ArcView 3.3	Command Line
Mathematical approach	Probabilistic	Deterministic

Therefore, the reliability of both models was evaluated through the Contingency table (FAWCETT, 2006), and SI/EI index (SORBINO; et. al., 2010). Figure 6.46 presents the comparison between the SINMAP and TRIGRS results for Vila Baiana.

Figure 6.46. Comparison between SINMAP and TRIGRS results for Vila Baiana.

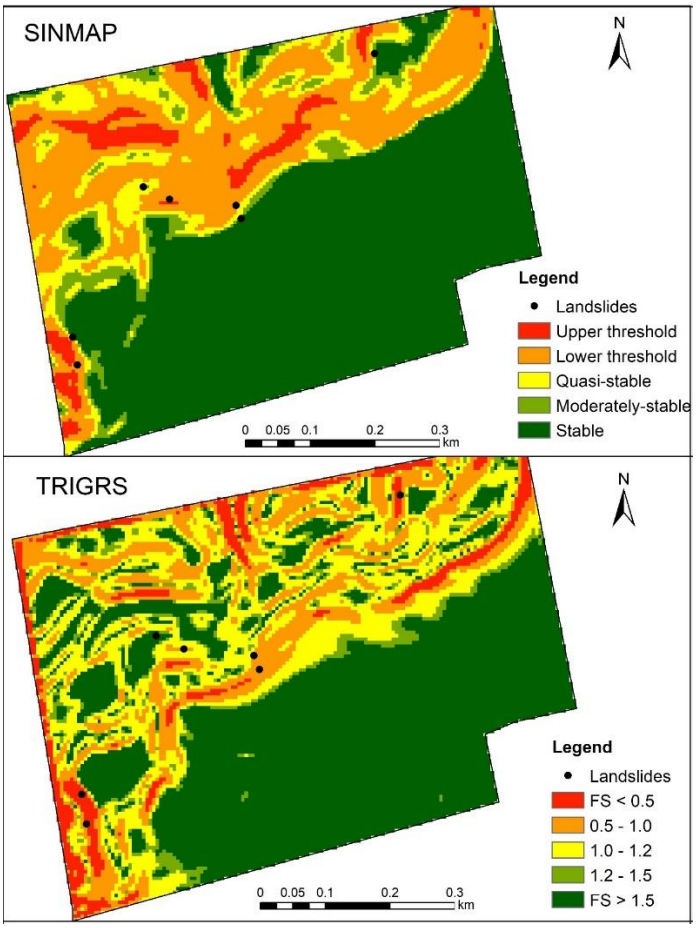

Observing Figure 6.46, there is a visual difference in the unstable classes for both models. The SINMAP model classified 27.75% of areas within the upper and lower threshold limit (SI < 1.0) and the TRIGRS model identified 22.65% of the area as unstable (FS <1.0). Moreover, the probabilistic model classified only 5.21% of Vila Baiana as Quasi-stable (1.0 > SI < 1.2), and TRIGRS computed 21.57% of the area. The model SINMAP estimated 63.05% of Vila Baiana as stable (SI > 1.2; Moderately stable and stable limits) and 55.78% of the area for TRIGRS. Figure 6.47 presents the comparison between stability classes computed by both models.

Figure 6.47. Stability classes computed by TRIGRS and SINMAP for Vila Baiana.

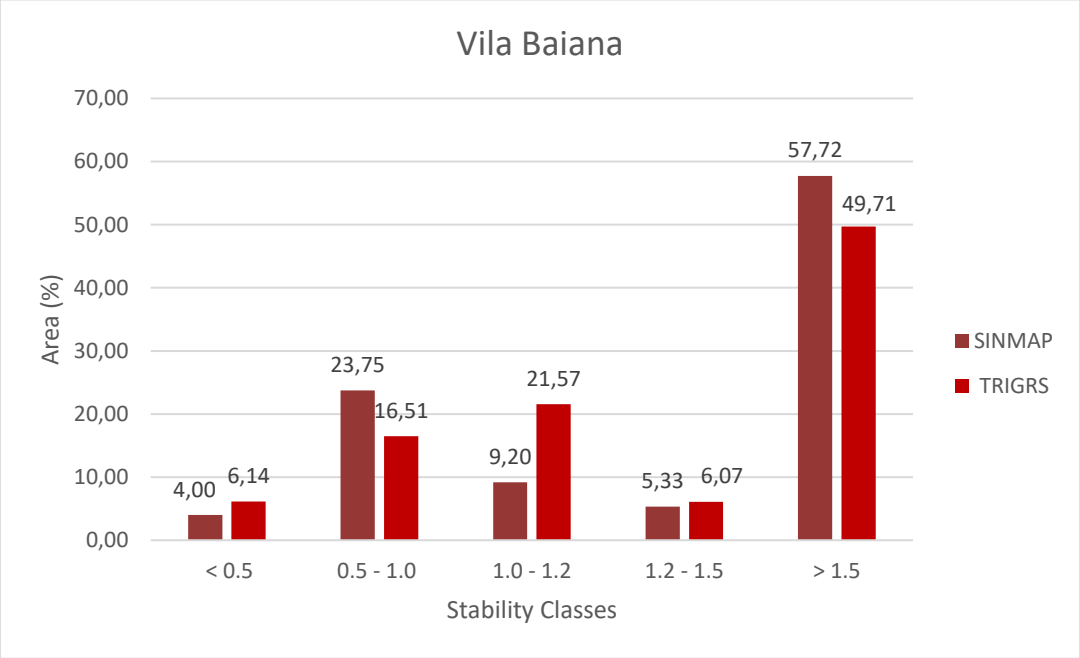

Figure 6.48 shows the comparison between SINMAP and TRIGRS results for Guarujá municipality, and the stability areas computed by both models are presented in Figure 6.49.

TRIGRS model estimated 18.98% of the study area as unstable (FS < 1.0), while SINMAP calculated 17.11% of areas with SI < 1.0 (upper and lower limits). Notwithstanding, the probabilistic model determined 5.21% of the area as Quasi-stable (1.0 > SI < 1.2), and TRIGRS computed that 11.83% of Guarujá has 1.0 > FS < 1.2. The stable classes represented 69.19% of the municipality for TRIGRS and 77.68% for SINMAP.

Figure 6.48. Comparison between SINMAP and TRIGRS results for Guarujá.

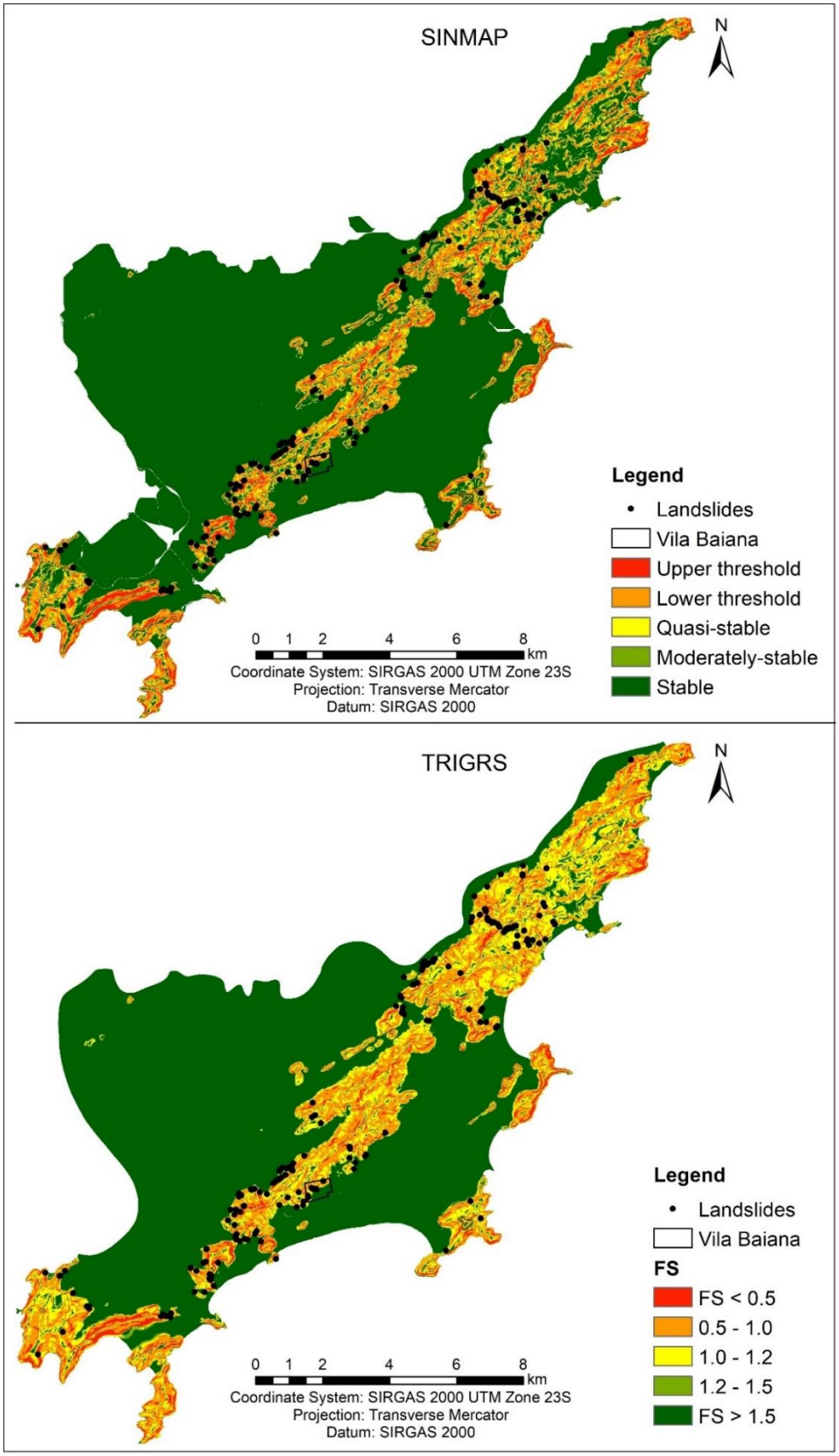

Figure 6.49. Stability classes computed by TRIGRS and SINMAP for Guarujá.

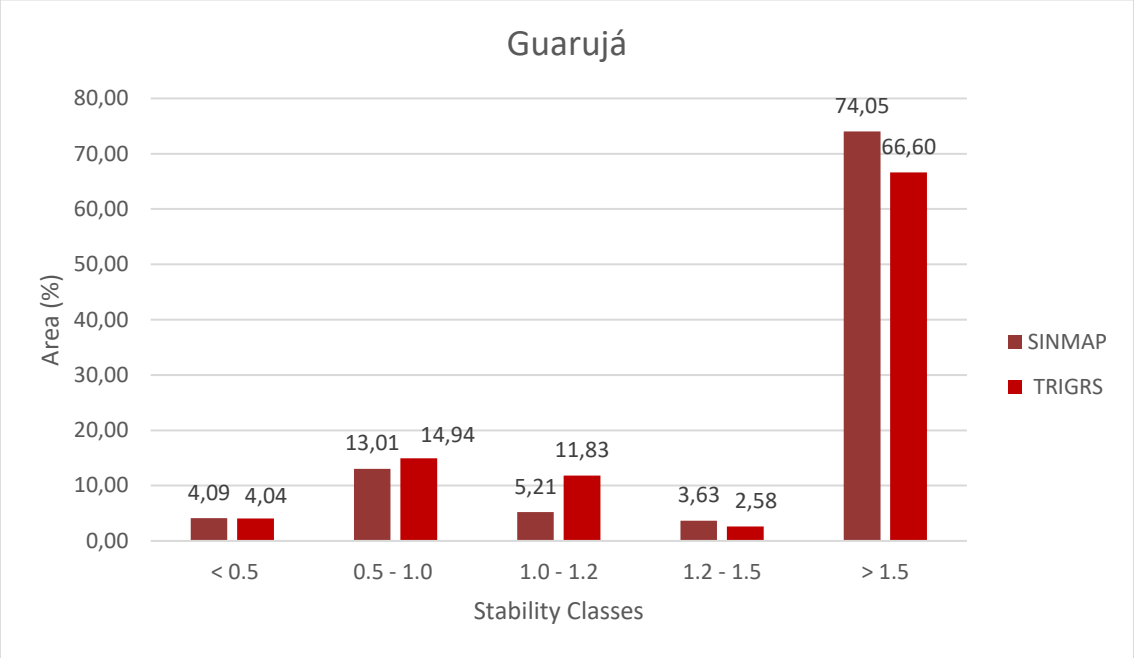

Comparing the SI and EI indexes from both models (Table 6-24), the model SINMAP had a lower value of SI and EI than TRIGRS. According to Sorbino et al., (2010), the ratio between SI and EI indicates the model's efficiency to represent the area's reality. The model with a higher value of SI/EI had the best performance.

Table 6.24. Comparison between Success and Error indexes from both mathematical models.

Model	Success Index (SI)	Error Index (EI)	SI/EI
SINMAP	17.48	6.71	2.60
TRIGRS	54.24	17.11	3.17

The analysis of Table 6.24, shows that TRIGRS had the best performance to identify landslide-prone areas in comparison with SINMAP.

The contingency table, based on Fawcett (2006), is a two-by-two confusion matrix, that compares the model's results. The comparison is determined by the four outcomes: true positive (TP), false negative (FN), true negative (TN), and false positive (FP). For a landslide analysis, the TP is when a landslide occurred in unstable areas. A false negative

is a landslide in stable areas. True negative refers to stable areas without landslides scars, and False positive is related to unstable areas without landslides. Table 6.25 presents the contingency table. Therefore, the following indexes can be determined: accuracy, precision, sensitivity, and specificity, as presented in Table 6.26. The performance is determined by the ratio between sensitivity and the False Positive Ratio (FPR); thus, higher values indicate better performance.

Table 6.25. Contingency table, based on Fawcett (2006).

Positive (P)	**Negative (N)**
True Positive (TP)	False Positive (FP)
False Negative (FN)	True Negative (TN)

Table 6.26. Statistical indexes are calculated from the Contingency table.

Index	**Parameters**	**Performance**
Accuracy	$\frac{VP + VN}{P + N}$	$\frac{Sensitivity}{FPR}$
Precision	$\frac{TP}{TP + FP}$	
Sensitivity	$\frac{TP}{P}$	
Specificity	$\frac{TN}{FP + TN}$	
False Positive Ratio (FPR)	$\frac{FP}{N}$	

Table 6.27 presents the results of the contingency table for both TRIGRS and SINMAP.

Table 6.27. Contingency table for SINMAP and TRIGRS models.

Index	SINMAP	TRIGRS
Accuracy	0.829	0.820
Precision	0.003	0.026
Sensitivity	0.415	0.965
Specificity	0.829	0.819
False Positive Ratio	0.171	0.181
Performance	**2.435**	**5.348**

The analysis of Table 6.27 shows that the TRIGRS model had a better performance than SINMAP. Since SINMAP is a probabilistic model, there is a tendency to overestimate the unstable areas. The best model to identify unstable areas is that one whose results of the most unstable class coincide with the landslides scars, and which represents the minor area of the study basin (HUANG; KAO, 2006; DIETRICH; et. al., 2011; PARK; et. al., 2013; ZIZIOLI et al., 2013; MICHEL; et. al., 2014; NERY; VIEIRA, 2015).

The TRIGRS model has provided the most realistic scenarios when compared to Sinmap, due to its capability to evaluate the transient pore-water pressure during rainfall events. The steady-state hydrology approach from Sinmap leads to widespread landslide- prone areas (FRATTINI et al., 2004; SORBINO; et. al., 2010; ZHUANG et al., 2017). Notwithstanding, TRIGRS can be applied as an early warning system for landslides.

6.8 Landslides early warning system using TRIGRS

The model TRIGRS shows its applicability in predicting landslides-prone areas during a rainfall event. Therefore, this model can be used as an early warning system.

To accomplish that, a Python script was developed to automatically acquire the weather forecast data from Climatempo's API and perform the TRIGRS modeling for Vila Baiana. The script (presented in Appendix C) provides the variation of FS for the next 24h, 48h, and 72h, and if needed, an alert is sent.

The script uses Climatempo's API to request Guarujá's weather forecast, hourly for the following 72h. The rain values from Climatempo are shown in millimeters per hour (mm/h), while TRIGRS uses meters per second as a unit. Therefore, the rainfall values are converted to the units used in the mathematical model. The following step is to define and set TRIGRS configuration parameters for 3 days of rain forecast. The model is executed,

creating the three maps of FS for 24h, 48h, and 72h. To quantify the FS variation, the program calculates the sum of the FS values of the area for each timeframe. Following that, the Python script compares the values for the periods considered. Moreover, the automated process provides the percentage of cells with FS ≤ 1 for each map. The alert is sent when the FS sum decreases by 0.22%. This workflow is presented in Appendix D.

To determine the FS threshold, several landslides that happened in Vila Baiana were chosen (Table 6.28), and the FS variation was computed using TRIGRS. The PPDC determined a rainfall threshold of 80mm in 72h for Guarujá. Therefore, to verify the FS variation and its correlation with the rainfall, nine landslides were selected. Three of the landslides selected happened with rainfall values lower than 80mm/72h. Three occurrences had values closer to 80mm/72h, and the last three selected data happened during extreme rainfall events (values above 80mm/72h).

Table 6.28. Landslides in Vila Baiana to determine the FS threshold.

Data	Rainfall 24h (mm)	Rainfall 72h (mm)	FS 24h (%)	FS 72h (%)
10/02/2010	7.3	38.6	-0.03	-0.19
19/03/2009	43.0	43.0	-0.16	-0.43
18/10/2009	49.2	66.9	-0.18	-0.59
14/12/2010	59.4	79.6	-0.22	-0.74
17/04/2005	80.0	80.0	-0.30	-0.91
27/02/2013	82.7	82.7	-0.31	-0.95
26/03/1991	70.9	95.9	-0.26	-0.93
26/02/2009	82.1	191.5	-0.31	-1.37
23/03/1991	70.4	230.5	-0.26	-1.44

Table 6.28 shows that the decrease in slope stability is directly related to the accumulated rainfall. Notwithstanding, this correlation validates the use of an FS threshold as an alert. The improvement of using TRIGRS as an early warning system is the fact that the model computes slope stability based on how much rain infiltrates in the soil, and the increase in soil moisture decreases the FS. In addition to that, the results are maps, that help visualize how the area will be affected by the predicted rain. Today, the early warning defined by PPDC analyzes only the accumulated rainfall in 72h. Using this new system, the alerts will be based on FS variation that takes soil moisture over time into consideration.

It is important to observe that extreme events in a very short period, have become commonplace. As presented in Table 6.9, several landslides were triggered by heavy rainfall in 24h. From 1991-2020, 48.58% of the landslides happened with a threshold higher than 70mm in 24 hours.

Moreover, to determine an FS threshold that could predict these extreme events, an analysis using the methodology proposed by Tatizana et al., (1987a, 1987b) and applied by Molina et al. (2015) e Santoro et al. (2010) e Tachini et al. (2021), among others were conducted.

This methodology consists of determining the correlation between landslides and precipitations levels, using scatter plots adjusted accordingly with Equation 6.4.

$$I = k * (Pac)^{-b} \quad (6.4)$$

In Equation 6.4, "I" is the hourly intensity, Pac is the accumulated precipitation, k and b are constant values of geometric adjustment. The respective values of k and b were automatically defined by the software (Excel) using the Least Squares method, and hourly intensity referring to the previous 24h of accumulated rainfall.

The coefficient of determination, denoted as R^2, was calculated to validate the curve projected by the scatter plot, and values close to 1 mean an improved curve adjustment.

Two criteria were used to determine the best correlation of landslide and rainfall in 24h and 72h, as shown in Table 6.29. The results are presented in Figure 6.50 and Figure 6.51.

Table 6.29. Criteria to determine the correlation between landslide and rainfall events.

Rainfall threshold criteria		
Criteria	24 hours	72 hours
1	60 mm	80 mm
2	80 mm	100 mm

Figure 6.50. Scatter plot of Criteria 1 to determine the best correlation of landslides and rainfall.

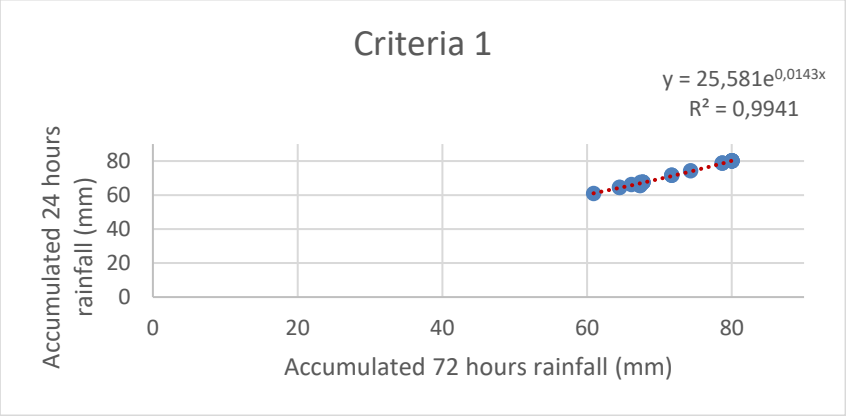

Figure 6.51. Scatter plot of Criteria 2 to determine the best correlation of landslides and rainfall.

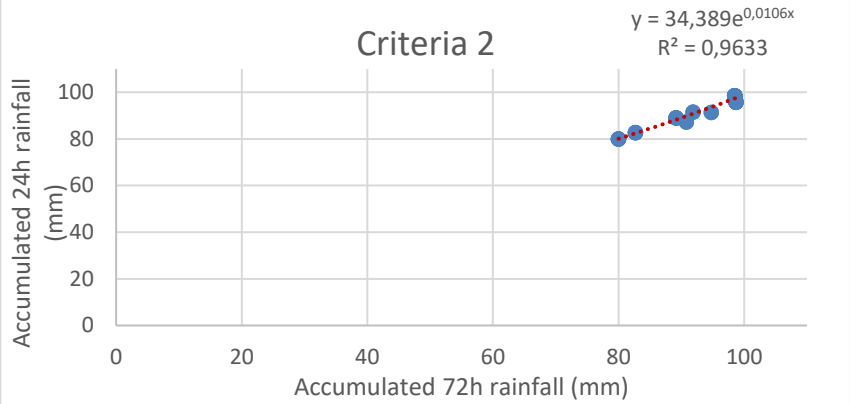

The best-adjusted curve corresponds to a threshold of 60 mm and 80 mm for 24 hours. Therefore, most of the landslide occurrences happened withing this range of accumulated rainfall values. Consequently, considering the landslide involucre from criteria 1 and 2, an additional threshold of 60mm for 24 hours is recommended.

The PPDC already uses an accumulated of 80mm/72h as an alert. Then, to improve the reliability of the alerts, and predict extreme events, a few tests of the FS variation, considering 60mm of rainfall in 24h was performed. To determine the FS threshold for 24h, TRIGRS simulated scenarios for 55mm, 60mm, 65mm, 70mm, 75mm and 80mm of rainfall in 24h, as presented in Table 6.30.

Table 6.30. Simulated scenarios for 24h accumulated rainfall.

Rainfall 24h (mm)	FS variation in 24h (%)
55.0	-0.20
60.0	-0.22
65.0	-0.24
70.0	-0.26
75.0	-0.28
80.0	-0.30

According to Table 6.30, with 60mm of rainfall in 24h, the FS variation is 0.22%. The FS decreases according to the increase in rainfall, thus this correlation is a linear regression, as presented in Figure 6.52.

Figure 6.52. Correlation between the rainfall infiltration in 24 and the FS variation.

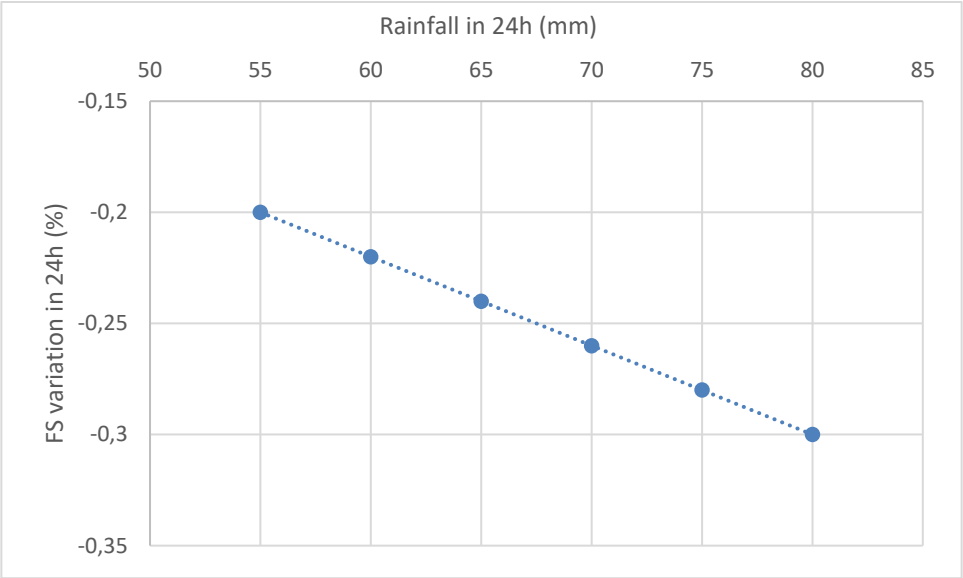

For the early warning system, TRIGRS will calculate the slope stability based on the weather forecast and rainfall infiltration. Rainfall of lower intensities, but with long duration, could trigger landslides due to the increase in soil moisture. Therefore, the advantage of using TRIGRS as an early warning system is because this model calculates the slope stability based on how the rain forecast will increase the soil moisture of Vila Baiana. Moreover, the results presented in Table 6.30 indicate that the FS threshold for this early warning system is 0.22%.

When the system starts, it acquires the weather forecast from Climatempo's website and calculates the slope stability. If the scenario computed indicates an FS variation equal to or higher than the defined threshold for 24h (FS ≥ 0.22), an alert will be emitted. Despite the alert, the script always shows the forecast and FS variation for 24h, 48h, and 72h. The unstable areas can be observed in the map that results from the TRIGRS calculation.

To better illustrate using concrete examples, four dates were chosen: August 8th, December 12th, 13th, and 16th of 2022. August 8th was chosen because it exemplifies how the variation of soil moisture during time changes slope stability. December 12th and 13th were chosen due to the strong rainfall events happening in the study area. And December 16th represents a day with a lower rainfall forecast.

Figure 6.53 presents the results of the FS variation forecast for August 8th of 2022.

Figure 6.53. FS variation forecast for August 8th, 2022, in Vila Baiana.

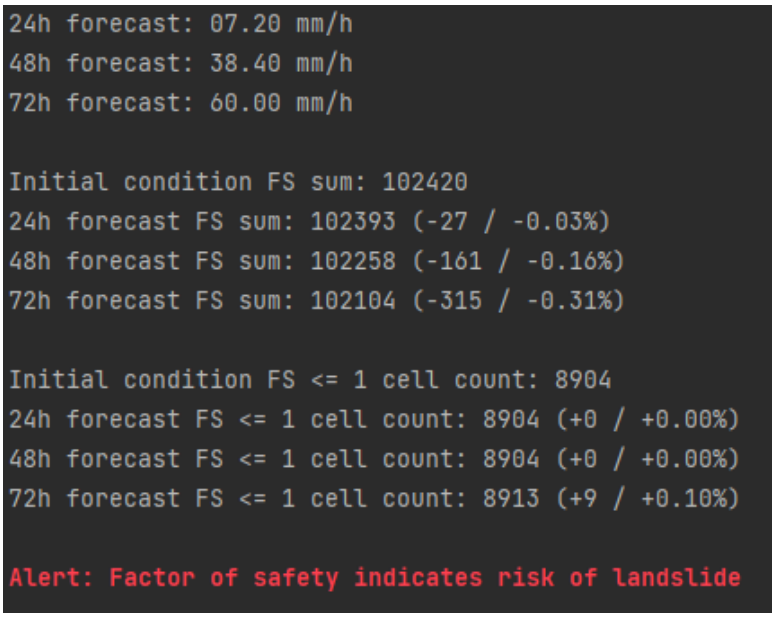

Figure 6.53 shows a decrease in the FS of Vila Baiana for the following 72h. The weather forecast indicates a 7.20 mm/h of rainfall in the next 24h, thus TRIGRS calculates a decrease of 0.03% on the FS. For 48h, with a forecast of 38.40 mm/h of rainfall, the model indicates a decrease in the FS (- 0.16%), when compared to the initial condition. And for

60 mm/h of rainfall, the model determined that Vila Baiana FS decreases by 0.31%. This means that there is an increased possibility of landslides occurring.

This example perfectly illustrates how the water infiltration in the soil over time, decreases the slope stability. The accumulated rainfall for 72h is 60mm, lower than the PPDC threshold. However, there is an increase in soil moisture during this period, decreasing the FS. The model can prevent landslides that would occur even when the rainfall forecast is lower than the PPDC threshold.

Figure 6.54 presents the maps with FS variation for 24h, 48h, and 72h forecast, and the most unstable areas (in red).

Figure 6.54. FS variation for 24h, 48h, and 72h forecast in Vila Baiana on August 8th of 2022.

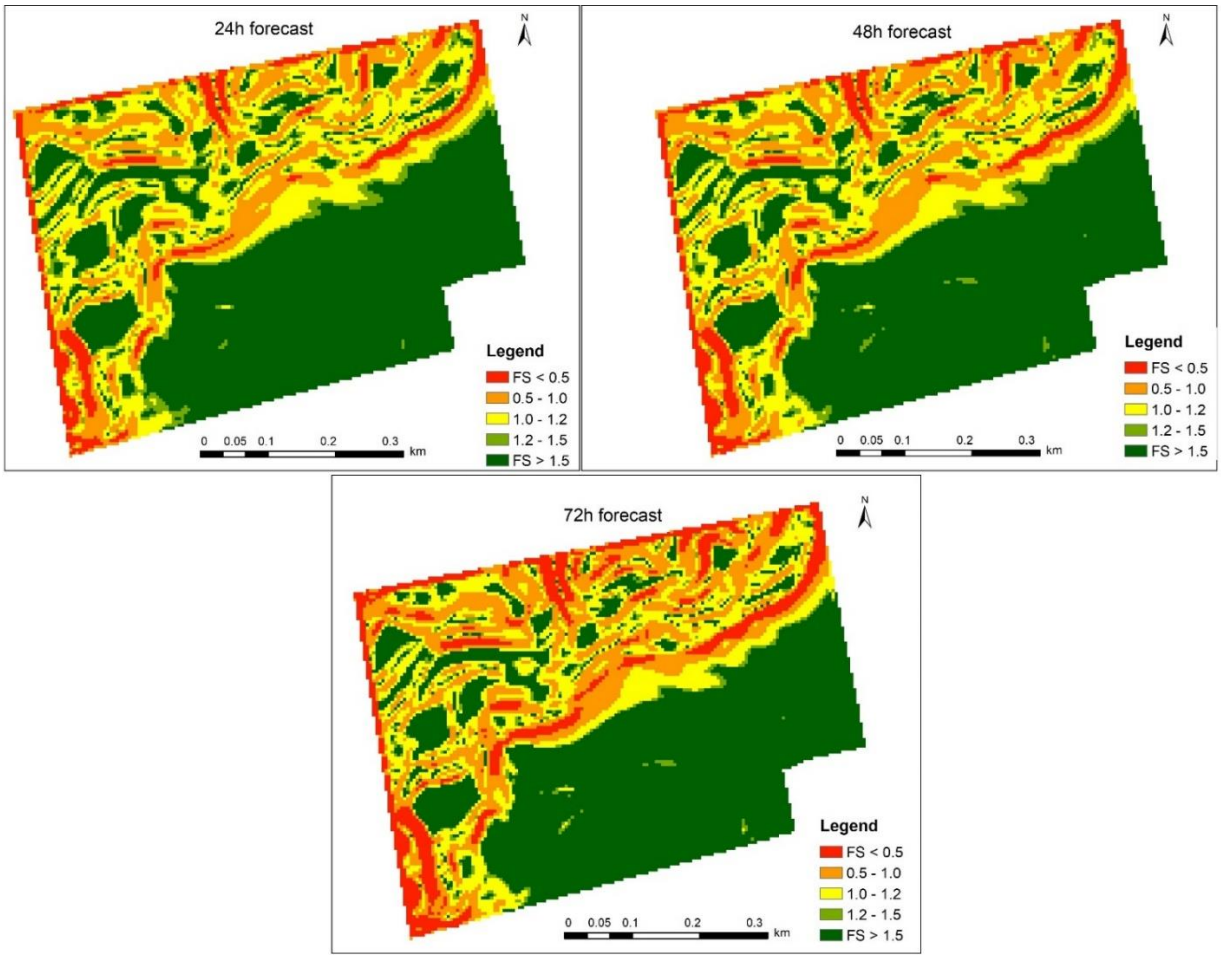

Figure 6.54 presents the TRIGRS results for a 72h forecast. It is observed an increase in areas with FS <1, and mostly the areas in red, indicating FS<0.5. These areas have higher chances of suffering from landslides.

Figure 6.55 shows the early warning system for December 12th of 2022, and Figure 6.56 presents the maps, resulting from TRIGRS calculations.

Figure 6.55. FS variation forecast for December 12th of 2022 in Vila Baiana.

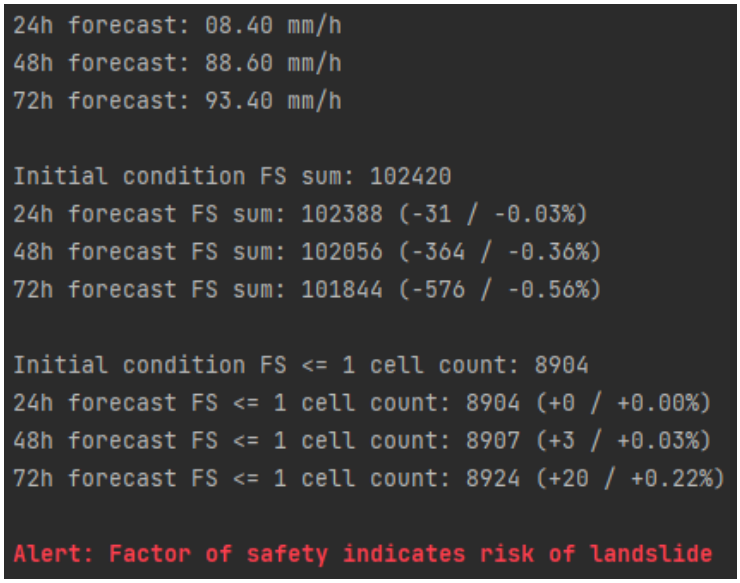

Figure 6.55 shows the FS variation of Vila Baiana for the following 72h. It is expected to rain 8.40mm in the next 24h, indicating a decrease in the FS of 0.03%. For 48h, the forecast is 88.60mm, thus TRIGRS calculates that FS decrease by 0.36%. With this volume of rainfall, the soil moisture rapidly increases, and landslides can be triggered. And for 72h forecast, the accumulated rainfall is 93.4mm, with an FS varying by 0.56%, therefore the landslide alert is emitted. Figure 6.56 shows the maps with the FS variation in Vila Baiana.

In Figure 6.56, the FS variation is easily perceptive. There is an increase in areas with FS<1 for 48h forecast, and a few more for 72h. Vila Baiana is known for its high number of landslides, and TRIGRS demonstrates how fast the slope stability can change.

Figure 6.56. FS variation for 24h, 48h, and 72h forecast in Vila Baiana for December 12th of 2022.

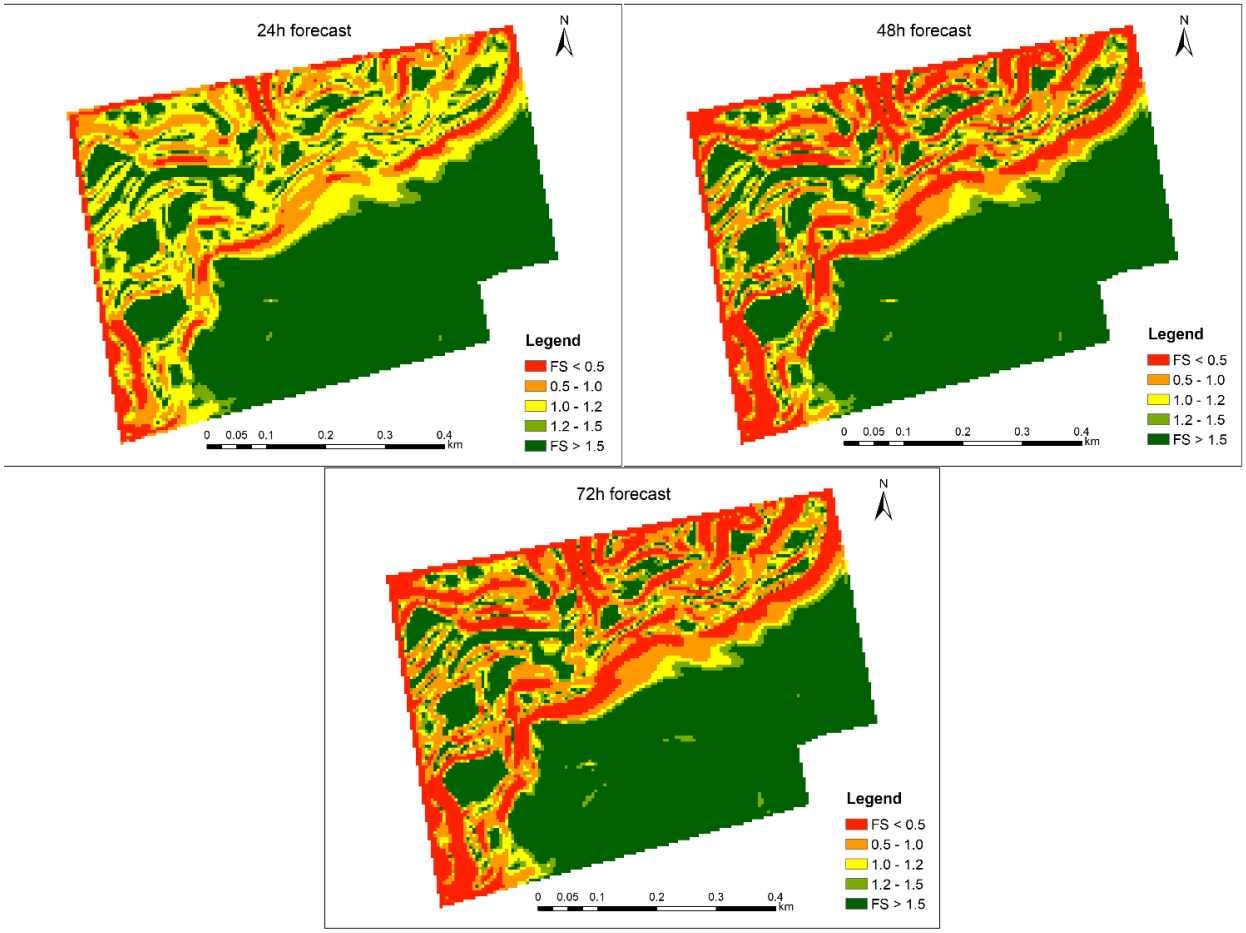

The early warning system was tested on consecutive days, to see its performance with a possibility of changes in the rainfall forecast. Therefore, Figure 6.57 presents the results obtained on December 13th of 2022.

Figure 6.57 shows the forecast for December 13th of 2022. The weather forecast shows heavy rainfall with 80.20mm in 24h, and an accumulated of 85.0mm in 72h. This early warning system emitted the alert of a decrease in FS. Extreme rainfall in a short time can trigger landslides and become a disaster. The FS during 24h decreased by 0.30%. For 48h and 72h, the FS continued at 0.30% since the accumulated for the next few days was only 5mm.

Figure 6.57. FS variation forecast for December 13th of 2022 in Vila Baiana.

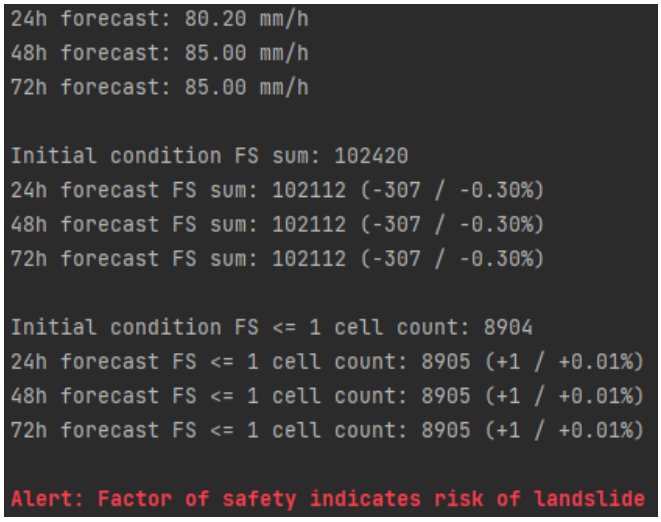

Figure 6.58 presents the three maps produced by TRIGRS with the visual variation of FS for December 13th of 2022.

Figure 6.58. FS variation for 24h, 48h, and 72h forecast in Vila Baiana for December 13th of 2022.

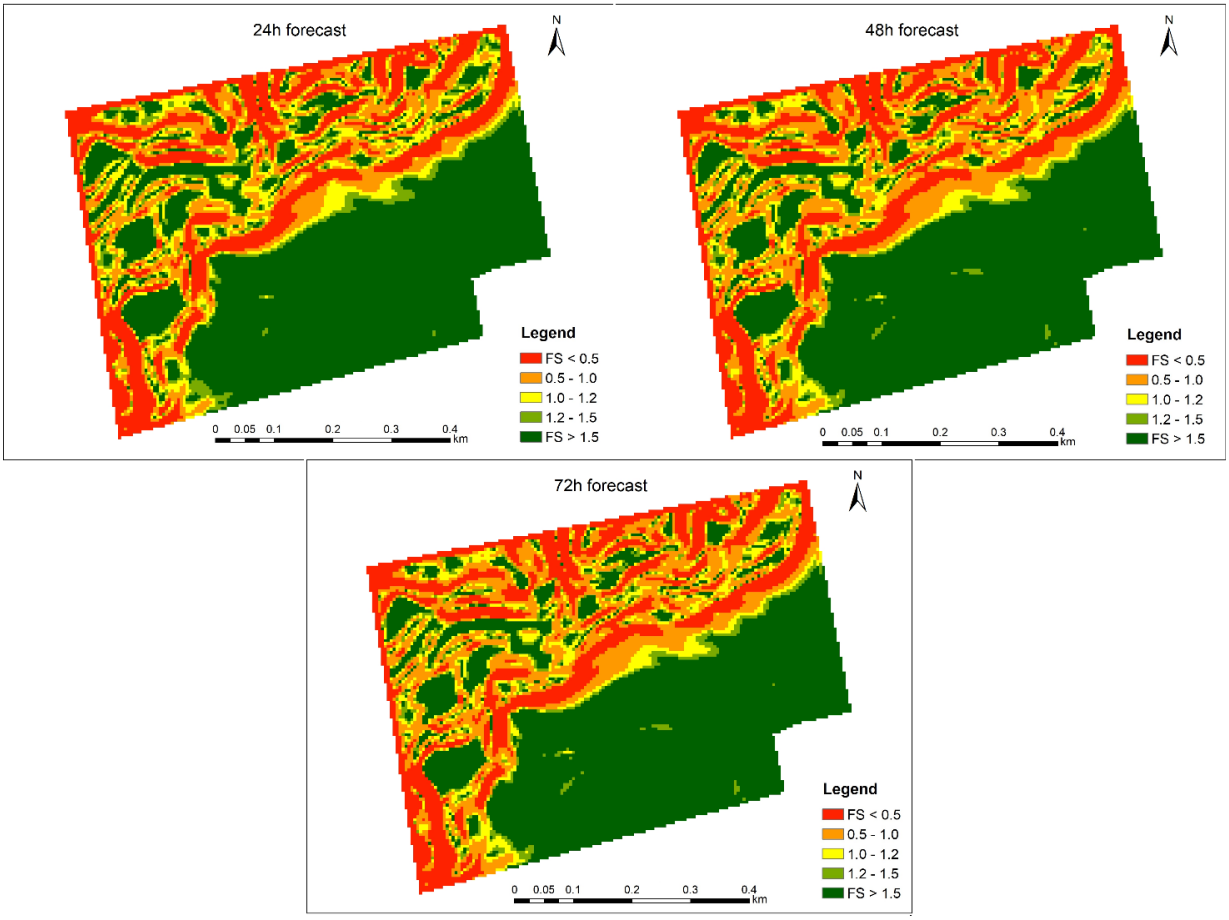

Analyzing two consecutive days (December 12th and 13th) of heavy rainfall events shows how the forecast can change within 24h. For example, on December 12th, the forecast predicted 88.60mm of rainfall in the next 48 hours (meaning December 13th). And on December 13th, the rainfall expected for the first 24h was already 80.20mm. Either way, the alert was emitted, due to the decrease in FS. The early warning system adapted the FS variation, according to the new rainfall forecast.

The last example was performed on December 16th of 2022, as presented in Figure 6.59.

Figure 6.59. FS variation forecast for December 16th of 2022 in Vila Baiana.

```
24h forecast: 04.80 mm/h
48h forecast: 09.60 mm/h
72h forecast: 26.40 mm/h

Initial condition FS sum: 102420
24h forecast FS sum: 102402 (-18 / -0.02%)
48h forecast FS sum: 102373 (-47 / -0.05%)
72h forecast FS sum: 102297 (-122 / -0.12%)

Initial condition FS <= 1 cell count: 8904
24h forecast FS <= 1 cell count: 8904 (+0 / +0.00%)
48h forecast FS <= 1 cell count: 8904 (+0 / +0.00%)
72h forecast FS <= 1 cell count: 8904 (+0 / +0.00%)
```

For December 16th, the rainfall forecast predicted 4.80mm in 24h, and the FS decreased by 0.02%. During 48h, it is expected 9.60mm of accumulated rainfall, and the FS of Vila Baiana decreased to 0.05%. And for 72h, the FS was 0.12% with a, accumulated rainfall of 26.4mm. This scenario is under the FS threshold (FS $\geq$ 0.22%), and no alert was emitted. The variation of FS is presented in Figure 6.60.

Figure 6.60 shows the FS variation for 72h from December 16th. The areas with a decrease in the FS are minimal, and a visual comparison of the maps is difficult. However, the area represented in red, has FS<0.5, even with lower values of rainfall. Meaning that these areas are the most susceptible ones for landslides.

The script was tested with different rainfall forecasts, and the results are promising. Using TRIGRS as an early warning system allows for the identification of unstable areas. The FS variation threshold increases the chances of predicting landslides that happen with lower values of precipitation, or rainfall events of long duration.

Figure 6.60. FS variation for 24h, 48h, and 72h forecast in Vila Baiana for December 16th of 2022.

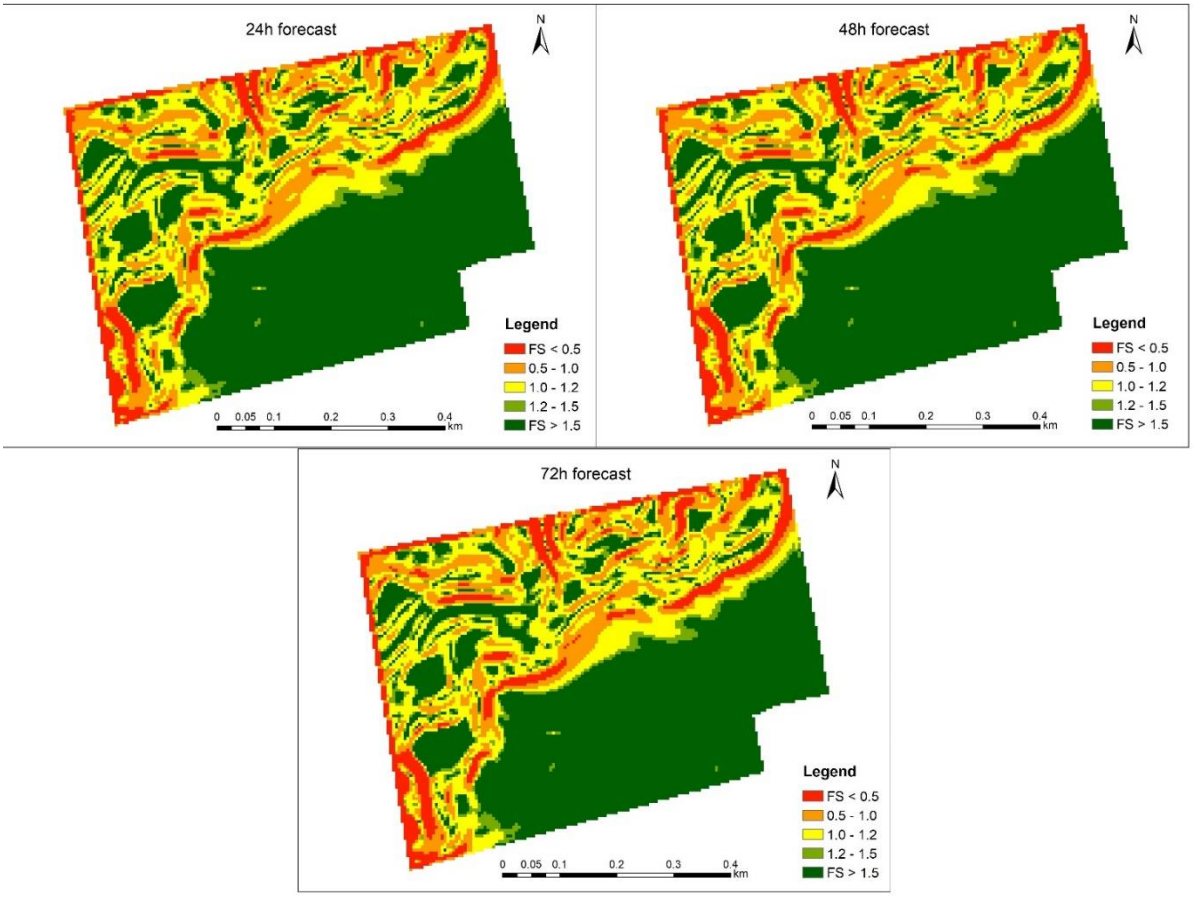

7. CONCLUSIONS

The identification and analysis of landslide-prone areas are essential to avoid disasters. The use of satellite images from the Landsat sensor allows a temporal analysis of the urban sprawl from 1990-2021. Moreover, the populational growth foments the construction of houses in steep slope areas. Consequently, the natural vegetation was removed, and the total vegetation cover of Guarujá has decreased. Machine learning techniques and data mining contributed to classifying the orthophoto of the Vila Baiana neighborhood and discriminated the objects of the area. Several constructions were observed in steep slope areas, and most of them have precarious building standards. Pavement streets are present only in flat areas, where it is possible to discriminate the blocks. A vegetation cover is rare. Therefore, the area has a lot of anthropic changes, which contribute to become more susceptible to landslides.

The rainfall events have correlations with the documented landslides in Guarujá. However, several occurrences happened with lower levels of rainfall. And an increase in heavy rainfalls (extreme events) in a short period, has become more common. The importance of developing an early warning system based on the variation of Factor of Safety is to predict the landslides considering not only the rainfall values but also the soil moisture.

Two mathematical models were tested to verify which has better results to become part of the early warning system: SINMAP and TRIGRS. The results show that TRIGRS has the best capability to identify landslide-prone areas and calculate how the FS decreases according to the volume of rainfall expected.

The early warning system, developed in Python, used TRIGRS to determine the slope stability of Vila Baiana, and the results are coherent with reality. The model sends an alert when the predicted FS is lower than the defined threshold. It can be replicated in different areas, adapting it to a different context. Thus, this system does not replace the rainfall threshold determined by PPDC and applied by the Civil Defense. On the contrary, it should be used in parallel, as a new tool to predict landslides based on FS variation.

8. RECOMMENDATIONS FOR FUTURE STUDIES

For future studies, it is recommended to use geotechnical parameters collected in situ, to improve the reliability of the results. The mathematical model TRIGRS determines slope stability based on both weather forecasts and rainfall infiltration. The soil moisture has an important impact on triggering landslides. CEMADEN has sensors installed in several risk areas to analyze the soil moisture at different depths. Therefore, a partnership with the CEMADEN project is recommended, allowing automatic access to this data, through an API. More precise soil moisture data will improve the reliability of this early warning system, leading to improved results and accurate alerts.

REFERENCES

AHRENDT, A. **Movimentos de massa gravitacionais:** proposta de um sistema de previsão: aplicação na área urbana de Campos do Jordão – SP. 2005. 390p. Tese (Doutorado em Geotecnia) - Escola de Engenharia de São Carlos, Universidade de São Paulo, São Carlos, 2005.

ARAKI, R.; SERGIO, F.; LADEIRA, B. Vulnerabilidade associada a precipitações e fatores antropogênicos no Município de Guarujá (SP): Período De 1965 a 2001. In: WORKSHOP PROJETO SERRA DO MAR, 2. 2001. **Anais…** 2001.

AVEN, T. On some recent definitions and analysis frameworks for risk, vulnerability, and resilience. **Risk Analysis**, v. 31, n. 4, p. 515–522, 2011.

BAI, S. B.; WANG, J.; LÜ, G. N.; ZHOU, P. G.; HOU, S. S.; XU, S. N. GIS-based and data-driven bivariate landslide-susceptibility mapping in the three gorges area, China Project supported by the National Natural Science Foundation of China, the Foundation for China Geological Survey. **Pedosphere**, v. 19, n. 1, p. 14–20, 2009.

BAUM, R. L.; SAVAGE, W. Z.; GODT, J. W. **TRIGRS: a Fortran program for transient rainfall infiltration and grid-based regional slope-stability analysis, version 2.0**. [S.l.]: U.S. Geological Survey, 2008.

BENTO, B. M. P. **Avaliação dos classificadores por árvores de decisão e árvore de regressão em cenas urbanas do sensor WorldView-2**. 2016. Dissertação (Mestrado em Sensoriamento Remoto) - Instituto Nacional de Pesquisas Espaciais, São José dos Campos, 2016.

BITAR, O. Y.; FREITAS, C. G. L.; MACEDO, E. S.. **Guia cartas geotécnicas: orientações básicas aos municípios**. [S.l.: s.n.], 2015.

BOCKHEIM, J. G.; GENNADIYEV, A. N.; HAMMER, R. D.; TANDARICH, J. P. Historical development of key concepts in pedology. **Geoderma**, v. 124, n. 1–2, p. 23–36, 2005.

BROLLO, M. J.; FERREIRA, C. J. Gestão de risco de desastres devido a fenômenos geodinâmicos no estado de São Paulo: cenário 2000-2015. **Boletim do Instituto Geológico**, n. 67, p. 72, 2016.

CANAVESI, V.; CAMARINHA, P. I. M.; IVO, P. I. S. E; ALGARVE, V. R. Análise da susceptibilidade a deslizamentos de terra: estudo de caso de Paraibuna, SP. In: SIMPÓSIO BRASILEIRO DE SENSORIAMENTO REMOTO, 16., 2013. **Anais...** São José dos Campos: INPE, 2013.

CARDOZO, C.; LOPES, E.; MONTEIRO, A. M. Shallow landslide susceptibility assessment using SINMAP in Nova Friburgo (Rio de Janeiro, Brazil). **Revista Brasileira de Cartografia**, v. 70, n. 4, p. 1206–1230, 2018.

CARRARA, A.; CARDINALI, M.; DETTI, R.; GUZZETTI, F.; PASQUI, V.; REICHENBACH, P. GIS techniques and statistical models in evaluating landslide hazard. **Earth Surface Processes and Landforms**, v. 16, n. 5, p. 427–445, 1991.

CARVALHO, M. V. A. DE. **Classificação da cobertura e uso do solo com imagens Worldview-2 utilizando mineração de dados e análise baseada em objetos**. 204 p. Dissertação (Mestrado em Sensoriamento Remoto) - Instituto Nacional de Pesquisas Espaciais, São José dos Campos, 2011.

CARVALHO, L. M. V.; JONES, C.; LIEBMANN, B. Extreme precipitation events in southeastern South America and large-scale convective patterns in the South Atlantic covergence zone. **Journal of Climate**, v. 15, n. 17, p. 2377–2394, 2002.

CENTRO DE ESTUDOS E PESQUISAS EM ENGENHARIA E DEFESA CIVIL (CEPED-UFSC). **Atlas brasileiro de desastres naturais 1991 a 2012.** Florianópolis: UFSC, 2013.

CENTRO DE ESTUDOS E PESQUISAS EM ENGENHARIA E DEFESA CIVIL (CEPED-USFC). **A P&DC e os 30 anos de desastres no Brasil**. 2020. Available from: <https://www.gov.br/mdr/pt-br/centrais-de-conteudo/publicacoes/protecao-e-defesa-civil-sedec/A_p_amp_dc_e_os_30_anos_de_desastres_no_Brasil_20221_compressed.pdf>.

CENTRO NACIONAL DE GERENCIAMENTO DE RISCOS E DESASTRES (CENAD). **Anuário braileiro de desastres naturais: 2012**. [S.l.]: CENAD, 2013.

CENTRO NACIONAL DE MONITORAMENTO E ALERTAS DE DESASTRES NATURAIS (CEMADEN). **Histórico da criação do CEMADEN**. Available from: <http://www.cemaden.gov.br/historico-da-criacao-do-cemaden/ >. Access on: Jan. 24 2016.

CENTRO NACIONAL DE MONITORAMENTO E ALERTAS DE DESASTRES NATURAIS (CEMADEN). **Boletim da sala de situação- 1 trimestre 2020**. Available from: <http://www2.cemaden.gov.br/wp-content/uploads/2020/06/Boletim-da-Sala-de-Situa%c3%a7%c3%a3o-1%c2%ba-Trimestre-de-2020.pdf >. Access on: July 20 2020.

CERVI, F.; BERTI, M.; BORGATTI, L.; RONCHETTI, F.; MANENTI, F.; CORSINI, A. Comparing predictive capability of statistical and deterministic methods for landslide susceptibility mapping: a case study in the northern Apennines (Reggio Emilia Province, Italy). **Landslides**, v. 7, n. 4, p. 433–444, 2010.

CHEN, G.; WENG, Q.; HAY, G. J.; HE, Y. Geographic object-based image analysis (GEOBIA): emerging trends and future opportunities. **GIScience and Remote Sensing**, v. 55, n. 2, p. 159–182, 2018.

CHIEN-YUAN, C.; TIEN-CHIEN, C.; FAN-CHIEH, Y.; SHENG-CHI, L. Analysis of time-varying rainfall infiltration induced landslide. **Environmental Geology**, v. 48, n. 4/5, p. 466–479, 2005.

CIURLEO, M.; MANDAGLIO, M. C.; MORACI, N. Landslide susceptibility assessment by TRIGRS in a frequently affected shallow instability area. **Landslides**, v. 16, n. 1, p. 175–188, 2019.

CLIMATEMPO. **Home page.** Available from: < https://www.Climatempo.com.br/ >. Access on: Ago 07 2022.

COORDENADORIA MUNICIPAL DE PROTEÇÃO E DEFESA CIVIL DO GUARUJÁ (COMPDEC-Guarujá). **Relação de escorregamentos de 1991 a 2019** [comunicação pessoal]. Menssage received by Tèhrrie König in Feb. 14, 2020.

CRUDEN, D.; VARNES, D. Landslides: investigation and mitigation. In: _____ (Ed.). **Landslides: analysis and control.** Washington: National Academic Press, 1996.

DAS, B. B.; KONDRAIVENDHAN, B. Implication of pore size distribution parameters on compressive strength, permeability and hydraulic diffusivity of concrete. **Construction and Building Materials**, v. 28, n. 1, p. 382–386, 2012.

DEB, S. K.; EL-KADI, A. I. Susceptibility assessment of shallow landslides on Oahu, Hawaii, under extreme-rainfall events. **Geomorphology**, v. 108, n. 3/4, p. 219–233, 2009.

DEPARTAMENTO DE ÁGUA E ENERGIA ELETRICA (DAEE). **Banco de dados hidrológicos.** Available from: < http://www.hidrologia.daee.sp.gov.br/ >. Access on: Aug. 6 2021.

DIETRICH, W. E.; MONTGOMERY, D. R. **Shalstab: a digital terrain model for mapping shallow landslide potential**. [S.l.]: NCASI, 1998.

DIETRICH, W. E.; BELLUGI, D.; REAL DE ASUA, R. Validation of the shallow landslide model, SHALSTAB, for forest management. **Water Science and Application**, v. 2, n. 1, p. 195–227, 2011.

DRONOVA, I. Object-based image analysis in wetland research: a review. **Remote Sensing**, v. 7, n. 5, p. 6380–6413, 2015.

EMPRESA BRASILEIRA DE PESQUISA AGROPECUÁRIA (EMBRAPA). **Sistema brasileiro de classificação de solos**. [S.l.]: Embrapa, 2018. 353p.

ENGESAT. **Imagens de satélite**. Available from: <http://www.engesat.com.br/imagem-de-satelite/landsat-8/>. Access on: Nov. 9 2020.

FAWCETT, T. An introduction to ROC analysis. **Pattern Recognition Letters**, v. 27, n. 8, p. 861–874, 2006.

FAYYAD, U.; PIATETSKY-SHAPIRO, G.; SMYTH, P. From data mining to knowledge discovery in databases. **AI Magazine**, v.17, n.3, p.37-54, 1996.

FELL, R.; COROMINAS, J.; BONNARD, C.; CASCINI, L.; LEROI, E.; SAVAGE, W. Z. Guidelines for landslide susceptibility, hazard and risk zoning for land use planning. **Engineering Geology**, v. 102, n. 3/4, p. 85–98, 2008.

FRATTINI, P.; CROSTA, G. B.; FUSI, N.; DAL NEGRO, P. Shallow landslides in pyroclastic soils: a distributed modelling approach for hazard assessment. **Engineering Geology**, v. 73, n. 3/4, p. 277–295, 2004.

FUNDAÇÃO SISTEMA ESTADUAL DE ANÁLISE DE DADOS (SEADE). **População**. Available from: <https://populacao.seade.gov.br/>. Access on: Mar.25 2020.

GAO, J. Identification of topographic settings conductive to landsliding from Nelson County, Virginia, U.S.A. **Earth Surface Processes and Landforms**, v. 18, n.7, p. 579-591, 1993.

GARCÍA-ARISTIZÁBAL, E. F.; ARISTIZABAL GIRALDO, E. V.; MARÍN SÁNCHEZ, R. J.; GUZMAN MARTINEZ, J. C. Implementación del modelo TRIGRS con análisis de confiabilidad para la evaluación de la amenaza a movimientos en masa superficiales detonados por lluvia. **TecnoLógicas**, v. 22, n. 44, p. 111–129, 2019.

GEO-SLOPE. **Stability modeling with Slope/W**. Calgary, Canada: Geo-Slope/W, 2012.

GEO-SLOPE, I. GeoStudio. **LatinFinance**, n. 172, p. 46–47, 2016.

GHOSH, P. Effect of reinforcement on stability of slopes using GEOSLOPE. **International Journal of Computer** Applications, p. 29–32, 2012.

GRELLE, G.; SORIANO, M.; REVELLINO, P.; GUERRIERO, L.; ANDERSON, M. G.; DIAMBRA, A.; FIORILLO, F.; ESPOSITO, L.; DIODATO, N.; GUADAGNO, F. M. Space-time prediction of rainfall-induced shallow landslides through a combined probabilistic/deterministic approach, optimized for initial water table conditions. **Bulletin of Engineering Geology and the Environment**, v. 73, n. 3, p. 877–890, 2014.

GODT, J. W.; BAUM, R. L.; SAVAGE, W. Z.; SALCIARINI, D.; SCHULZ, W. H.; HARP, E. L. Transient deterministic shallow landslide modeling: requirements for susceptibility and hazard assessments in a GIS framework. **Engineering Geology**, v. 102, n. 3/4, p. 214–226, 2008.

GOLDSCHMIDT, R.; PASSOS, E. **Data mining**: um guia prático. Rio de Janeiro: Elsevier, 257 p. 2005.

GUILD, L. S.; COHEN, W. B.; KAUFFMAN, J. B. Detection of deforestation and land conversion in Rondônia, Brazil using change detection techniques. **International Journal of Remote Sensing**, v. 25, n. 4, p. 731–750, 2004.

GUIMARÃES, R. F. **Utilização de um modelo de previsão de áreas susceptíveis a escorregamentos rasos com controle topográfico: adequação e calibração em duas bacias de drenagem**. Tese (Doutorado) - Universidade Federal do Rio de Janeiro, Rio de Janeiro, 2000.

HAN, J.; KAMBER, M.; PEI, J. **Data mining**: concepts and techniques. 3.ed. Rio de Janeiro: Elsevier, 2012.

HAY, G. J.; CASTILLA, G. Object-based image analysis: Strengths, weaknesses, opportunities and threats (SWOT). **The International Archives of the Photogrammetry, Remote Sensing and Spatial Information Sciences**, p. 4–5, 2006.

HENRIQUE, E.; ARAÚJO, G.; JOHANN, H.; KUX, H.; FLORENZANO, T. G. Orhtorrectification of Quickbird satellite images for urban applications. **Spectrum**, n. 60, 2008.

HOUGHTON, J. **Global warming the complete briefing**. Cambridge: [s.n.], 2003.

HUANG, J. C.; KAO, S. J. Optimal estimator for assessing landslide model performance. **Hydrology and Earth System Sciences**, v. 10, n. 6, p. 957–965, 2006.

INSTITUTO BRASILEIRO DE GEOGRAFIA E ESTATÍSTICA (IBGE). **Cidades e estados do Brasil**. Available from: <http://cidades.ibge.gov.br/ >. Access on: Mar. 27 2020.

INSTITUTO DE PESQUISAS TECNOLÓGICAS (IPT). **Indicação preliminar de áreas prioritárias para recomposição da cobertura vegetal na Serra do Mar na área de Cubatão**. São Paulo: IPT, 1986.

INSTITUTO DE PESQUISAS TECNOLÓGICAS (IPT). E**studo das instabilizações de encostas da Serra do Mar na região de Cubatão objetivando a caracterização do fenômeno de corrida de lama e da prevenção dos seus efeitos**. São Paulo: IPT, 1988.

IVERSON, R. M. Landslide triggering by rain infiltration. **Water Resources Research**, v. 36, p. 1897-1910, 2000.

JENNY, H. **Factors of soil formation: a system of quantitative pedology**. [S.l.: Dover Publications, 1945.

KOBIYAMA, M.; MENDONÇA, M.; MORENO, D. A.; MARCELINO, I. P. V. D. O.; MARCELINO, E. V.; GONÇALVES, E. F.; BRAZETTI, L. L. P.; GOERL, R. F.; MOLLERI, G. S. F.; RUDORFF, F. D. M. **Prevenção de desastres naturais: conceitos básicos**. [S.l.]: Organic Trading, 2006.

KÖNIG, T. **Identificação e análise de áreas de suscetibilidade a deslizamentos de encostas em Campos do Jordão-SP utilizando o modelo SHALSTAB e imagens do WorldView-2.** Dissertação (Mestrado em Sensoriamento Remoto) - Instituto Nacional de Pesquisas Espaciais, São José dos Campos-SP, 2018.

KÖNIG, T.; KUX, H. J. H.; CORSI, A. C. Landslide risk management using the mathematical model TRIGRS. **Revista Geociências**, v. 41, p. 243–254, 2022.

KÖNIG, T.; KUX, H. J. H.; MENDES, R. M. Shalstab mathematical model and WorldView-2 satellite images to identification of landslide-susceptible areas. **Natural Hazards**, v. 97, n. 3, 2019.

KÖNIG, T.; KUX, H. J. H.; MENDES, R. M. Identificação de áreas de suscetibilidade a escorregamentos de encosta utilizando o modelo matemático Shalstab. **Boletim de Geografia**, v. 37, n. 3, p. 228–243, 2020.

KORTING, T. S.; FONSECA, L. M. G.; CAMARA, G. GeoDMA-geographic data mining analyst. **Computer and Geosciences**, v. 57, p. 133-145, 2013.

LARRAMENDY, M. L.; SOLONESKI, S. **Use and misuse and teir impact pesticides**. London, UK: IntechOpen, 2019. ISBN 9789535179986.

LARSEN, M. C.; TORRES-SANCHEZ, A. J. The frequency and distribution of recent landslides in three. **Geomorphology**, n. 24, p. 309–331, 1998.

LI, C.; MA, T.; SUN, L.; LI, W.; ZHENG, A. Application and verification of a fractal approach to landslide susceptibility mapping. **Natural Hazards**, v. 61, n. 1, p. 169–185, 2012.

LIAO, Z.; HONG, Y.; KIRSCHBAUM, D.; ADLER, R. F.; GOURLEY, J. J.; WOOTEN, R. Evaluation of TRIGRS (transient rainfall infiltration and grid-based regional slope-stability analysis)'s predictive skill for hurricane-triggered landslides: a case study in Macon County, North Carolina. **Natural Hazards**, v. 58, n. 1, p. 325–339, 2011.

LIBONATI, R.; DACAMARA, C. C.; SETZER, A. W.; MORELLI, F.; MELCHIORI, A. E. An algorithm for burned area detection in the Brazilian Cerrado using 4 μm MODIS imagery. **Remote Sensing**, v. 7, n. 11, p. 15782–15803, 2015.

LIEBMANN, B.; JONES, C.; CARVALHO, L. M. V. Interannual variability of daily extreme precipitation events in the state of Saõ Paulo, Brazil. **Journal of Climate**, v. 14, n. 2, p. 208–218, 2001.

LISTO, F. D. L. R. Modelos matemáticos aplicados à previsão de escorregamentos translacionais rasos: exemplos em áreas naturais e de risco. **CLIO – Arqueológica**, v. 31, n. 3, p. 91, 2016.

LISTO, F. D. L. R.; GOMES, M. C. V.; VIEIRA, B. C. Avaliação da variação do fator de segurança com o modelo trigrs. **Revista Brasileira de Geomorfologia**, v. 19, n. 1, p. 207–220, 2018.

LISTO, F. D. L. R.; VIEIRA, B. C. Influência de parâmetros geotécnicos e hidrológicos na previsão de áreas instáveis a escorregamentos translacionais rasos utilizando o modelo Trigrs. **Revista Brasileira de Geomorfologia**, v. 16, n. 3, 2015.

LÜDEKE, M. K. B.; RAMGE, P. H.; KOHLMAIER, G. H. The use of satellite NDVI data for the validation of global vegetation phenology models: application to the frankfurt biosphere model. **Ecological Modelling**, v. 91, n. 1/3, p. 255–270, 1996.

MACEDO, E. S.; BRESSANI, L. A. (Org.). **Diretrizes para o zoneamento da suscetibilidade, perigo e risco de deslizamentos para planejamento do uso do solo**. São Paulo: ABGE, ABMS, 2013.

MACEDO, E. S.; SANTORO, J.; ARAÚJO, R. E. Plano preventivo de defesa civil (PPDC) para deslizamentos, Estado de São Paulo, Brasil. In: SIMPÓSIO BRASILEIRO DE DESASTRES NATURAIS, 2004. **Anais...** 2004. p. 908–919.

MARCELINO, E. V.; NUNES, L. H.; KOBIYAMA, M. Banco de dados de desastres naturais: análise de dados globais e regionais. **Caminhos de Geografia**, v. 7, n. 19, p. 130–149, 2006.

MARÍN, R. J.; GUZMÁN-MARTÍNEZ, J. C.; MARTÍNEZ CARVAJAL, H. E.; GARCÍA-ARISTIZÁBAL, E. F.; CADAVID-ARANGO, J. D.; AGUDELO-VALLEJO, P. Evaluación del riesgo de deslizamientos superficiales para proyectos de infraestructura: caso de análisis en vereda El Cabuyal. **Ingeniería y Ciencia**, v. 14, n. 27, p. 153–177, 2018.

MARÍN, R. J.; SALAS, J. P. O. Modelación de la contribución arbórea en análisis de susceptibilidad a deslizamientos superficiales. **Revista EIA**, v. 14, n. 28, p. 13–27, 2017.

MEISINA, C.; SCARABELLI, S. A comparative analysis of terrain stability models for predicting shallow landslides in colluvial soils. **Geomorphology**, v. 87, n. 3, p. 207–223, 2007.

MENDES, R. M.; ANDRADE, M. R. M. D.; TOMASELLA, J.; MORAES, M. A. E. D.; SCOFIELD, G. B. Understanding shallow landslides in Campos do Jordão municipality – Brazil: disentangling the anthropic effects from natural causes in the disaster of 2000. **Natural Hazards and Earth System Sciences**, v. 18, n. 1, p. 15–30, 2018a.

MENDES, R. M.; DE ANDRADE, M. R. M.; GRAMINHA, C. A.; PRIETO, C. C.; DE ÁVILA, F. F.; CAMARINHA, P. I. M. Stability analysis on urban slopes: case study of an anthropogenic-induced landslide in São José dos Campos, Brazil. **Geotechnical and Geological Engineering**, v. 36, n. 1, p. 599–610, 2018b.

MENDES, R. M.; VALÉRIO FILHO, M. Real-time monitoring of climactic and geotechnical variables during landslides on the slopes of Serra do Mar and Serra da Mantiqueira (São Paulo State, Brazil). **Engineering**, v. 7, n. 3, p. 140–159, 2015.

MENEGHETTI, G. T.; KUX, H. J. H. Land cover mapping of Raposa (MA) municipality using WorldView-II images, the InterIMAGE system and data mining. **Revista Brasileira de Cartografia**, v. 2, n.66, p. 365–377, 2014.

MENEZES, M. B. M.; PEJON, O. J. Análise da influência do teor de umidade na absorção d'água e sucção dos solos em estudos de erodibilidade. **Geociencias**, v. 29, n. 2, p. 211–228, 2010.

MENG, J.; DU, X.; WU, B. Generation of high spatial and temporal resolution NDVI and its application in crop biomass estimation. **International Journal of Digital Earth**, v. 6, n. 3, p. 203–218, 2013.

MICHEL, G. P.; KOBIYAMA, M.; GOERL, R. F. Análise comparativa entre os modelos Shalstab e SINMAP na identificação de áreas susceptíveis à escorregamentos translacionais. In: ENCONTRO NACIONAL DE ENGENHARIA DE SEDIMENTOS, 10., 2012. **Anais...** 2012. p. 1–21.

MICHEL, G. P.; KOBIYAMA, M.; GOERL, R. F. Comparative analysis of SHALSTAB and SINMAP for landslide susceptibility mapping in the Cunha River basin, southern Brazil. **Journal of Soils and Sediments**, v. 14, n. 7, p. 1266–1277, 2014.

MODENESI-GAUTTIERI, M. C.; HIRUMA, S. T. A expansão urbana no planalto de Campos do Jordão. diagnóstico geomorfológico para fins de planejamento. **Revista do Instituto Geológico**, v. 25, p. 1–28, 2004.

MOLINA, E.; CARDOSO, A.; NOGUEIRA, F. Relação precipitação-deslizamento no Município de São Bernardo do Campo - SP. **Ciência e Natura**, v. 37, p. 46–54, 2015.

MONTGOMERY, D. R.; DIETRICH, W. E. A physically based model for the topographic control on shallow landsliding. **Water Resources Research**, v. 30, n. 4, p. 1153–1171, 1994.

NAGAMANI, K.; KANNAN, J.; JEYAGOPAL, S.; SURESH, Y. **Study on error matrix analysis of classified remote sensed data for Pondicherry Coast mangrove ecosystem**. [S.l.: s.n.], 2015.

NERY, T. D.; VIEIRA, B. C. Susceptibility to shallow landslides in a drainage basin in the Serra do Mar, São Paulo, Brazil, predicted using the SINMAP mathematical model. **Bulletin of Engineering Geology and the Environment**, v. 74, n. 2, p. 369–378, 2015.

NICHOLLS, N. Atmospheric and climatic hazards: improved monitoring and prediction for disaster mitigation. **Natural Hazards**, v. 23, n. 2–3, p. 137–155, 2001.

NOVACK, T. **Classificação da cobertura da terra e do uso do solo urbano utilizando o sistema InterIMAGE e imagens do sensor QuickBird.** 2009. 214 p. Dissertação (Mestrado em Sensoriamento Remoto) - Instituto Nacional de Pesquisas Espaciais, São José dos Campos, 2009.

NOVO, E. M. L. M. **Sensoriamento remoto: princípios e aplicações**. 4 ed. São Paulo: Blucher, 2010. 288 p.

O'LOUGHLIN, E. M. O. Prediction of surface saturation zones in natural catchments by topographic analysis. **Water Resources**, v. 22, n. 5, p. 794–804, 1986.

PACK, R. T. The SINMAP approach to terrain stability mapping. In: CONGRESS OF THE INTERNATIONAL ASSOCIATION OF ENGINEERING GEOLOGY, 8., 1998. **Proceedings…** 1998.

PACK, R. T.; TARBOTON, D. G.; GOODWIN, C. N. **Terrain stability mapping with SINMAP, technical description and users guide for version 1.00**. [S.l.]: Terratech Consulting, 1998.

PARK, D. W.; NIKHIL, N. V.; LEE, S. R. Landslide and debris flow susceptibility zonation using TRIGRS for the 2011 Seoul landslide event. **Natural Hazards and Earth System Sciences**, v. 13, n. 11, p. 2833–2849, 2013.

PAUL, L. R.; SCHWARZ, H.; MICHEL, G. P. Identificação de áreas propensas a escorregamentos translacionais nas bacias do Taboão E Matador, Rio do Sul - SC. In: ENCONTRO NACIONAL DE DESASTRES, 1., 2018. **Anais...** 2018

PECHINCHA, M. G. H.; ZAIDAN, R. T. Zoneamento de risco à ocorrência de escorregamentos: uma aplicação na bacia do Córrego Matirumbide, Juiz de Fora, MG. **Revista Espinhaço**, v. 4, n. 2, p. 45–57, 2015.

PESCK, V. A.; DISPERATI, A. A. Comparação de técnicas de fusão aplicadas à imagem Quickbird-2. **Floresta e Ambiente**, v. 18, n. 2, p. 127–134, 2011.

PHILLIPS, J. D. Soil complexity and pedogenesis. **Soil Science**, v. 182, n. 4, p. 117–127, 2017.

PIELKE, R. A. Making sense of trends in disaster losses. **The OST's Publication on Science & Technology Policy**, v. 7, 2005.

PIELKE, R. A. Disasters, death, and destruction making sense of recent calamities. **Oceanography**, v. 19, n. 2, p. 138–147, 2006.

PINHO, C.; FEITOSA, F.; KUX, H. Classificação automática de cobertura do solo urbano em imagem IKONOS: comparação entre a abordagem pixel-a-pixel e orientada a objetos. In: SIMPÓSIO BRASILEIRO DE SENSORIAMENTO REMOTO, 12., 2005, Goiânia. **Anais...** São José dos Campos: INPE, 2005. p. 4217–4224.

PINHO, C. M. D.; FONSECA, L. M. G.; KORTING, T. S.; DE ALMEIDA, C. M.; KUX, H. J. H. Land-cover classification of an intra-urban environment using high-resolution images and object-based image analysis. **International Journal of Remote Sensing**, v. 33, n. 19, p. 5973–5995, 2012.

POLIZEL, S. P.; MARQUES, M. L.; COSTA, N. R.; ROSSI, E.; FERREIRA, M. V. Aplicação e avaliação de técnicas de fusão em imagens Ikonos e GeoEye. In: SIMPÓSIO BRASILEIRO DE SENSORIAMENTO REMOTO, 15., 2011, Curitiba. **Anais...** São José dos Campos: INPE, 2011. p. 447–451.

PRIETO, C. C.; MENDES, R. M.; JORGE, S.; SIMÕES, C.; NOBRE, C. A.; PIETRO, C. C. Comparison between the application of SHALSTAB model with slide susceptibility and risk maps in Piracuama stream basin in Campos do Jordão - SP Cen. **Revista Brasileira de Cartografia**, v. 1, p. 71–87, 2017.

PU, R.; LANDRY, S. A comparative analysis of high spatial resolution IKONOS and WorldView-2 imagery for mapping urban tree species. **Remote Sensing of Environment**, v. 124, p. 516–533, 2012.

RODRIGUES, T. C. S. **Classificação da cobertura e do uso da terra com imagens WorldView-2 de setores norte da Ilha do Maranhão por meio do aplicativo interIMAGE e de mineração de dados**. Dissertação (Mestrado em Sensoriamento Remoto) - Instituto Nacional de Pesquisas Espaciais, São José dos Campos, 2014.

ROY, S.; KUMAR BHALLA, S. Role of geotechnical properties of soil on civil engineering structures. **Resources and Environment**, v. 7, n. 4, p. 103–109, 2017.

SANTORO, J.; MENDES, R. M.; PRESSINOTTI, M. M. N.; MANOEL, G. R. . Correlação entre chuvas e deslizamentos ocorridos durante a operação do Plano Preventivo de Defesa Civil em São Paulo, SP. In: SIMPÓSIO BRASILEIRO DE CARTOGRAFIA GEOTÉCNICA E GEOAMBIENTAL, 7., 2010. **Anais...** 2010. p.1-15.

SANTOS, C. S.; CASTRO, C. M. S.; RIBEIRO, T. R. Aplicações de imagens de satélite de alta resolução no planejamento urbano: o caso do cadastro técnico multifinalitário de Mata de São João, Bahia. In: SIMPÓSIO BRASILEIRO DE SENSORIAMENTO REMOTO, 15., 2011, Curitiba, PR. **Anais...** São José dos Campos: INPE, 2011. p. 3843–3850.

SCHWARZ, H.; MICHEL, G. P. Avaliação de estabilidade de encostas com uso do modelo Trigrs no município de Ibirama - SC. In: SIMPÓSIO BRASILEIRO DE RECURSOS HÍDRICOS, 20., 2016, Florianópolis, SC. **Anais...** 2016. p. 1–8.

SORBINO, G.; SICA, C.; CASCINI, L. Susceptibility analysis of shallow landslides source areas using physically based models. **Natural Hazards**, v. 53, n. 2, p. 313–332, 2010.

SOUZA, C. G. (Coord.). **Manual técnico de pedologia**. [S.l.: s.n.], 1995.

TACHINI, M.; SEVERO, D. L.; SILVA, H. S. Análise das correlações entre as chuvas acumuladas e os deslizamentos em Blumenau - SC. **Geosul**, v. 36, n. 79, p. 457–472, 2021.

TAN, C.; KU, C.; CHI, S.; CHEN, Y.; FEI, L.; LEE, J.; SU, T. Assessment of regional rainfall-induced landslides using 3S-based hydro-geological model. In: CHEN, Z.; ZHANG, J. M.; HO, K.; WU, F. Q.; LI, Z. K. (Ed.). **Landslides and engineereslopes: from the past to the future**. [S.l.]: Taylor and Francis, 2008. p. 1639–1645.

TATIZANA, C.; OGURA, A. T.; CERRI, L. E. S.; ROCHA, M. C. M. Análise da correlação entre chuvas e escorregamentos aplicados às encostas da Serra do mar, município de Cubatão. In: CONGRESSO BRASILEIRO DE GEOLOGIA E ENGENHARIA, 5., 1987. **Anais...** 1987a. p. 225–236.

TATIZANA, C.; OGURA, A. T.; CERRI, L. E. S.; ROCHA, M. C. M. Modelamento numérico da análise de correlação entre chuvas e escorregamentos aplicado às encostas da Serra do Mar no município de Cubatão. In: CONGRESSO BRASILEIRO DE GEOLOGIA E ENGENHARIA, 5., 1987. **Anais...** 1987b. p.237-248.

THIEBES, B.; BELL, R.; GLADE, T.; WANG, J.; BAI, S. Application of SINMAP and analysis of model sensitivity: case studies from Germany and China. **Romanian Journal of Geography**, v. 60, n. 1, p. 3–25, 2016.

TOBIN, G. A.; WHITEFORD, L. M. Provisioning capacity: a critical component of vulnerability and resilience under chronic volcanic eruptions. In: PFEIFER, K.; PFEIFER, N. (Ed.). **Forces of nature and cultural responses**. Berlin: Springer, 2013. p. 139–166.

VARNES, D. J. Slope movement types and processes. In: SCHUSTER, R. L. (Ed.). **Landslides: analysis and control.** [S.l.]: Transportation Research Board, 1978. p. 11–33.

VIEIRA, B. C. **Previsão de escorregamentos translacionais rasos na Serra do Mar (SP) a partir de modelos matemáticos em bases físicas**. 2007. 213 p. Tese (Doutorado em Geografia) - Universidade Federal do Rio de Janeiro, Rio de Janeiro, 2007.

VIEIRA, B. C.; RAMOS, H. **Aplicação do modelo Shalstab para mapeamento da suscetilidade a escorregamentos rasos em Caraguatatuba, Serra do Mar (SP)**. São Paulo: USP, 2015.

WISNER, B.; BLAIKIE, P.; CANNON, T.; DAVIS, I. **At Risk: Natural Hazards Peoples Vulnerability and Disasters**. [S.l.]: Routledge, 2003.

WOLLE, C. M. **Análise dos escorregamentos translacionais rasos numa região da Serra do Mar**. Tese (Doutorado) - Universidade de São Paulo, São Paulo, 1988.

WU, W.; SIDLE, R. C. A distributed slope stability model for steep forested basins. **Water Resources**, v. 31, n. 8, p. 2097–2110, 1995.

WU, W.; SIDLE, R. C. Application of a distributed Shallow Landslide Analysis Model (dSLAM) to managed forested catchments in Oregon, USA. **IAHS-AISH Publication**, v. 245, n. 245, p. 213–221, 1997.

ZÊZERE, J. L.; TRIGO, R. M.; TRIGO, I. F. Shallow and deep landslides induced by rainfall in the Lisbon region (Portugal): assessment of relationships with the North Atlantic Oscillation. **Natural Hazards and Earth System Science**, v. 5, n. 3, p. 331–344, 2005.

ZHUANG, J.; PENG, J.; WANG, G.; IQBAL, J.; WANG, Y.; LI, W.; XU, Q.; ZHU, X. Prediction of rainfall-induced shallow landslides in the Loess Plateau, Yan'an, China, using the TRIGRS model. **Earth Surface Processes and Landforms**, v. 42, n. 6, p. 915–927, 2017.

ZIZIOLI, D.; MEISINA, C.; VALENTINO, R.; MONTRASIO, L. Comparison between different approaches to modeling shallow landslide susceptibility: a case history in Oltrepo Pavese, Northern Italy. **Natural Hazards and Earth System Sciences**, v. 13, n. 3, p. 559–573, 2013.

APPENDIX A - DECISION TREE GENERATED BY CART ALGORITHM IN VILA BAIANA CLASSIFICATION.

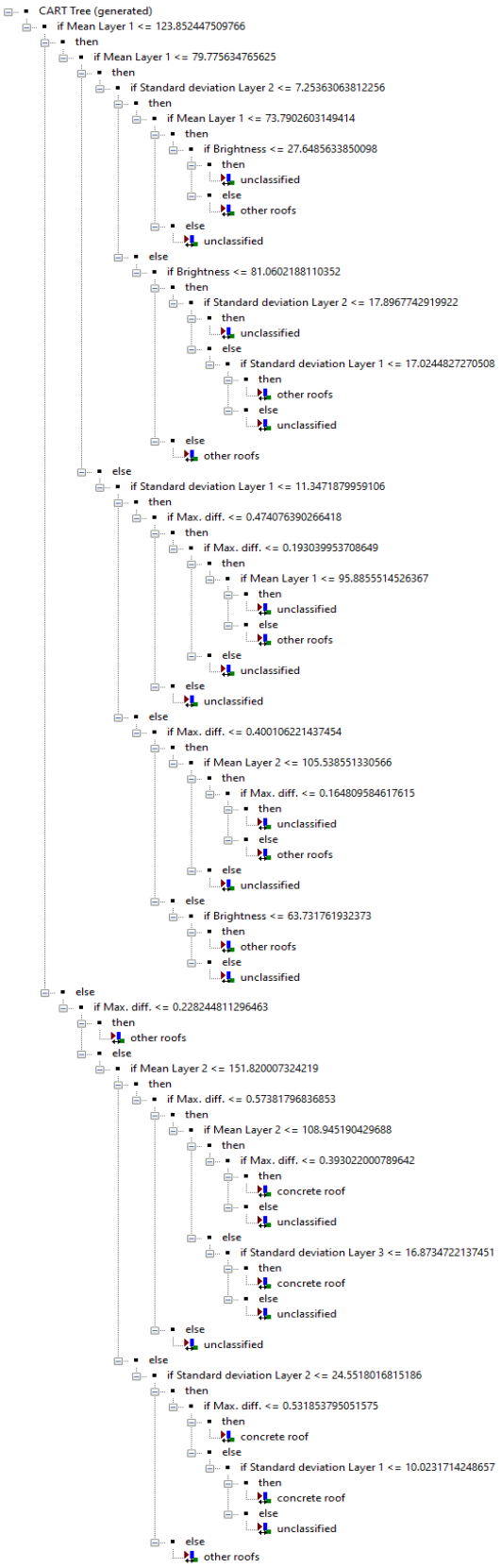

APPENDIX B – COMPARISON BETWEEN URBAN SPRAWL FROM 2013 AND 2021.

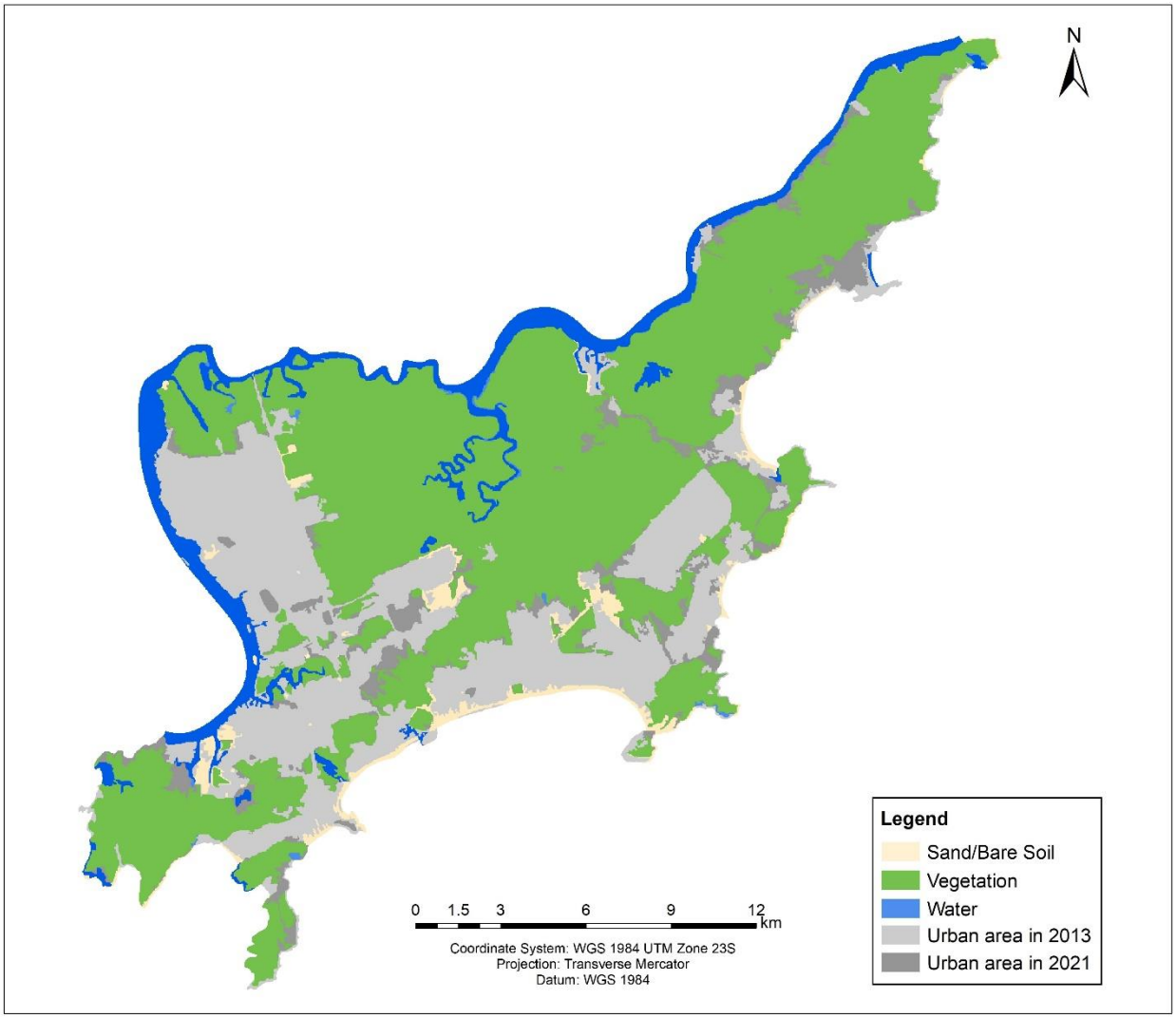

APPENDIX C – SCRIPT OF THE MATHEMATICAL MODEL TRIGRS USED AS AN EARLY WARNING SYSTEM.

```
import json
import requests
import pandas as pd
import subprocess
import pathlib
import numpy as np
import os

# Climatempo's API access token
token = ''  # Removed to preserve the confidentiality of the token

# API URL for the 72h forecast - 4234 = Guaruja
api_url =
'https://apiadvisor.Climatempo.com.br/api/v1/forecast/locale/4234/hour
s/72?token=' + token

# Receives the APIs response
response = requests.get(api_url)
response_json = response.json()

# Turns the API's response into a Pandas' DataFrame
response_df = pd.DataFrame(response_json['data'])

# Creates variables for each day of forecast
rain_24_sum = 0
rain_48_sum = 0
rain_72_sum = 0

# Iteration control variable
prediction_hour = 0

# For each of the 72h of forecast, sum the hour's precipitation of the
appropriate variable
for prediction_rain in response_df['rain']:
    if prediction_hour < 24:
        rain_72_sum += prediction_rain.get('precipitation')
        rain_48_sum += prediction_rain.get('precipitation')
        rain_24_sum += prediction_rain.get('precipitation')

    else:
        if prediction_hour < 48:
            rain_72_sum += prediction_rain.get('precipitation')
            rain_48_sum += prediction_rain.get('precipitation')

        else:
            rain_72_sum += prediction_rain.get('precipitation')

    # Increases the hour counter ahead of the loop wrap
    prediction_hour += 1

# Prints the forecast on the console
print('24h forecast: %04.2f mm/h' % round(rain_24_sum, 2))
print('48h forecast: %04.2f mm/h' % round(rain_48_sum, 2))
print('72h forecast: %04.2f mm/h' % round(rain_72_sum, 2))
```

```
# Converts mm/24h to m/s
rain_24_sum_ms = rain_24_sum / 86400000
rain_48_sum_ms = rain_48_sum / 86400000
rain_72_sum_ms = rain_72_sum / 86400000

# TRIGRS runs in 24-hour windows
rain_48_sum_ms_window = rain_48_sum_ms - rain_24_sum_ms
rain_72_sum_ms_window = rain_72_sum_ms - rain_48_sum_ms

# Defines and sets TRIGRS configuration parameters for 3 days of rain
forecast
trigrs_input_text = """Name of project (up to 255 characters)
PrevisaoScript
imax, row, col, nwf, tx, nmax
15889  141  165  21874,  1,  30
nzs, mmax, nper,  zmin,  uww,     t, zones
10,    100,   3,   0.001,  9.8e3,  259200,  2
zmax,   depth,   rizero,  Min_Slope_Angle (degrees)
-3.001,  -2.4,  1.0e-9,       0.
zone, 1
cohesion,phi,  uws,   diffus,   K-sat, Theta-sat,Theta-res,Alpha
4.0e+03, 39., 1.95e+04,  6.0e-06, 1.0e-05,   0.45,    0.05,    -0.5
zone, 2
cohesion,phi,  uws,   diffus,   K-sat, Theta-sat,Theta-res,Alpha
1.0e+03, 34., 1.71e+04,  6.0e-06, 1.0e-05,   0.45,    0.06,   -8.
cri(1), cri(2), ..., cri(nper)
%.2e, %.2e, %.2e
capt(1), capt(2), ..., capt(n), capt(n+1)
0,86400,172800,259200.
File name of slope angle grid (slofil)
{file/location/for/slope}
File name of property zone grid (zonfil)
{file/location/for/zone}
File name of depth grid (zfil)
{file/location/for/zmax}
File name of initial depth of water table grid   (depfil)
{file/location/for/depthwt}
File name of initial infiltration rate grid   (rizerofil)
None
List of file name(s) of rainfall intensity for each period, (rifil())
None
None
None
File name of grid of D8 runoff receptor cell numbers (nxtfil)
{file/location/for/TIdscelGrid}
File name of list of defining runoff computation order (ndxfil)
{file/location/for/TIcelindxList}
File name of list of all runoff receptor cells  (dscfil)
{file/location/for/TIdscelList}
File name of list of runoff weighting factors  (wffil)
{file/location/for/TIwfactorList}
Folder where output grid files will be stored  (folder)
%s
Identification code to be added to names of output files (suffix)
ThesisScript
Save grid files of runoff? Enter T (.true.) or F (.false.)
F
Save grid of minimum factor of safety? Enter Enter T (.true.) or F
(.false.)
```

```
T
Save grid of depth of minimum factor of safety? Enter Enter T (.true.)
or F (.false.)
F
Save grid of pore pressure at depth of minimum factor of safety? Enter
Enter T (.true.) or F (.false.)
F
Save grid files of actual infiltration rate? Enter T (.true.) or F
(.false.)
F
Save grid files of unsaturated zone basal flux? Enter T (.true.) or F
(.false.)
F
Save listing of pressure head and factor of safety ("flag")? (Enter -2
detailed, -1 normal, 0 none)
-2
Number of times to save output grids
4
Times of output grids
0,86400,172800,259200.
Skip other timesteps? Enter T (.true.) or F (.false.)
F
Use analytic solution for fillable porosity?  Enter T (.true.) or F
(.false.)
T
Estimate positive pressure head in rising water table zone (i.e. in
lower part of unsat zone)?  Enter T (.true.) or F (.false.)
T
Use psi0=-1/alpha? Enter T (.true.) or F (.false.) (False selects the
default value, psi0=0)
F
Log mass balance results?   Enter T (.true.) or F (.false.)
T
Flow direction (enter "gener", "slope", or "hydro")
gener
Add steady background flux to transient infiltration rate to prevent
drying beyond the initial conditions during periods of zero
infiltration?
T
""" % (rain_24_sum_ms, rain_48_sum_ms_window, rain_72_sum_ms_window,
str(pathlib.Path(__file__).parent.resolve()) + "\Outputs\\")

# Creates a new, or replaces the current 'tr_in.txt' in the folder
with open('tr_in.txt', 'w') as f:
    f.write(trigrs_input_text)

# Checks whether an Outputs folder exists and creates one if necessary
pathlib.Path(str(pathlib.Path(__file__).parent.resolve()) +
"\Outputs").mkdir(parents=True, exist_ok=True)

# Runs TRIGRS to calculate the safety factors
subprocess.run([str(pathlib.Path(__file__).parent.resolve()) +
"\TRIGRS.exe"], stdout=open(os.devnull, 'wb'), stderr=open(os.devnull,
'wb'))

# Reads TRIGRS safety factor output files
trigrs_output_1 = np.loadtxt('Outputs\TRfs_min_Previsao_1.txt',
skiprows=6)
trigrs_output_2 = np.loadtxt('Outputs\TRfs_min_Previsao_2.txt',
```

```
skiprows=6)
trigrs_output_3 = np.loadtxt('Outputs\TRfs_min_Previsao_3.txt',
skiprows=6)
trigrs_output_4 = np.loadtxt('Outputs\TRfs_min_Previsao_4.txt',
skiprows=6)

# Replaces the '-9999.' into '0' in order to be ignored (Forces the
data to be within the values 0 and 10)
np.clip(trigrs_output_1, 0, 10, out=trigrs_output_1)
np.clip(trigrs_output_2, 0, 10, out=trigrs_output_2)
np.clip(trigrs_output_3, 0, 10, out=trigrs_output_3)
np.clip(trigrs_output_4, 0, 10, out=trigrs_output_4)

# Calculates the sum of all values
trigrs_output_1_sum = np.sum(trigrs_output_1)
trigrs_output_2_sum = np.sum(trigrs_output_2)
trigrs_output_3_sum = np.sum(trigrs_output_3)
trigrs_output_4_sum = np.sum(trigrs_output_4)

# Calculates the percentage of FS that dropped compared to the initial
state
output_percent_24h = (100 * trigrs_output_2_sum / trigrs_output_1_sum)
- 100
output_percent_48h = (100 * trigrs_output_3_sum / trigrs_output_1_sum)
- 100
output_percent_72h = (100 * trigrs_output_4_sum / trigrs_output_1_sum)
- 100

# Writes the initial condition and forecasts on the console
print('\nInitial condition FS sum: %d' % round(trigrs_output_1_sum))
print('24h forecast FS sum: %d (%d / %.2f%%)' %
(round(trigrs_output_2_sum), trigrs_output_2_sum -
trigrs_output_1_sum, output_percent_24h))
print('48h forecast FS sum: %d (%d / %.2f%%)' %
(round(trigrs_output_3_sum), trigrs_output_3_sum -
trigrs_output_1_sum, output_percent_48h))
print('72h forecast FS sum: %d (%d / %.2f%%)' %
(round(trigrs_output_4_sum), trigrs_output_4_sum -
trigrs_output_1_sum, output_percent_72h))

# Counts the number of cells where the safety factor is 1 or lower,
ignoring zeros
trigrs_output_1_sub1count = np.count_nonzero(trigrs_output_1 <= 1)
trigrs_output_2_sub1count = np.count_nonzero(trigrs_output_2 <= 1)
trigrs_output_3_sub1count = np.count_nonzero(trigrs_output_3 <= 1)
trigrs_output_4_sub1count = np.count_nonzero(trigrs_output_4 <= 1)

# Writes the initial condition and forecast FS cell count on the
console
print('\nInitial condition FS <= 1 cell count: %d' %
trigrs_output_1_sub1count)
print('24h forecast FS <= 1 cell count: %d (+%d / +%.2f%%)' %
(trigrs_output_2_sub1count, trigrs_output_2_sub1count -
trigrs_output_1_sub1count, (100 * trigrs_output_2_sub1count /
trigrs_output_1_sub1count) - 100))
print('48h forecast FS <= 1 cell count: %d (+%d / +%.2f%%)' %
(trigrs_output_3_sub1count, trigrs_output_3_sub1count -
trigrs_output_1_sub1count, (100 * trigrs_output_3_sub1count /
trigrs_output_1_sub1count) - 100))
```

```
print('72h forecast FS <= 1 cell count: %d (+%d / +%.2f%%)' %
(trigrs_output_4_sub1count, trigrs_output_4_sub1count -
trigrs_output_1_sub1count, (100 * trigrs_output_4_sub1count /
trigrs_output_1_sub1count) - 100))

# In case the forecast predicts a decrease of 0.22% or greater, a
warning is issued
if (output_percent_24h <= -0.22) | (output_percent_48h <= -0.22) |
(output_percent_72h <= -0.22):

    # Commands that make it bold and red
    print('\n' + '\033[1m' + '\033[91m' + "Alert: Factor of safety
indicates risk of landslide" + '\033[0m')
```

APPENDIX D – EARLY WARNING SYSTEM WORKFLOW